

**Simulations of 2015  
Hydrodynamics and Water Quality  
in the Massachusetts Bay System using  
the Bays Eutrophication Model**

---

Massachusetts Water Resources Authority  
Environmental Quality Department  
Report 2016-16



Citation:

Zhao L, Chen C, Beardsley RC, Codiga DL, Leo WS. 2016. **Simulations of 2015 Hydrodynamics and Water Quality in the Massachusetts Bay System using the Bays Eutrophication Model**. Boston: Massachusetts Water Resources Authority. Report 2016-16. 112pp.

## Acronyms

### *Related to models used*

|              |   |
|--------------|---|
| BEM          | Bays Eutrophication Model (water quality model UG-RCA and hydrodynamics model MB-FVCOM together)                                      |
| FVCOM        | Finite-Volume Community Ocean Model   |
| MB-FVCOM     | FVCOM applied to Massachusetts Bay  |
| NECOFS       | Northeast Coastal Ocean Forecast System (components of which include the GOM3-FVCOM regional model, and Global-FVCOM)                 |
| GOM3-FVCOM   | FVCOM for Gulf of Maine (GOM), Scotian and southern New England shelves, and Georges Bank: 45 vertical layers, nested in Global-FVCOM |
| GOM1-FVCOM   | “ “ but 30 vertical layers, not nested in Global-FVCOM  |
| Global-FVCOM | FVCOM applied to the global oceans  |
| RCA          | Row Column Advanced (RCA), a water quality model originally developed by Hydroqual  |
| UG-RCA       | Unstructured-grid version of RCA  |
| WRF          | Weather Research and Forecast meteorological model  |

### *Related to modeled quantities*

|   |  |
|---|--|
| DIN   | Dissolved Inorganic Nitrogen (Sum of Nitrogen in $\text{NH}_4^+$ , $\text{NO}_3^-$ , and $\text{NO}_2^-$ ) |
| DO  | Dissolved Oxygen   |
| DOC, DON, DOP                                       | Dissolved Organic Carbon, Nitrogen, and Phosphorous  |
| $\text{NH}_4^+$ , $\text{NO}_3^-$ , $\text{NO}_2^-$ | Ammonium, Nitrate, Nitrite   |
| $\text{PO}_4^{3-}$ , $\text{SiO}_3^{2-}$            | Phosphate, Silicate  |
| POC, PON, POP                                       | Particulate Organic Carbon, Nitrogen, and Phosphorous  |
| SOD   | Sediment Oxygen Demand   |

**Simulations of 2015 Hydrodynamics and Water Quality  
in the Massachusetts Bay System using the Bays Eutrophication Model**

Submitted to

Massachusetts Water Resources Authority  
Environmental Quality Department  
100 First Avenue  
Charlestown Navy Yard  
Boston, MA 02129  
(617) 242-6000

Prepared by

Liuzhi Zhao and Changsheng Chen  
School for Marine Science and Technology  
University of Massachusetts-Dartmouth  
New Bedford, MA 02744

Robert C. Beardsley  
Woods Hole Oceanographic Institution  
Woods Hole, MA 02543

Daniel L. Codiga and Wendy S. Leo  
Massachusetts Water Resources Authority  
Boston, MA 02129

April 2017

## EXECUTIVE SUMMARY

The hydrodynamics (including temperature, salinity, and currents) and water quality (including nutrients, chlorophyll, and dissolved oxygen) of Massachusetts Bay, Cape Cod Bay, and Boston Harbor during 2015 were simulated by University of Massachusetts Dartmouth. Methods were as in simulations of 2014 (MWRA Technical Report, <http://www.mwra.state.ma.us/harbor/enquad/pdf/2016-03.pdf>) except that the system was upgraded to use the regional hydrodynamic model of the North East Coastal Ocean Forecast System (NECOFS). Advantages of the new approach include higher grid resolution and improvements to offshore boundary forcing from use of a global-scale simulation; in addition NECOFS is an operational product that is generated for, and being used by, many others so a regional hydrodynamics simulation dedicated to this project is no longer necessary. Hydrodynamic results were in good agreement with available observations for the geographic and vertical structure, and temporal variability, of temperature and salinity distributions (including density stratification) and currents (non-tidal and tidal).

The water quality simulation captured general patterns in observed seasonal variations, geographic distributions, and vertical structure for many variables. This included the late spring reduction in near-surface dissolved inorganic nitrogen (DIN), due to phytoplankton uptake, and its replenishment when stratification broke down in fall. It also included seasonal dissolved oxygen variations, with peak values in spring at shallow depths due to colder water and phytoplankton growth, and late summer minima deep in the water column where stratification inhibits reaeration by air-sea exchange. In addition to those more bay-wide patterns, DIN was elevated near the seafloor within 10-20 km of the outfall. Model-observation agreement was modest for dissolved and particulate organic nitrogen and weakest for particulate organic carbon, particularly its vertical structure, and for chlorophyll. In general, as in prior years, most modeled water quality variables exhibited a smaller range of values, and smaller surface-bottom differences during stratified conditions, than did field observations. The simulations support the conclusion of the field monitoring program, that bay-wide ecological function is not appreciably influenced by the outfall.

A 1995-2015 hindcast simulation was used for an initial investigation of the importance of variations in physical transport, due to the flow into Massachusetts Bay south of Cape Ann, to variations of dissolved oxygen and chlorophyll in northern Massachusetts Bay including the outfall site. The results of this preliminary analysis, while not definitive, are consistent with prior studies that suggested transport plays a role in seasonal and inter-annual variations of oxygen.

## Table of Contents

|  |     |
|--|-----|
| EXECUTIVE SUMMARY .....  | 3   |
| 1. Introduction.....   | 9   |
| 1.1 Project overview.....  | 9   |
| 1.2 Background on oceanographic processes influencing water quality .....  | 9   |
| 1.3 Summary of observed 2015 conditions.....   | 11  |
| 2. Methods.....  | 13  |
| 2.1 Overview .....   | 13  |
| 2.2 Transition to GOM3-based modeling system .....   | 17  |
| 3. Forcing conditions .....  | 24  |
| 3.1 Wind, heat flux, light, and rivers.....  | 24  |
| 3.2 Loading of organic carbon, nitrogen, and phosphorous.....  | 28  |
| 3.3 Open boundary of the UG-RCA water quality model.....   | 31  |
| 4. Hydrodynamics .....   | 35  |
| 4.1 Model-observation comparisons .....  | 35  |
| 4.2 Model monthly-mean temperature, salinity, and circulation .....  | 45  |
| 5. Water quality.....  | 53  |
| 5.1 Light .....  | 55  |
| 5.2 Dissolved inorganic nitrogen .....   | 59  |
| 5.3 Chlorophyll.....   | 64  |
| 5.4 Primary productivity .....   | 69  |
| 5.5 Dissolved and particulate organic nitrogen.....  | 71  |
| 5.6 Particulate organic carbon.....  | 78  |
| 5.7 Dissolved oxygen .....   | 82  |
| 5.8 Sediment fluxes.....   | 91  |
| 5.9 Summary .....  | 94  |
| 6. Synthesis: Preliminary study of bay oxygen and chlorophyll variations in relation to inflow from offshore ..... | 95  |
| 7. Summary.....  | 106 |
| References.....  | 109 |

## Table of Figures

|   |    |
|---|----|
| Figure 1-1. Geography, bathymetry, schematic long-term mean circulation. ....                       | 10 |
| Figure 2-1. GOM3-FVCOM grid and Global-FVCOM grid.....  | 14 |
| Figure 2-2. Model grids: GOM3-FVCOM, MB-FVCOM, and UG-RCA. ....                                     | 15 |
| Figure 2-3. Water quality model dynamics, schematic (reproduced from Hydroqual, 2004). ....         | 17 |
| Figure 2-4. Comparison of GOM3-based model results with observed temperature and salinity. ..       | 21 |
| Figure 2-5. Comparison of GOM1-based results with observed temperature and salinity. ....           | 22 |
| Figure 2-6. Comparison of GOM3-based (“model”) and GOM1-based (“MB-GOM1”) results. ....             | 23 |
| Figure 3-1. Surface wind forcing, monthly averages.....   | 25 |
| Figure 3-2. Surface heat flux. ....   | 26 |
| Figure 3-3. Merrimack River daily/cumulative flux, and anomaly relative to long-term mean.....      | 27 |
| Figure 3-4. Mean daily 2015 non-oceanic loads (carbon, nitrogen, phosphorous). ....                 | 29 |
| Figure 3-5. MWRA outfall mean annual flow and carbon/nitrogen/phosphorous loads, 2005-15. .         | 30 |
| Figure 3-6. Station groups: northern (circles), southern (squares), and harbor (triangles).....     | 32 |
| Figure 3-7. Open boundary forcing, water quality model: chlorophyll, oxygen, and nutrients. ....    | 33 |
| Figure 3-8. Open boundary forcing, water quality model: organics. Presented as in Figure 3-7. ....  | 34 |
| Figure 4-1. Temperature time series, model-observation comparison. ....                             | 36 |
| Figure 4-2. Salinity time series, model-observation comparison. ....                                | 37 |
| Figure 4-3a. Temperature spatial structure, at/near sea surface, model-observation comparison. .... | 39 |
| Figure 4-3b. Temperature spatial structure, at/near seafloor, model-observation comparison. ....    | 40 |
| Figure 4-4a. Salinity spatial structure, at/near sea surface, model-observation comparison. ....    | 41 |
| Figure 4-4b. Salinity spatial structure, at/near seafloor, model-observation comparison. ....       | 42 |
| Figure 4-5a. Currents time series model-observation comparison, Jan – Jun. Winds top frame.....     | 43 |
| Figure 4-5b. Currents time series model-observation comparison, Jul - Dec.....                      | 44 |
| Figure 4-6a. Model temperature, monthly-mean spatial structure, at sea surface. ....                | 46 |
| Figure 4-6b. Model temperature, monthly-mean spatial structure, at seafloor.....                    | 47 |
| Figure 4-7a. Model salinity, monthly-mean spatial structure, at sea surface. ....                   | 48 |
| Figure 4-7b. Model salinity, monthly-mean spatial structure, at seafloor. ....                      | 49 |
| Figure 4-8a. Model currents, monthly-mean spatial structure, at sea surface. ....                   | 51 |
| Figure 4-8b. Model currents, monthly-mean spatial structure, 15 m deep.....                         | 52 |
| Figure 5-1. Model-observation correlations/regressions for key water quality parameters. ....       | 54 |
| Figure 5-2a. Light extinction. Northern stations. Line: Model. Symbols: Observations.....           | 56 |
| Figure 5-2b. Light extinction. Southern stations. Line: Model. Symbols: Observations. ....          | 57 |

|   |     |
|---|-----|
| Figure 5-2c. Light extinction. Harbor stations. Line: Model. Symbols: Observations.....                         | 58  |
| Figure 5-3a. Dissolved inorganic nitrogen. Northern stations. Model-observation comparisons. ...                | 60  |
| Figure 5-3b. Dissolved inorganic nitrogen. Southern stations. Model-observation comparisons. ...                | 61  |
| Figure 5-3c. Dissolved inorganic nitrogen. Harbor stations. Model-observation comparisons. ....                 | 62  |
| Figure 5-3d. Dissolved inorganic nitrogen ( $\mu\text{M}$ ). Model results, east-west transect (Fig. 3-7). .... | 63  |
| Figure 5-4a. Chlorophyll. Northern stations. Model-observation comparisons. ....                                | 65  |
| Figure 5-4b. Chlorophyll. Southern stations. Model-observation comparisons. ....                                | 66  |
| Figure 5-4c. Chlorophyll. Harbor stations. Model-observation comparisons. ....                                  | 67  |
| Figure 5-4d. Chlorophyll ( $\mu\text{g L}^{-1}$ ). Model results, east-west transect (Fig. 3-7). ....           | 68  |
| Figure 5-5. Primary production, vertically integrated, model-observation comparison.....                        | 70  |
| Figure 5-6a. Dissolved organic nitrogen. Northern stations. Model-observation comparisons. ....                 | 72  |
| Figure 5-6b. Dissolved organic nitrogen. Southern stations. Model-observation comparisons. ....                 | 73  |
| Figure 5-6c. Dissolved organic nitrogen ( $\mu\text{M}$ ). Model results, east-west transect (Fig. 3-7).....    | 74  |
| Figure 5-7a. Particulate organic nitrogen. Northern stations. Model-observation comparisons. ....               | 75  |
| Figure 5-7b. Particulate organic nitrogen. Southern stations. Model-observation comparisons. ....               | 76  |
| Figure 5-7c. Particulate organic nitrogen ( $\mu\text{M}$ ). Model results, east-west transect (Fig. 3-7). .... | 77  |
| Figure 5-8a. Particulate organic carbon. Northern stations. Model-observation comparisons.....                  | 79  |
| Figure 5-8b. Particulate organic carbon. Southern stations. Model-observation comparisons. ....                 | 80  |
| Figure 5-8c. Particulate organic carbon ( $\mu\text{M}$ ). Model results, east-west transect (Fig. 3-7).....    | 81  |
| Figure 5-9a. Oxygen concentration. Northern stations. Model-observation comparisons. ....                       | 84  |
| Figure 5-9b. Oxygen concentration. Southern stations. Model-observation comparisons. ....                       | 85  |
| Figure 5-9c. Oxygen concentration ( $\text{mg L}^{-1}$ ). Model results, east-west transect (Fig. 3-7).....     | 86  |
| Figure 5-10a. Oxygen percent saturation. Northern stations. Model-observation comparisons. ....                 | 87  |
| Figure 5-10b. Oxygen percent saturation. Southern stations. Model-observation comparisons. ....                 | 88  |
| Figure 5-10c. Oxygen percent saturation. Model results, east-west transect (Fig. 3-7). ....                     | 89  |
| Figure 5-11. Oxygen time series, Mooring A01 site, model-observation comparison.....                            | 90  |
| Figure 5-12. Sediment $\text{NH}_4^+$ flux. Model 2015 (line), observed 2001-2010 (box-whiskers). ....          | 92  |
| Figure 5-13. Sediment oxygen demand. Model 2015 (line), observed 2001-2010 (box-whiskers). ...                  | 93  |
| Figure 6-1. Transport anomaly and DO concentration anomalies, 3-day resolution.....                             | 96  |
| Figure 6-2. Transport anomaly and DO concentration anomalies, monthly-means. ....                               | 97  |
| Figure 6-3. Transport anomaly and DO concentration anomalies, annual means. ....                                | 98  |
| Figure 6-4. Transport anomaly and chlorophyll concentration anomalies, 3-day resolution. ....                   | 101 |

Figure 6-5. Transport anomaly and chlorophyll concentration anomalies, monthly means..... 102  
Figure 6-6. Transport anomaly and chlorophyll concentration anomalies, annual means. .... 103

## Table of Tables

|   |     |
|---|-----|
| Table 2-1. Statistics of differences between modeled and observed temperature and salinity.....                         | 20  |
| Table 6-1. Correlation coefficient of transport anomaly and DO concentration anomaly. ....                              | 100 |
| Table 6-2. Correlation coefficient of monthly-mean transport anomaly and lagged DO concentration anomaly. ....          | 100 |
| Table 6-3. Correlation coefficient of transport anomaly and chlorophyll concentration anomaly.                          | 104 |
| Table 6-4. Correlation coefficient of monthly-mean transport anomaly and lagged chlorophyll concentration anomaly. .... | 104 |

# 1. Introduction

## 1.1 *Project overview*

The Massachusetts Water Resources Authority (MWRA) has established a long-term monitoring program to evaluate the impact of MWRA sewage treatment plant effluent on the water quality and ecosystem function of Massachusetts Bay, Cape Cod Bay, and Boston Harbor. The monitoring program primarily consists of a series of ongoing field observation surveys and includes complementary water quality modeling as required by the permit for effluent discharge into Massachusetts Bay. The water quality simulations are carried out using the Bays Eutrophication Model (BEM), which consists of the UG-RCA (Unstructured Grid - Row Column Advanced) water quality model and the MB-FVCOM (Massachusetts Bay - Finite Volume Community Ocean Model) hydrodynamic model. This report presents simulation results for the 2015 calendar year.

## 1.2 *Background on oceanographic processes influencing water quality*

Massachusetts Bay and Cape Cod Bay (Figure 1-1) comprise a temperate coastal embayment system. Readers unfamiliar with its geography and the current understanding of its physical and biological oceanographic processes are referred to the introductory summaries found in sections 1.2 and 1.3 of MWRA Technical Report 2011-13 (Zhao et al., 2012), in the annual MWRA water column monitoring report (e.g., for calendar year 2015, Libby et al., 2016), and in references cited by them. (All MWRA Technical Reports, including those just cited, are available online at <http://www.mwra.state.ma.us/harbor/enquad/trlist.html>.) A brief summary follows here.

System hydrodynamics are characterized by a persistent general circulation pattern driving the flow of offshore Gulf of Maine waters into Massachusetts Bay via the Western Maine Coastal Current off Cape Ann, then southward before returning offshore just to the north of Cape Cod, with a portion of the flow first passing through Cape Cod Bay to the south. Rough estimates of the water residence time are about a month based on the surface currents, somewhat longer at mid-depth or deeper where currents are weaker, and also longer in Cape Cod Bay than in Massachusetts Bay. While this slow general circulation is important in determining long-term average transport pathways, superposed on it are stronger and more variable wind-driven currents, and oscillatory tidal motions. Temperatures follow the characteristic temperate seasonal pattern of minima in late winter and peaks in late summer. Salinities are freshest inshore and in the upper several meters; in

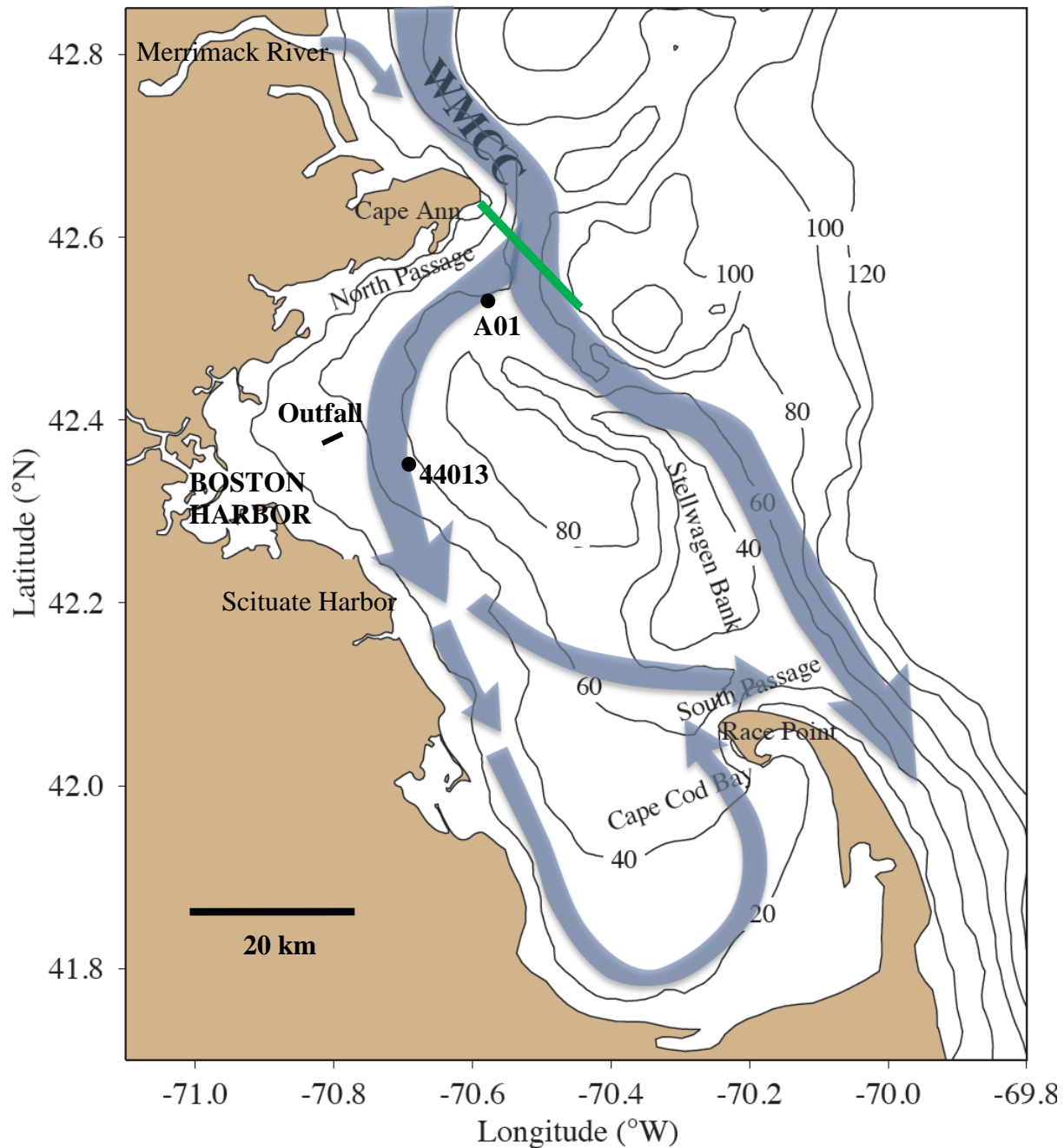


**Figure 1-1.** Geography, bathymetry, schematic long-term mean circulation.

WMCC = Western Maine Coastal Current.

A01 = Oceanographic mooring (Northeastern Regional Association of Coastal Ocean Observing Systems).

44013 = Weather buoy (National Data Buoy Center).

Contours = water depth in meters.

Green line = Transect used for volume transport analysis in Section 6.

Figure adapted from Xue et al. (2014).

addition to the influence of offshore oceanographic conditions, they vary mainly in response to riverine inputs including primarily those brought by the Western Maine Coastal Current and the Merrimack River outflow to the north, and to a lesser extent the smaller amounts delivered via Boston Harbor. There is a seasonal cycle in vertical structure that includes transitions between well-mixed conditions, present from fall through early spring due to higher winds and atmospheric cooling, and strong density stratification during the late spring and summer due mainly to preferential heating of surface water by the atmosphere.

The biology of the system is plankton-based and exhibits clear seasonal cycles that are tied closely to those hydrodynamic features, but with more pronounced spatial and interannual variability. Phytoplankton abundance typically peaks most strongly during bloom-favorable conditions in the late winter and early spring, as temperatures rise, light increases, and nutrients remain plentiful near the surface due to the active vertical mixing. Following the transition from spring to summer, near-surface nutrient concentrations become depleted as density stratification impedes the vertical mixing that replenishes them. Zooplankton abundance and biomass generally peak in late summer, following the spring increase in phytoplankton prey levels. Primary productivity is commonly sustained at modest levels through summer and typically there is a second increase in phytoplankton during fall, when vertical mixing increases again and delivers nutrients to the surface while temperature and light conditions are still favorable before winter. Dissolved oxygen concentrations are influenced by a combination of biological and physical processes; the net result is a seasonal peak in late spring, due to phytoplankton production increasing winter levels already high due to strong reaeration, then steady decreases to a late summer minimum due to respiration and reduced reaeration. Oxygen is depleted more strongly at depth, where stratification limits reaeration.

### **1.3 *Summary of observed 2015 conditions***

To provide context for descriptions of model simulations of 2015 throughout this report, a brief summary is given here of observed 2015 conditions based on MWRA monitoring results (Libby et al., 2016). For the fourth year in a row, February nutrient concentrations were at relatively low to moderate levels and chlorophyll concentrations were sustained at slightly elevated levels through the winter months, suggesting that the system remained more biologically productive through the winter than in a typical year. Winds were particularly strong in February and regional water temperatures were lower than normal in February to April. River flow was well below the median

throughout almost the entire year. No winter/spring diatom bloom was observed. There was a modest late-spring phytoplankton bloom, later than typical (in late April and May), due mainly to *Phaeocystis* which therefore led to depletion of nitrate but not silicate in near-surface waters. Chlorophyll concentrations in summer were lower than typical and no summer blooms were observed in coastal waters. In September and October there were fall blooms comparable to typical conditions, but the annual total phytoplankton abundance was the 21<sup>st</sup> lowest recorded during the past 24 years. Zooplankton abundances were nearly 10 times higher than typical levels in the prior 24 years, due mainly to exceptionally high bivalve veliger abundances in July and August, but also due to high copepod abundances. Dissolved oxygen levels followed the typical seasonal pattern and were relatively high, compared to past years, throughout most of 2015.

## 2. Methods

### 2.1 Overview

The present-day BEM is the result of extensive development begun in the early 1990s. Complete background information is in MWRA technical reports, where the model development and updating process has been documented. MWRA Technical Report 2015-02 (Zhao et al., 2015a) provides a comprehensive listing (their Table 1.1) of MWRA technical reports about the modeling (up to and including simulations of 2011), including for each report a summary of its topic, highlighted aspects of its content, the full citation, and (when viewed electronically) a hyperlink to the downloadable PDF file in the online repository. Section 1.4 of Zhao et al. (2012) reviews some of the key improvements incorporated to modeling methods, with emphasis on the several years leading up to the simulations of 2011. Simulations of years 2008 and later use MB-FVCOM for hydrodynamics and UG-RCA for water quality. The methods used in the simulations of 2015 are the same as for simulations of 2014 (Zhao et al., 2016), except for the important improvements described in Section 2.2 below. A brief overview of the methods is as follows.

The model grids consist of four domains. The largest domain is the Global-FVCOM simulation, with worldwide coverage (Figure 2-1; Chen et al., 2016). Nested within Global-FVCOM is the regional Gulf of Maine (GOM) FVCOM hydrodynamic model (GOM3-FVCOM; lower panel, Figure 2-2). Circulation in GOM3-FVCOM along its offshore boundary, including tidal variability, is driven (“forced”) by circulation of the Global-FVCOM simulation. Nested within the GOM3-FVCOM domain is the higher-resolution grid of the Massachusetts Bay FVCOM (MB-FVCOM) hydrodynamic model (upper panel, Figure 2-2). The MB-FVCOM domain extends offshore to an open boundary along an arc southeastward from north of Portsmouth, New Hampshire that passes about 25 km offshore from Cape Cod. Circulation in MB-FVCOM along this boundary, including tidal variability, is driven by circulation of the GOM3-FVCOM simulation. The fourth and smallest domain is that for the UG-RCA water quality model, which is the same as the MB-FVCOM grid except that it extends less far offshore, having an open boundary along an arc from near Cape Ann to the eastern shore of Cape Cod (upper panel, Figure 2-2). In MB-FVCOM and UG-RCA, horizontal resolution ranges from about 0.29 km near the coast to 0.7-2.5 km at the eastern boundary of UG-RCA and 5-10 km near the offshore MB-FVCOM nested boundary. In the vertical, the models have 45 grid levels. In areas shallower than 225 m deep, the levels are uniformly distributed; in deeper areas, the shallowest and deepest levels are concentrated

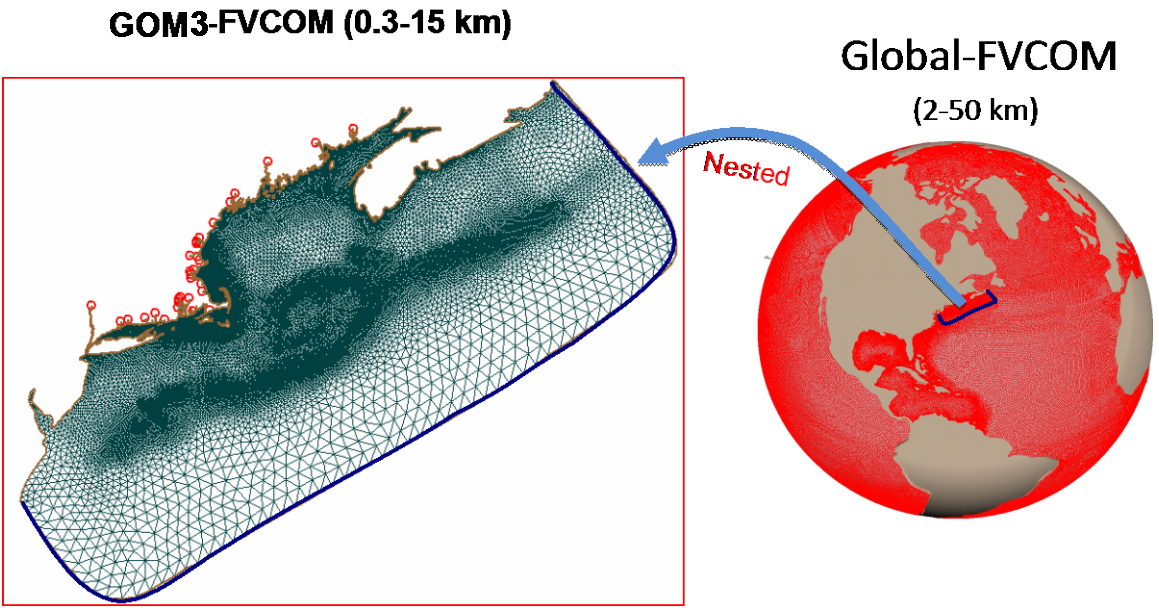


**Figure 2-1.** GOM3-FVCOM grid and Global-FVCOM grid.

GOM3-FVCOM is the new regional grid introduced for the 2015 simulation. It extends farther offshore and to the north and south, with finer coverage over the continental slope, as compared to the GOM1-FVCOM grid (shown in Figure 2-1 of Zhao et al., 2016) used in past years. Red dots in left panel show locations of freshwater input.

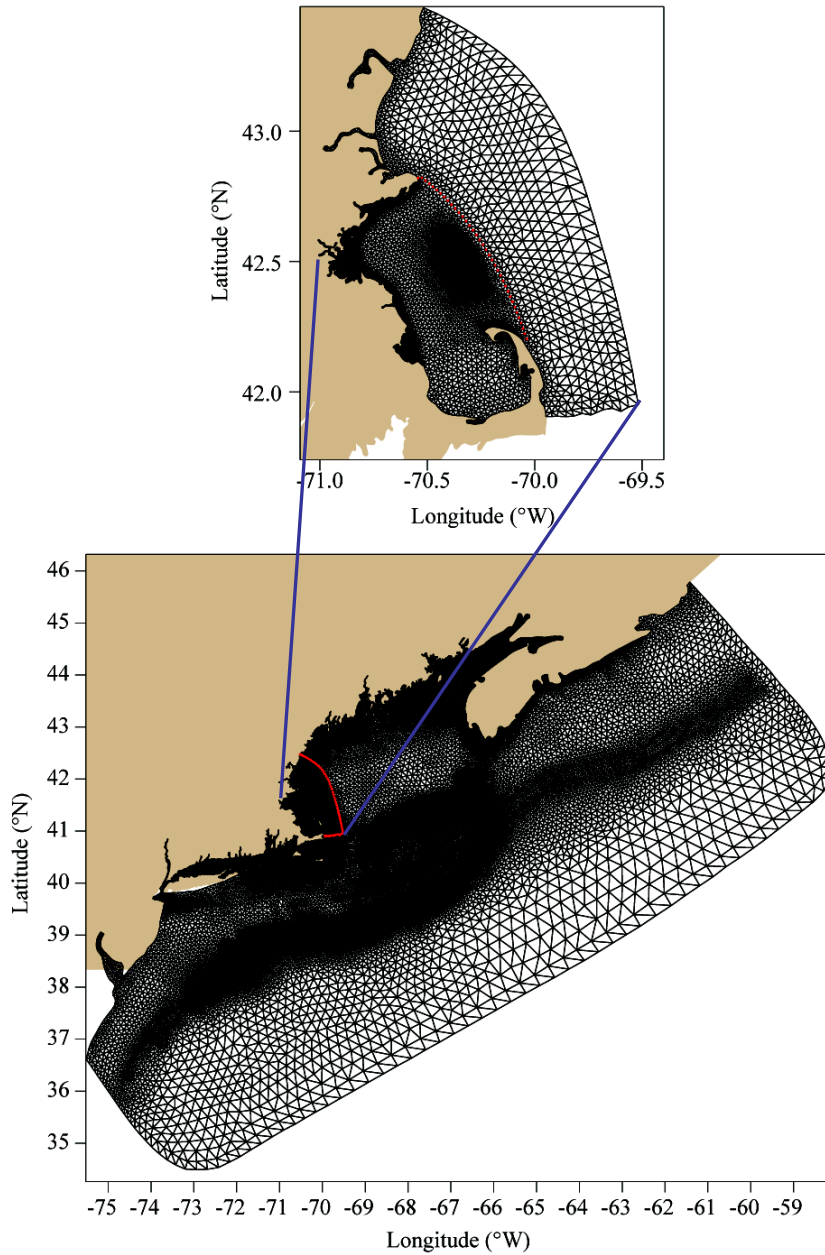


**Figure 2-2.** Model grids: GOM3-FVCOM, MB-FVCOM, and UG-RCA.

Lower panel: Gulf of Maine grid, GOM3-FVCOM; the red line shows the offshore boundary of the nested Massachusetts Bay grid, MB-FVCOM. Upper panel: nested MB-FVCOM domain; red line shows offshore boundary of the smaller domain of the water quality model, UG-RCA.

in constant-thickness boundary layers, between which the remaining levels are uniformly distributed. The GOM3-FVCOM and MB-FVCOM hydrodynamic models are forced at the surface by the data-assimilative Weather Research and Forecast (WRF) meteorological model, along the coast by freshwater inputs from rivers, and at the seafloor by the MWRA outfall. In addition to satellite sea surface temperature, the models assimilate all available observed temperature and salinity profiles and moored timeseries collected throughout their geographic coverage areas (as described in Zhao et al., 2016).

The water quality model UG-RCA is driven using the circulation and eddy diffusivity from the MB-FVCOM hydrodynamic model output. UG-RCA is an unstructured grid version of RCA-v3.0 (Hydroqual, 2004), which simulates 26 water column parameters and 23 sediment variables, a subset of which are shown in a schematic diagram of modeled processes (Figure 2-3). Three phytoplankton functional groups are included: a winter-spring group favoring low temperatures, low light, and high nutrients (representative of diatoms); a summer group that favors higher temperature and light conditions, and tolerates lower nutrients (representative of a mixture of species including dinoflagellates); and a fall group most responsive to moderate temperatures and lower nutrients (representative of a second diatom group). Growth of phytoplankton is based on solar radiation and nutrient availability. Grazing by zooplankton, which are not directly modeled, is treated as a transformation of mass in the phytoplankton groups to particulate and dissolved organic matter at rates that increase linearly with temperature. Nutrients (including nitrate  $\text{NO}_3^-$ , nitrite  $\text{NO}_2^-$ , ammonium  $\text{NH}_4^+$ , phosphate  $\text{PO}_4^{3-}$ , and dissolved silica  $\text{SiO}_3^{2-}$ ) are formed through mineralization of organic substances in the water column and at the sediment-water interface. Cycling of labile and refractory forms of dissolved and particulate organic carbon, nitrogen, and phosphorous is included. Dissolved oxygen concentration is computed by the reaeration flux at the sea surface, sediment oxygen demand at the bottom, and biological and biogeochemical dynamics in the water column including phytoplankton photosynthetic production, consumption by respiration, biogeochemical oxygen demand through the mineralization of particulate and dissolved organic matter, and nitrification. Open boundary condition fields are specified using MWRA monitoring program observations and the method of objective analysis (e.g., Tian et al., 2009). MWRA outfall nutrient and carbon loadings are specified using Deer Island Treatment Plant data.

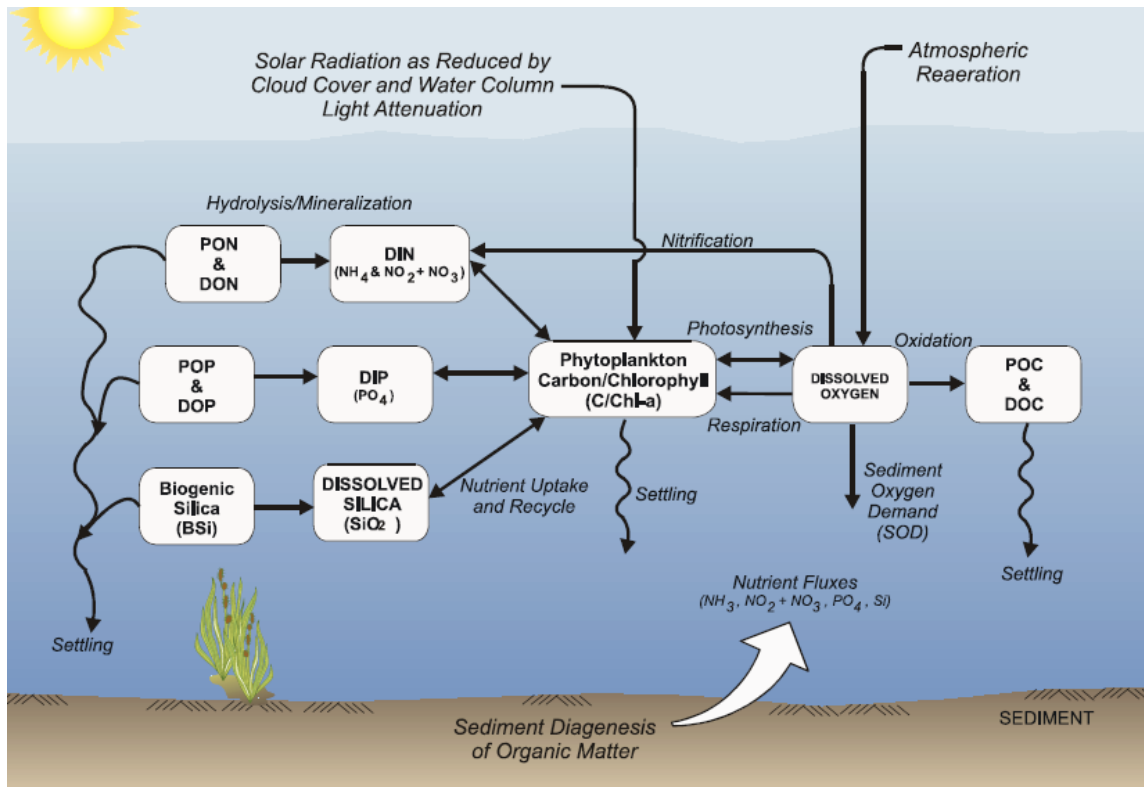


**Figure 2-3.** Water quality model dynamics, schematic (reproduced from HydroQual, 2004).

## 2.2 Transition to GOM3-based modeling system

For the 2015 simulation the Bays Eutrophication Model was updated by replacing the GOM1-FVCOM regional hydrodynamics model, used in past years, by GOM3-FVCOM. The main motivation was to capitalize on recently developed advances in capabilities of the Northeast Coastal Ocean Forecast System (NECOFS), because GOM3-FVCOM is already being run as part of NECOFS on an ongoing basis. NECOFS is an integrated atmosphere/surface wave/ocean forecast model system designed for the northeast U.S. coastal region covering a computational domain from central New Jersey to the eastern end of the Nova Scotia shelf. NECOFS includes the Weather Research and Forecasting (WRF) community mesoscale meteorological model, and a regional FVCOM (GOM3-FVCOM) with domain covering the Gulf of Maine, Georges Bank, and New England Shelf regions (Figure 2-2). GOM3-FVCOM features unstructured triangular meshes with horizontal resolution of ~0.3-25 km and 45 layers in the vertical. GOM3-FVCOM is nested in a global ocean model (Global-FVCOM, Chen et al., 2016; Figure 2-1), which provides the upstream and open ocean boundary conditions. NECOFS was placed into 24/7 forecast operations

in late 2007 and its core components continue to be improved to the present (<http://134.88.228.119:8080/fvcomwms/>). UMass Dartmouth used NECOFS to complete a 38-year (1978-2015) hindcast simulation with data assimilation of sea surface temperature, sea surface height, and hydrographic (temperature and salinity) profiles. This simulation includes 1) the surface heat flux, wind forcing, precipitation minus evaporation, and river discharges, 2) the inflow of the cool and lower salinity water from the upstream Scotian Shelf, and 3) interaction with the Gulf Stream. The hindcast successfully captured observed spatial and temporal variability in regional hydrodynamic fields as documented by Cowles et al. (2008) for vertical mixing and subtidal currents, Chen et al. (2011) for tidal elevations and currents, Li et al. (2015) for density stratification, and Sun et al. (2016) for spatially explicit patterns of surface currents.

The Bays Eutrophication Model used for simulations of 2006-2014 consisted (see Figure 2-1 of Zhao et al., 2016) of two hydrodynamic models (the regional GOM1-FVCOM, and nested within it the higher-resolution MB-FVCOM) and a water quality model (UG-RCA). GOM1-FVCOM and MB-FVCOM were coupled by a one-way nesting approach through common boundary cells and nodes. The water quality assessment was done by three steps. The first step was to run GOM1-FVCOM and output all variables on nesting boundary cells and nodes at every time step. The second step was to run MB-FVCOM under the same meteorological forcing, using boundary conditions specified by the GOM1-FVCOM output. The final step was to use the MB-FVCOM hydrodynamic fields to drive UG-RCA. Results from this system have been validated against observations and demonstrate the ability to capture the seasonal and inter-annual variability of water quality model fields, for example dissolved oxygen, in Massachusetts Bay both in MWRA simulations (e.g., Tian et al. 2009, Chen et al. 2010, Zhao et al. 2016) and in extensions to them that also included earlier years (e.g., 1995-2014 by Xue et al., 2014). However, GOM1-FVCOM had shortcomings associated with its open ocean boundaries. Water exchanges with the Gulf Stream, which mainly occur farther offshore over the outer slope, were not accounted for by GOM1-FVCOM because its grid extended offshore by a limited distance and did not have high resolution there. In addition, although GOM1-FVCOM had a means to include non-tidal inflow on the upstream Nova Scotia shelf (Cowles et al., 2008), the forcing specified on the GOM1-FVCOM open boundary included tidal variability only. Thus non-tidal variability, such as the important buoyancy-driven flow from offshore and upstream, was not optimally simulated.

In addition to the fact that GOM3-FVCOM is already being run operationally as part of NECOFS, so that its outputs are available without need to separately run a regional hydrodynamical model specifically for MWRA, there are several performance advantages of replacing GOM1-FVCOM with GOM3-FVCOM. In GOM3-FVCOM the grid extends farther offshore and a more realistic bathymetric dataset has been used. It thus produces more accurate tidal simulation results (e.g., Chen et al., 2011). The one-way nesting of GOM3-FVCOM in Global-FVCOM, through common nesting boundary cells and nodes, means that it captures non-tidal inflow from the upstream region, and water exchange with the Gulf Stream over the outer shelf, better than GOM1-FVCOM and is therefore capable of capturing climate change signals due to inter-annual variability of the inflow. Finally, GOM3-FVCOM has higher vertical and horizontal resolution. GOM3-FVCOM horizontal resolution reaches ~0.3 km near the coast, while the finest horizontal resolution of GOM1-FVCOM was ~1.3 km. In the vertical, GOM1-FVCOM had a  $\sigma$ -coordinate with 30 layers; GOM3-FVCOM has a hybrid terrain-following coordinate with 45 layers. The hybrid coordinate uses a  $\sigma$ -coordinate shallower than 225 m and an s-coordinate with 10 and 5 uniform layers near the surface and bottom, respectively, in deeper regions; at the transition between the two, the 225-m isobath, the thickness of all 45 layers is 5 m. This hybrid coordinate prevents numerical errors in the simulation of the surface mixed layer and bottom boundary layer dynamics offshore, while maintaining high resolution in shallower coastal regions.

To be consistent with GOM3-FVCOM, both the MB-FVCOM and the UG-RCA grids were upgraded to use the same 45 layers in the vertical.

The performance of the upgraded GOM3-based system was evaluated by running the 2015 simulations separately using both the GOM3-based system and the GOM1-based system, and comparing the two results at the Mooring A01 site (Figure 1-1) to time series observations collected there at 1m, 20m, and 50m deep. Statistics of the model-observation comparisons (Table 2-1) quantify the improved performance of the GOM3-based system in capturing the observations, as compared to the GOM1-based system. For GOM3-based results the magnitudes of mean model-observation differences are all substantially lower than GOM1-based results except for 1m deep salinity, which is essentially unchanged; the GOM3-based standard deviations are all modestly lower than GOM1-based results except for 1m deep temperature and 50m deep salinity, for which the two cases are comparable to each other.

**Table 2-1.** Statistics of differences between modeled and observed temperature and salinity.

| Parameter              | Depth | Statistic          | GOM3-based<br>(Figure 2-4) | GOM1-based<br>(Figure 2-5) |
|------------------------|-------|--------------------|----------------------------|----------------------------|
| Temperature<br>(deg C) | 1m    | Mean               | 0.069                      | 0.197                      |
|                        |       | Standard deviation | 0.759                      | 0.768                      |
|                        | 20m   | Mean               | -0.001                     | 0.581                      |
|                        |       | Standard deviation | 0.865                      | 1.134                      |
|                        | 50m   | Mean               | 0.298                      | 0.682                      |
|                        |       | Standard deviation | 0.600                      | 0.799                      |
| Salinity<br>(PSS)      | 1m    | Mean               | 0.064                      | -0.065                     |
|                        |       | Standard deviation | 0.230                      | 0.394                      |
|                        | 20m   | Mean               | 0.013                      | -0.149                     |
|                        |       | Standard deviation | 0.168                      | 0.200                      |
|                        | 50m   | Mean               | 0.018                      | -0.106                     |
|                        |       | Standard deviation | 0.136                      | 0.128                      |

The nature of the improvements underlying these statistics is illustrated by a series of plots. GOM3-based results are compared to observations in Figure 2-4. The model accurately captures both the overall seasonal patterns and the weather-band variations superposed on them. Agreement is best at 1 m and 20 m, while at 50 m deep the model temperature and salinity are both biased high (positive mean model-observation difference), particularly during the stratified period (mid-April to mid or late October). Results from the GOM1-based simulation, compared to the same observations (Figure 2-5), show similar agreement with the exception that the 20 m GOM1- based temperatures are notably higher than the observations during the late spring and early summer, and the deep temperature is biased high more strongly than in the GOM3-results. Super-posed GOM3-based model and GOM1-based model results (Figure 2-6) make these differences clear.

In summary, the success of the transition to the GOM3-based system has been demonstrated by comparisons between GOM3-based and GOM1-based simulations of the same year, and some aspects of the hydrodynamics results for the GOM3-based results are improved over the GOM1-based results.

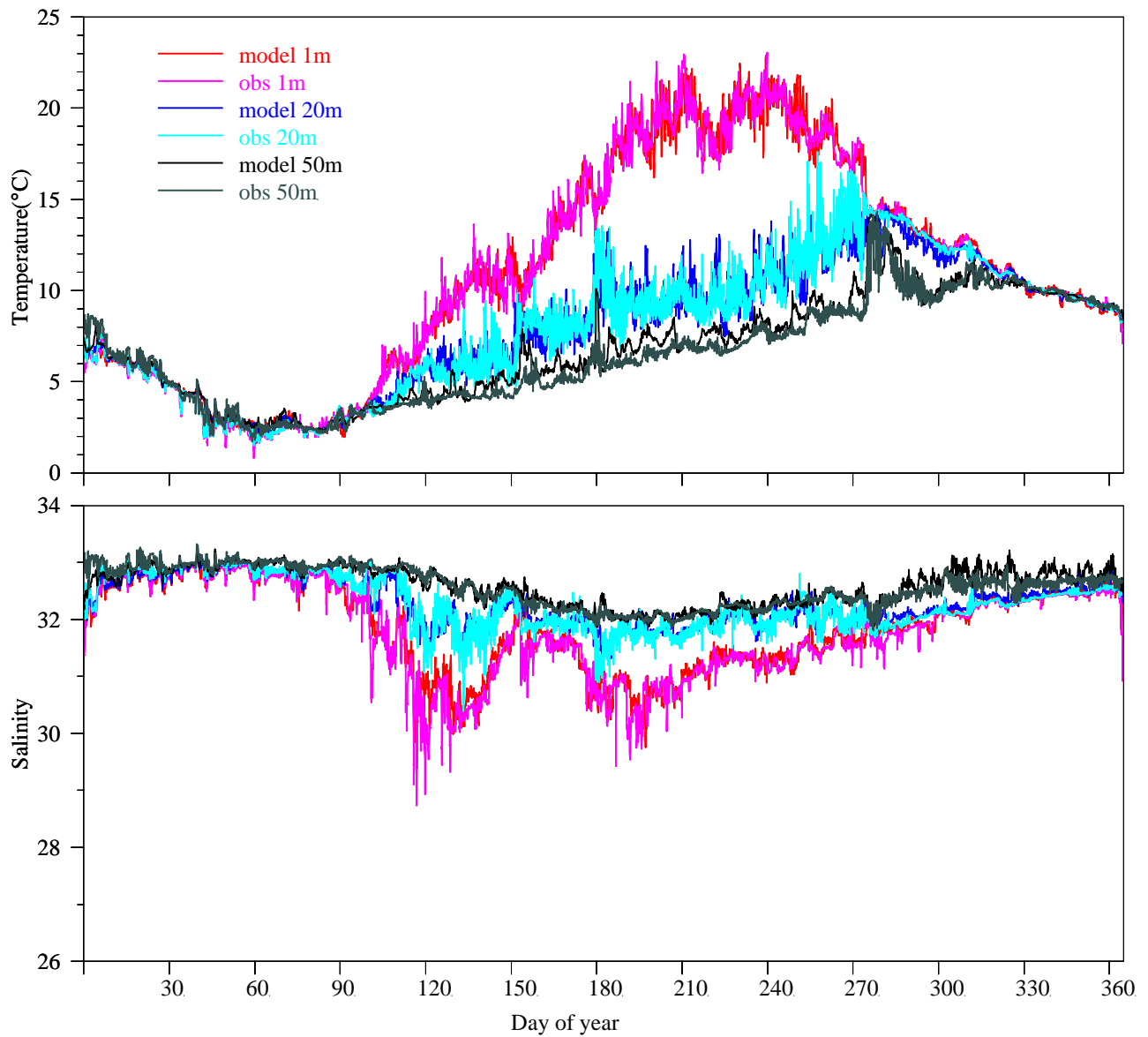


**Figure 2-4.** Comparison of GOM3-based model results with observed temperature and salinity. From Mooring A01 location (see Figure 1-1) at 1 m, 20 m, and 50 m depths. Temperature values given in units of degrees Celsius. Salinity values given on the Practical Salinity Scale (PSS).

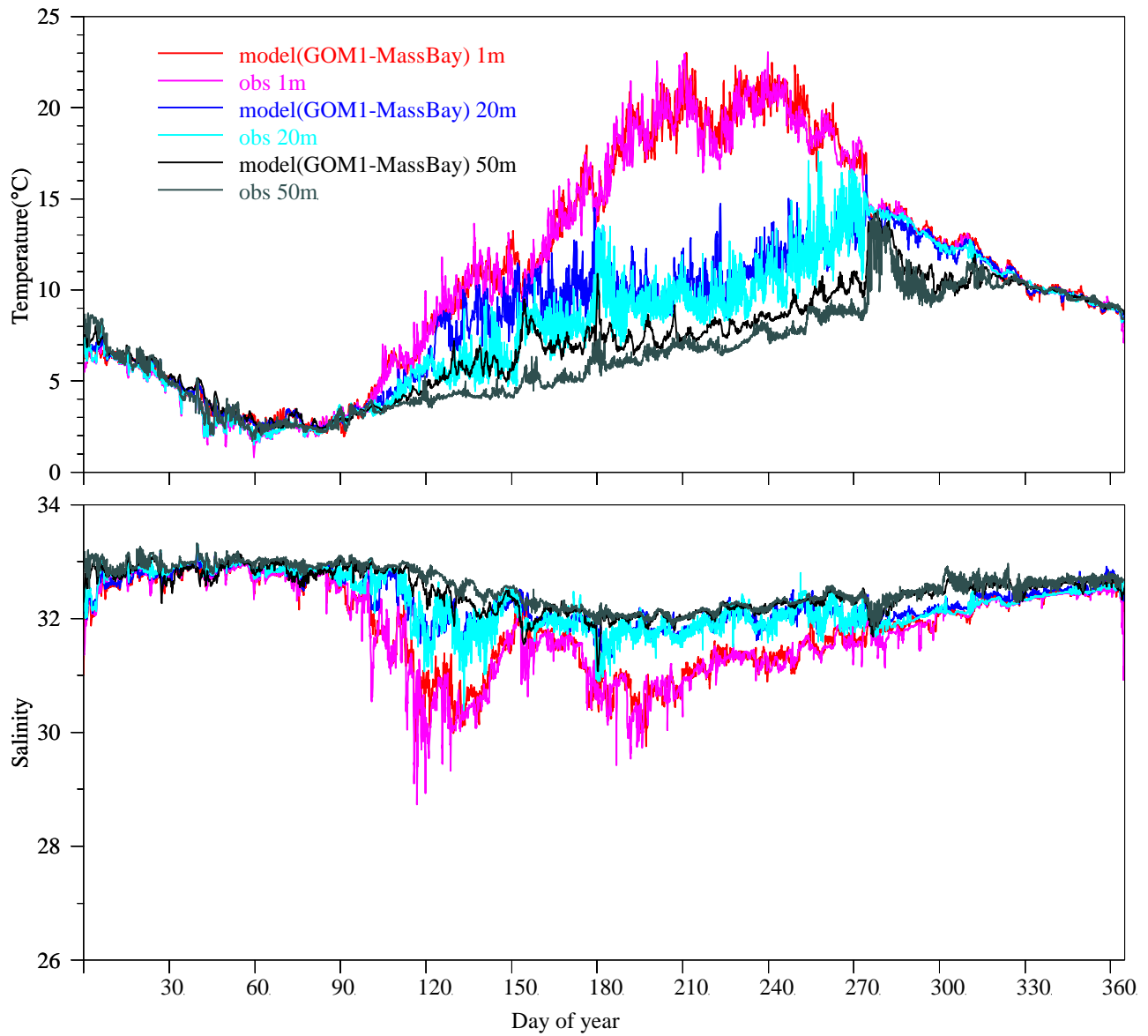


**Figure 2-5.** Comparison of GOM1-based results with observed temperature and salinity.

The GOM1-FVCOM grid (not shown; see Figure 2-1 of Zhao et al. 2016) was the regional grid used in simulations of years prior to 2015.

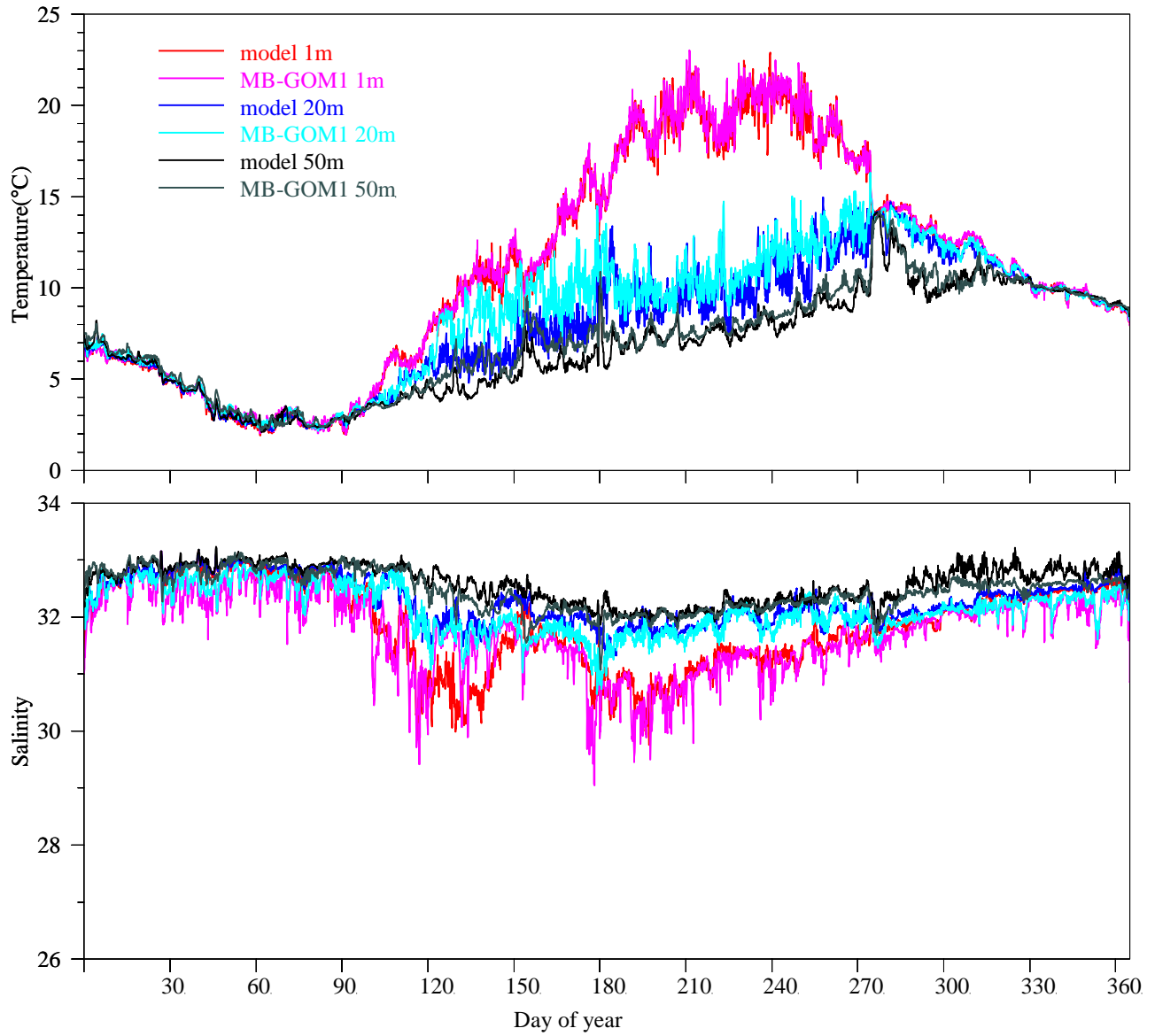


**Figure 2-6.** Comparison of GOM3-based (“model”) and GOM1-based (“MB-GOM1”) results.

### 3. Forcing conditions

#### 3.1 *Wind, heat flux, light, and rivers*

The main characteristics of 2015 wind forcing are revealed by comparisons with the long-term mean and standard deviation of previous years from 1995 to 2014 (Figure 3-1). The seasonal pattern of vector-averaged velocities (top frame) showed significantly larger magnitudes than the long-term mean in the months of January to March. In the months of May and June the mean wind was from the southwest and southeast, in contrast to the long-term mean which was from the southeast and southwest respectively. The wind speeds (second frame) in 2015 are generally larger than the long-term mean; in January and October, the monthly wind speed was larger than the maximum values in the past 20 years. The wind stress magnitude (third frame) showed the same pattern, and the north-south wind stress (bottom frame), a diagnostic for upwelling, was slightly higher than the long-term mean during the summer.

The main attributes of the 2015 air-sea heat flux are seen on comparisons with the long-term mean and standard deviation (Figure 3-2). The seasonal pattern in 2015 (top frame) had negative heat flux (loss of heat from surface; cooling of ocean) during winter and positive heat flux (heating of ocean) during summer, as does the long-term mean. The cumulative flux (middle frame) results emphasize that 2015 had a notably lower than average heat flux, which was lower than the long-term mean throughout the year. The anomaly of 2015 relative to the long-term mean (bottom frame) was therefore substantially negative throughout the year.

The largest riverine influence on Massachusetts Bay is the Merrimack River, which on entering coastal waters north of the bay joins the Western Maine Coastal Current and flows into the bay off Cape Ann (Figure 1-1). The 2015 Merrimack volume transport (Figure 3-3) was substantially smaller than the long-term mean throughout nearly the entire year, with cumulative values (middle frame) distinctly lower than the long-term average except during the first half of January, such that the cumulative anomaly (bottom frame) was large and negative.

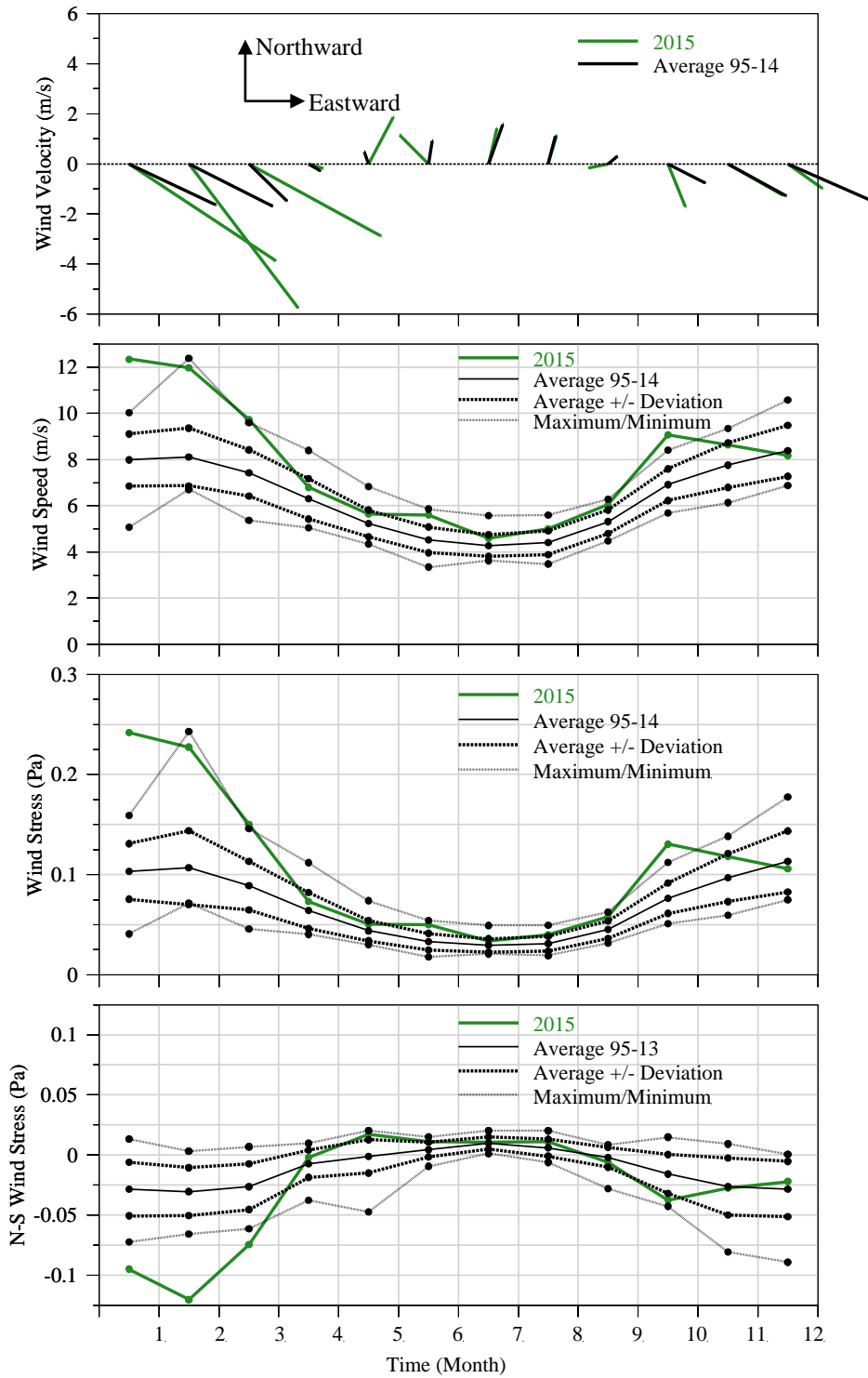


**Figure 3-1.** Surface wind forcing, monthly averages.

Top frame: Vector-averaged wind velocities. Second frame: Wind speed. Third frame: Wind stress magnitude. Bottom frame: North-south component of wind stress, an indicator for wind-driven upwelling.

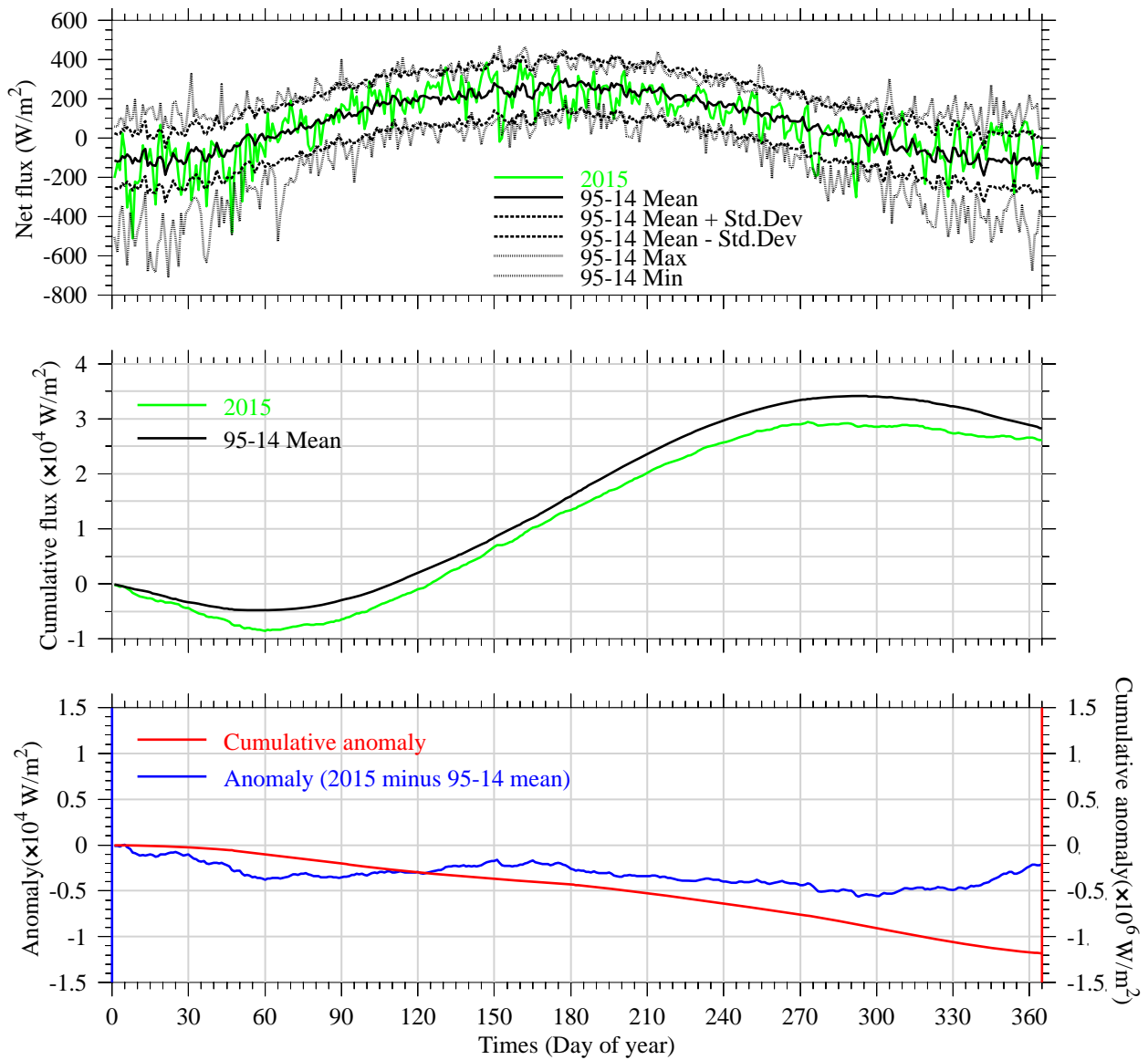


**Figure 3-2.** Surface heat flux.

Top frame: Net heat flux into ocean. Middle frame: Cumulative net heat flux relative to January 1. Bottom frame: Anomaly of 2015 net heat flux (blue, left vertical axis) relative to 1995-2014 average; cumulative anomaly relative to January 1 (red, right vertical axis).

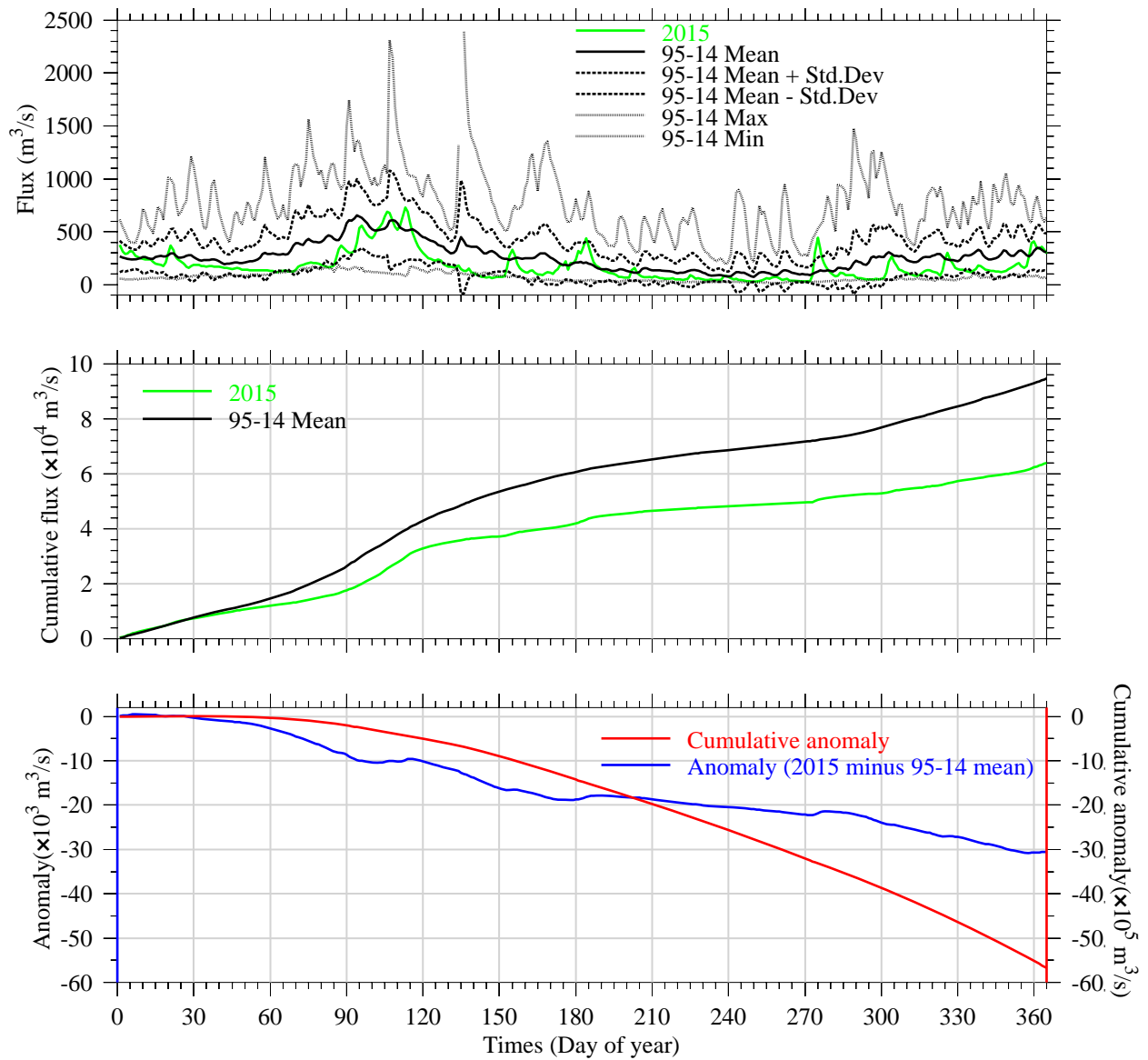


**Figure 3-3.** Merrimack River daily/cumulative flux, and anomaly relative to long-term mean.

Top frame: Merrimack River volume flux. Middle frame: Cumulative flux relative to January 1. Bottom frame: Anomaly of flux in 2015 relative to 1995-2014 average (blue, left vertical axis); cumulative anomaly relative to January 1 (red, right vertical axis).

### **3.2 Loading of organic carbon, nitrogen, and phosphorous**

There are both oceanic and non-oceanic sources of organic materials and nutrients to the bays. The oceanic component stems from exchange with adjacent offshore waters of the Gulf of Maine. These offshore waters are not characterized by particularly high concentrations, but the volume of the exchange is very large. A systemwide budget for total nitrogen in the bays, based on results from BEM simulations of 1992 conditions, concluded that approximately 93% originated offshore in the Gulf of Maine (Hunt et al., 1999; Hydroqual, 2000). Consequently, oceanic input is by far the single largest source of organic materials and nutrients to the bays. While conditions change from year to year and it is recognized there have been long-term changes to loads since 1992, the estimated 93% oceanic fraction remains broadly representative of today's conditions, and is likely roughly applicable to organic materials and nutrients other than total nitrogen.

The smaller non-oceanic sources include rivers, terrestrial runoff other than rivers (referred to as non-point sources), atmospheric deposition, and sewage outfalls (referred to as point sources). Point sources include both the MWRA outfall and non-MWRA outfalls. To help put the MWRA outfall contribution in context, estimates of the non-oceanic sources have been made and compared (Figure 3-4). In 2015 the non-MWRA outfalls contributed most to organic carbon loading, followed by the MWRA outfall, atmospheric deposition, non-point sources and rivers. The MWRA outfall was the largest input to nitrogen loading (ammonium, nitrate, and nitrite), followed by atmospheric deposition, non-MWRA outfalls, non-point sources, and rivers. For phosphorus loading, the MWRA outfall again contributed the largest portion, followed by non-MWRA outfalls, non-point sources, rivers, and atmospheric deposition. Note that for non-MWRA outfalls, use has been made of the only available dataset for conditions across the Massachusetts Bays system (Menzie-Cura and Associates, 1991), for which there are recognized limitations to applicability given that treatment levels at some non-MWRA outfalls have changed since that study.

For the MWRA outfall the annual mean volume flow in 2015 (Figure 3-5) was about 410 million m<sup>3</sup>/yr, substantially lower than the average over the past 10 years, and only slightly higher than the minimum recorded in 2012. The 2015 outfall carbon load was also below the average over the past 10 years. The 2015 nitrogen load was about the same as the average over the past 10 years. The 2015 phosphorous load was comparable to that of the past 5 years and lower than in most years prior to them.

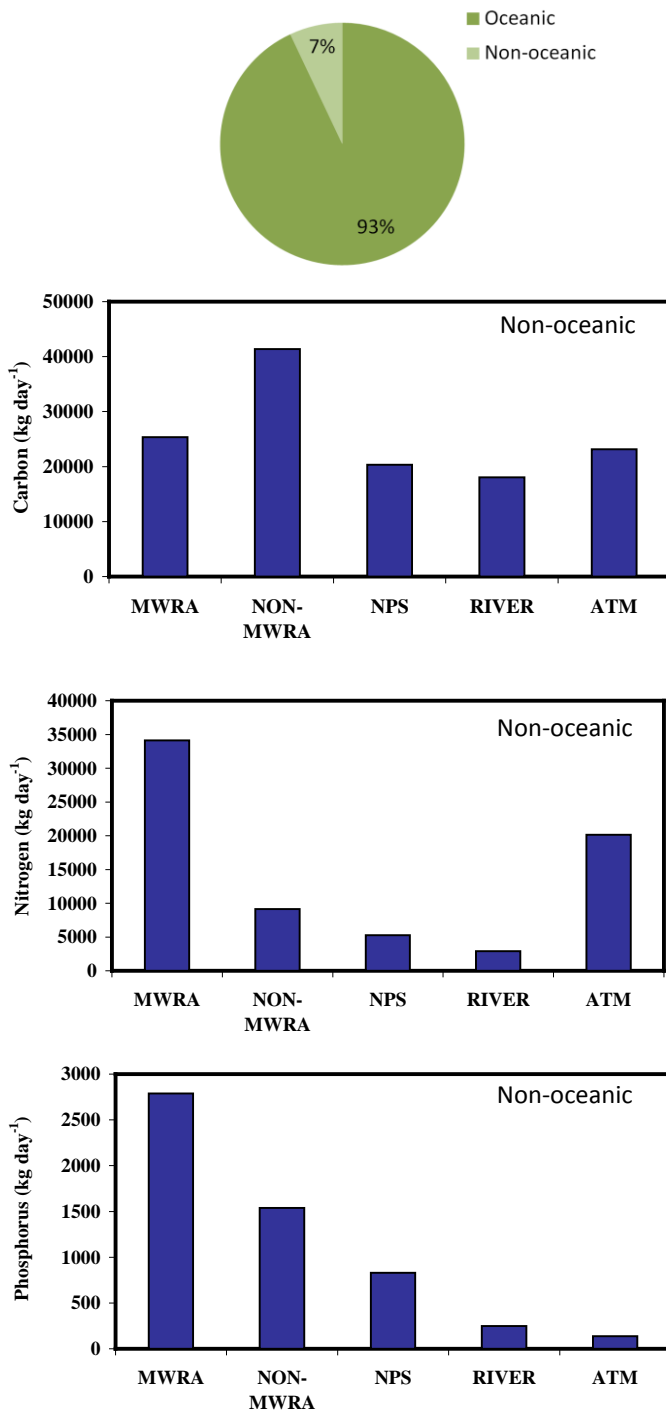


**Figure 3-4.** Mean daily 2015 non-oceanic loads (carbon, nitrogen, phosphorus).

MWRA = MWRA Outfall; NON-MWRA = Non-MWRA point sources; NPS = Non-point sources; RIVER = River loadings. ATM = Atmospheric deposition.

Top pie chart: Representative estimate of oceanic/non-oceanic sources of total nitrogen (see text).

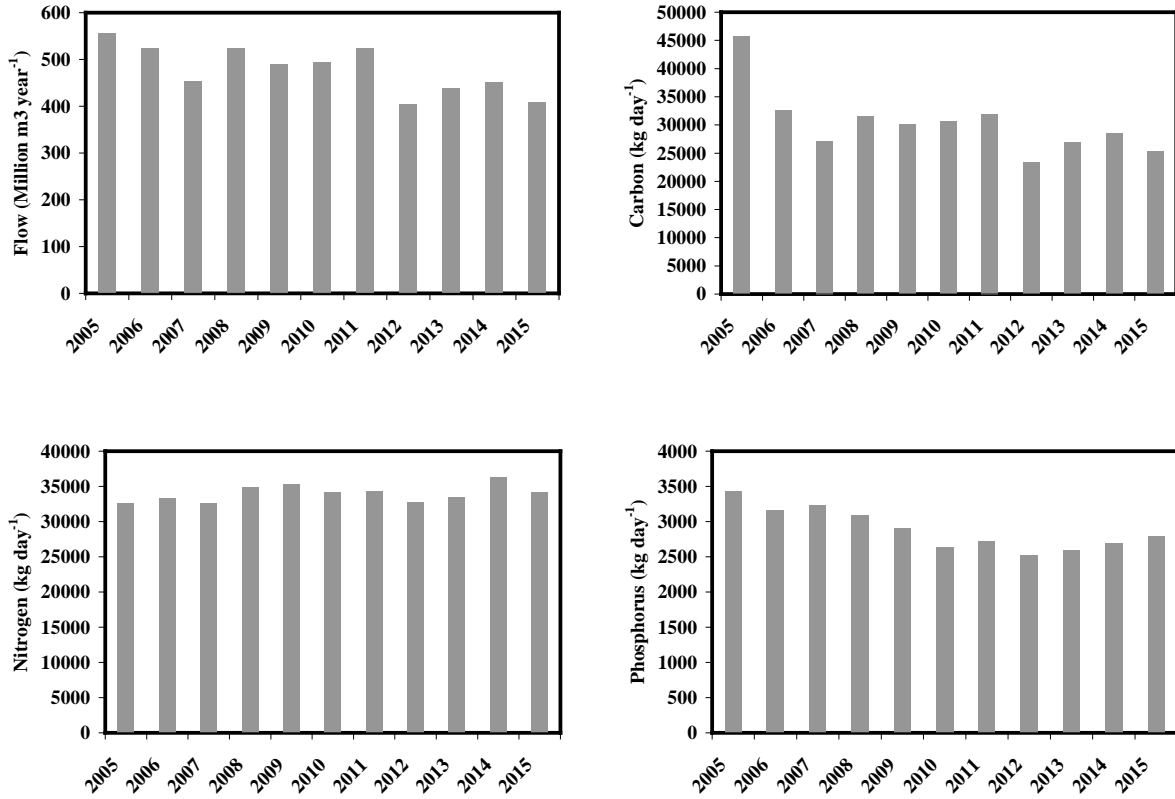


**Figure 3-5.** MWRA outfall mean annual flow and carbon/nitrogen/phosphorous loads, 2005-15.

### **3.3 *Open boundary of the UG-RCA water quality model***

The open boundary condition values for UG-RCA at the offshore edge of its grid domain (red line in upper frame of Figure 2-2) are determined using field survey observations from the MWRA monitoring program in Massachusetts and Cape Cod Bays and the objective analysis method (Tian et al., 2009). These observations are collected during 9 surveys annually, at 14 stations in the two bays. Figure 3-6 shows the representative subset (10 stations; with N and F prefixes) of these 14 stations that is used, for clarity of presentation, below in the water quality section of this report (all 14 stations are shown, for example, in Figure 3-1 on page 10 of Werme et al. 2015). Open boundary condition results for April 15, June 15, August 15, and October 15 illustrate representative seasonal changes (Figure 3-7 and Figure 3-8; colorscale ranges are the same as in earlier reports for ease of comparison). As explained in Zhao et al. (2012), for dissolved organic carbon and biogenic silica (not shown), which are no longer being sampled, a seasonal cycle constructed by averaging observations from 1992-2010 is used. The field observations on which the objective analysis method is based are collected relatively infrequently, and located at large distances from the open boundary, particularly for the South Passage near Cape Cod. It is therefore recognized that, while the method is appropriate and effective, the results include a high degree of uncertainty.

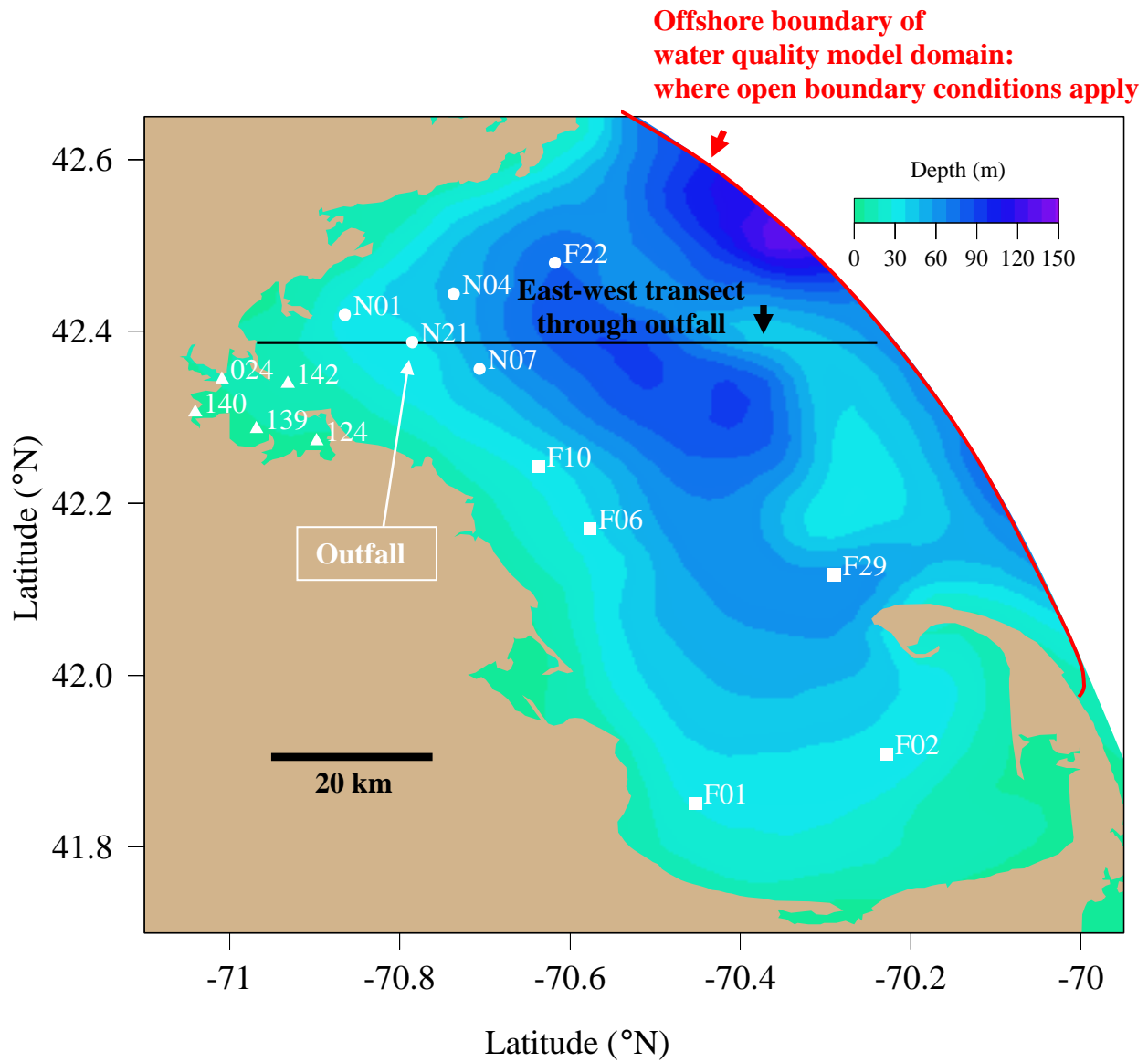


**Figure 3-6.** Station groups: northern (circles), southern (squares), and harbor (triangles).

For reference in later figures:

Red arc = Offshore boundary, water quality model domain, where open boundary conditions apply.

Black line = East-west transect through outfall.

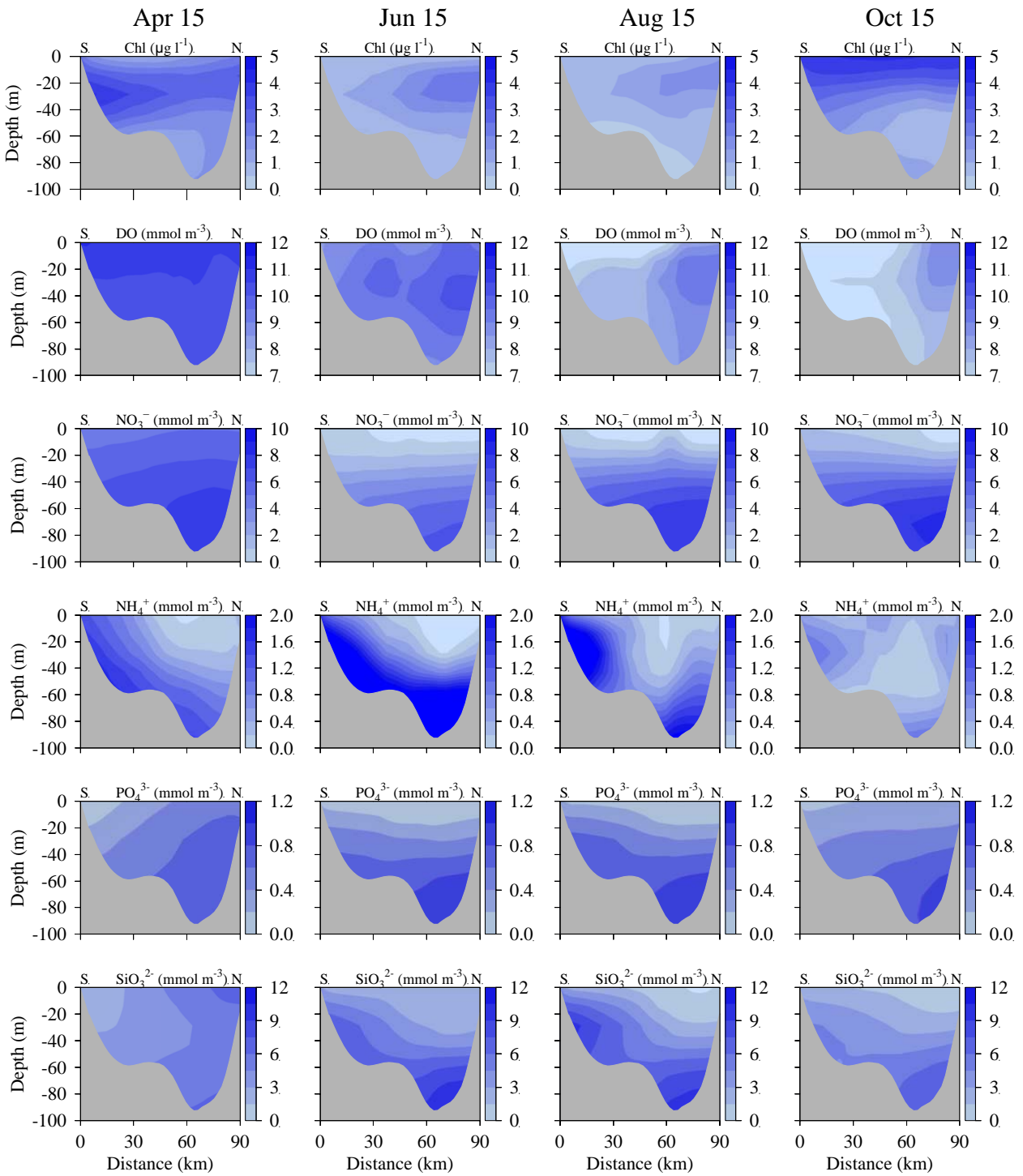


**Figure 3-7.** Open boundary forcing, water quality model: chlorophyll, oxygen, and nutrients.

Horizontal axis: distance along offshore arc (red in Figure 3-6) of open boundary, from its southernmost point; left endpoint (“S”, distance 0 km) is the southernmost end of arc at Cape Cod and right endpoint (“N”, distance 90 km) is the northernmost end of arc off Cape Ann.

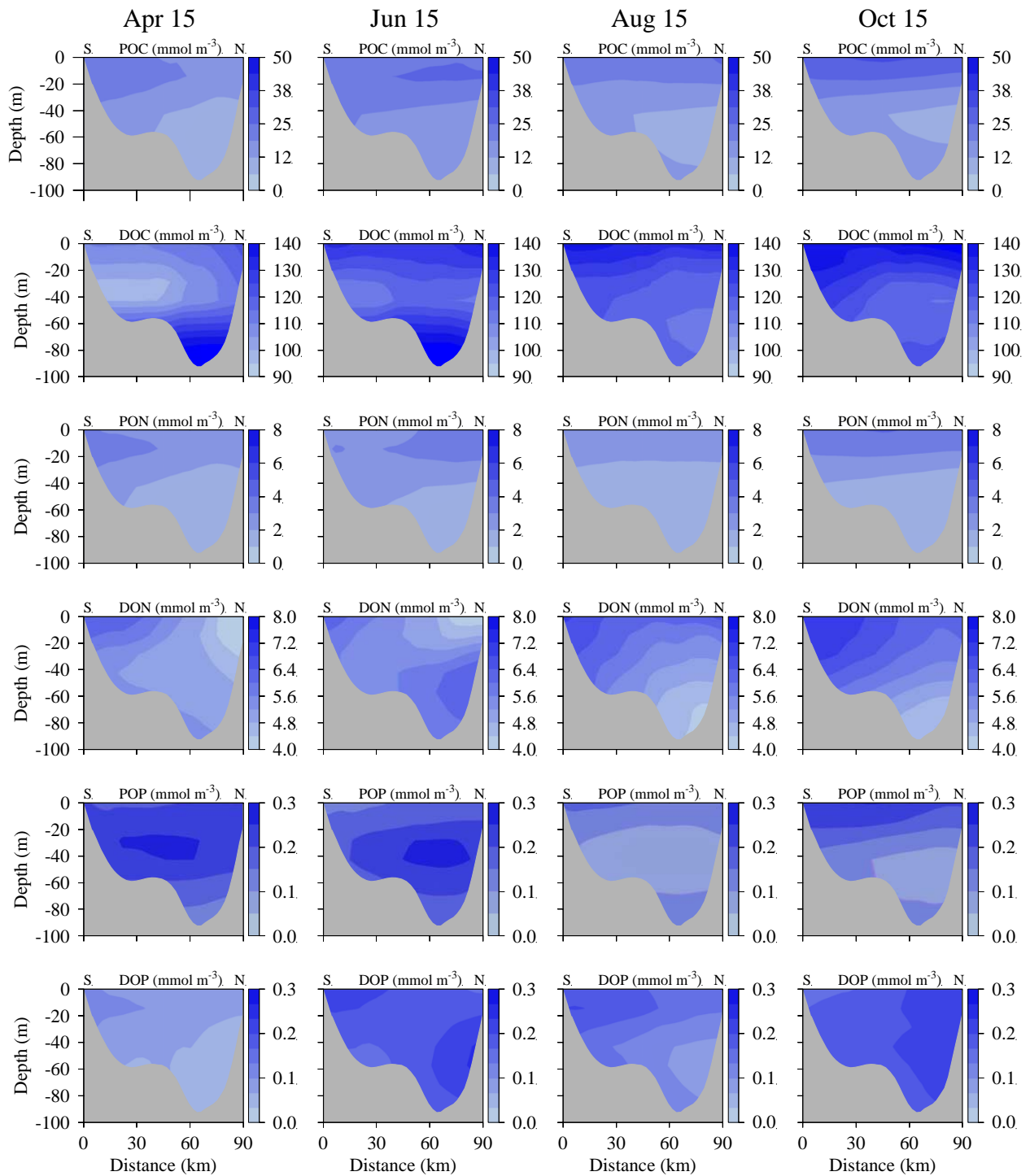


**Figure 3-8.** Open boundary forcing, water quality model: organics. Presented as in Figure 3-7.

POC = Particulate Organic Carbon, DOC = Dissolved Organic Carbon

PON = Particulate Organic Nitrogen, DON = Dissolved Organic Nitrogen

POP = Particulate Organic Phosphorus, DOP = Dissolved Organic Phosphorus

## 4. Hydrodynamics

The focus of BEM is water quality, which is strongly influenced by physical processes such as the evolution of temperature and salinity patterns and water circulation. The fidelity of the UG-RCA water quality simulations therefore depends on the capability of the MB-FVCOM hydrodynamic model to capture realistic physical processes of the bays. This section describes the hydrodynamic model characteristics and performance.

### 4.1 *Model-observation comparisons*

Comparisons between the model results and observations from 2015 make clear the level of agreement between them for the time evolution of the geographic and vertical structure of temperature (Figure 4-1) and salinity (Figure 4-2). Salinity is given in units on the Practical Salinity Scale throughout this report. Stations in these figures include locations spanning Massachusetts Bay (N01, F22, N07, F06), in and near Cape Cod Bay (F01, F02, F29), and at the mouth of Boston Harbor (F23; Figure 5-5 shows the location of F23, 1 km west of station 142 which is shown in Figure 3-6). Vessel-based observations from 9 survey dates in 2015 are shown as individual symbols, from both shallow (near-surface, less than 5m deep) and deep (near-bottom, within 5 m of seafloor) depths, at each station in Figure 4-1 and Figure 4-2. In addition, in the panels for Station F22, time series observations are shown from Mooring A01 (located about 5 km northeast of F22 and operated by University of Maine as part of the Northeast Regional Association of Coastal and Ocean Observing Systems) at 1m and 51 m deep. The model generally captured the seasonal cycle, and most event-timescale characteristics, of observed temperature and salinity. This indicates the effectiveness of data assimilation of both satellite sea surface temperature and *in situ* hydrographic measurements. Stratification developed in April, peaked between late July and early September, and was eliminated during October or November depending on the station. For temperatures the most notable model-observation differences were model temperatures not cold enough to match observations in February at some stations (F23, F01, F02), and the tendency for deep temperatures to be warmer than observed by up to several degrees except within a few days of observation dates, when the model values are reduced to nearer the observed values by data assimilation as expected. For salinities the most notable model-observation differences were model salinities fresher than observed during events in April and May at N01, and the tendency for deep salinities to be higher

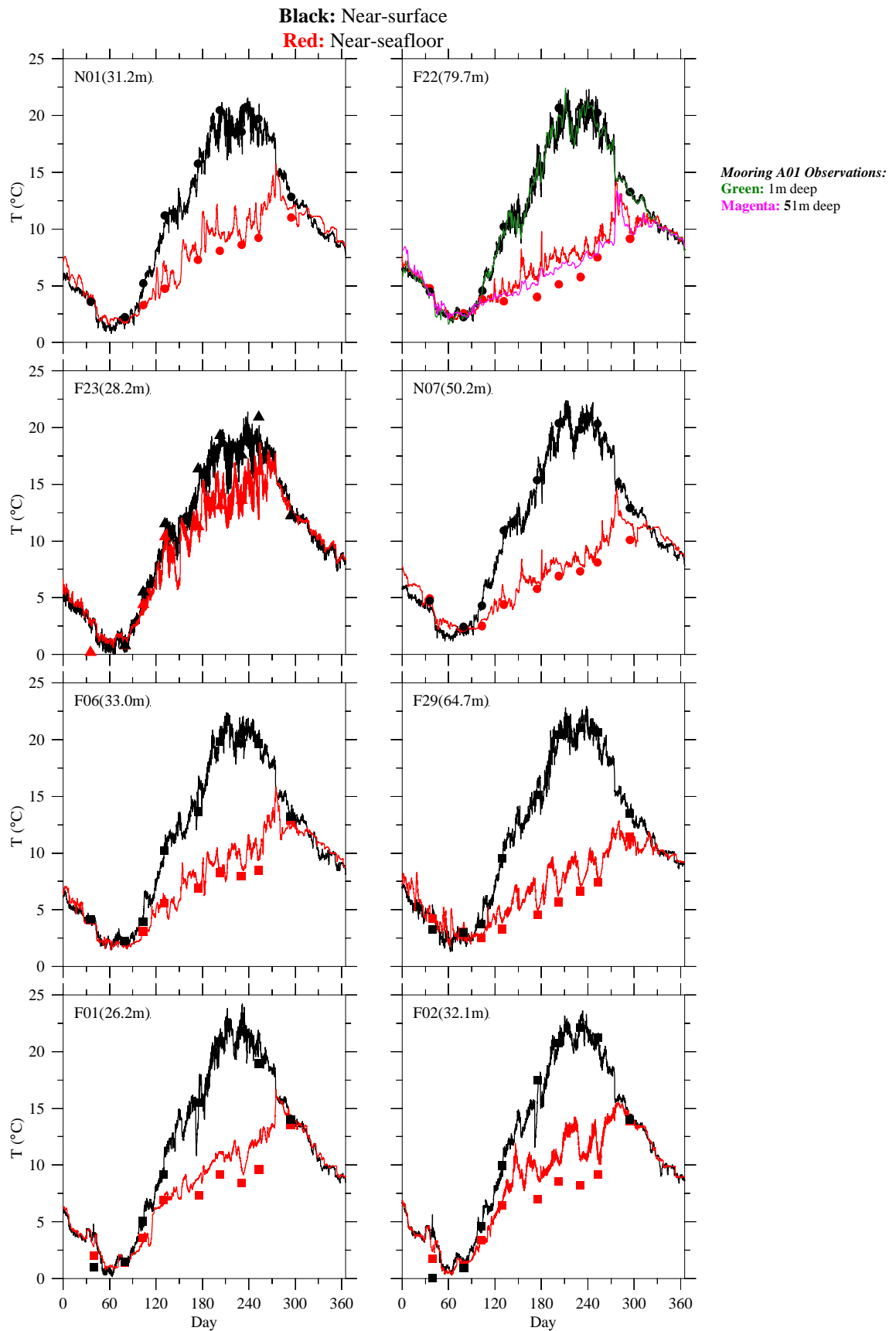


**Figure 4-1.** Temperature time series, model-observation comparison.

Model results: black/red lines. MWRA vessel-based survey observations: black/red symbols. Value in parentheses (after each station name) is the bathymetric depth of the station location.

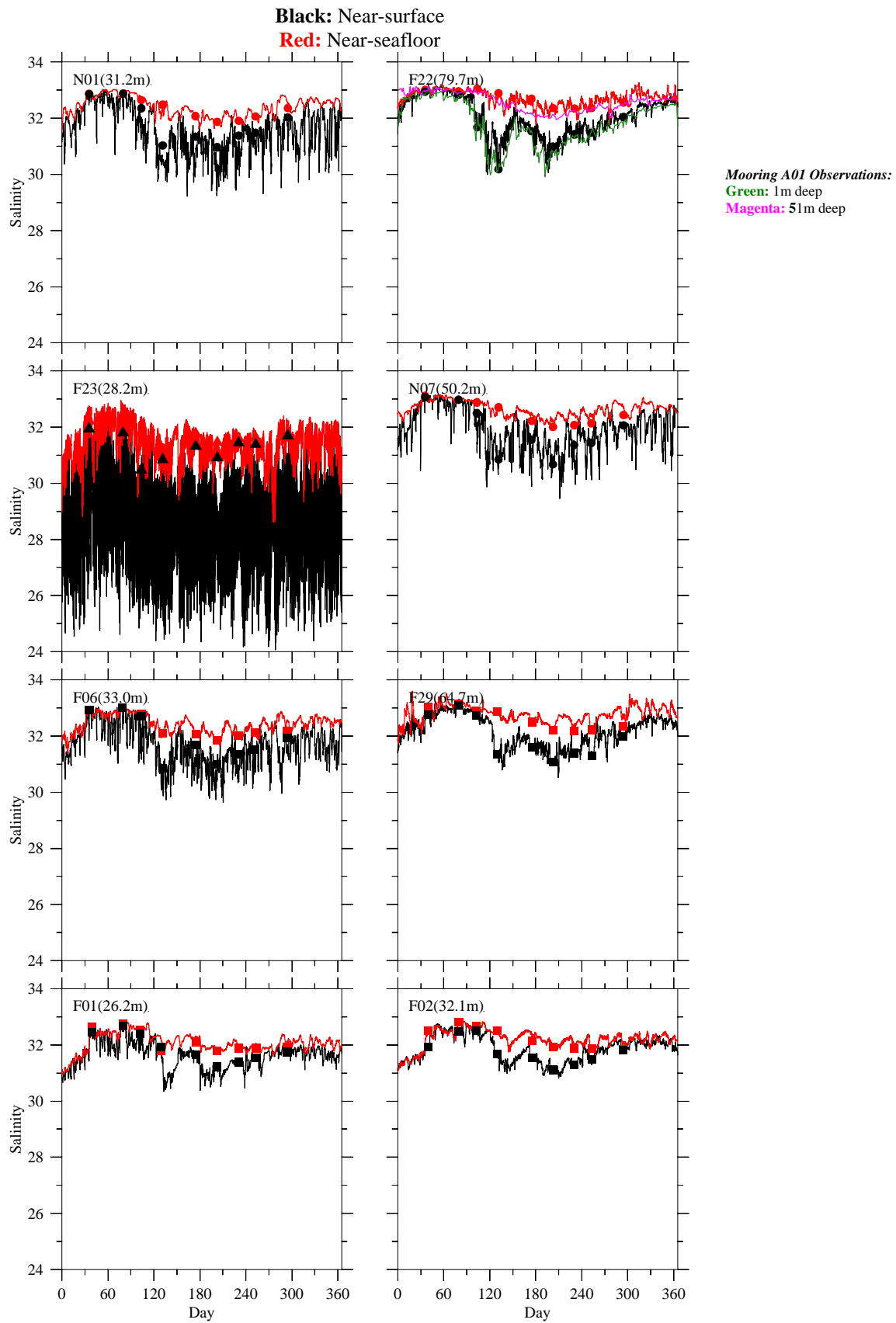


**Figure 4-2.** Salinity time series, model-observation comparison.

Shown as in Figure 4-1. Salinity units: Practical Salinity Scale.

than observed by as much as 0.5, at some stations (F22, F06, N07, F29) after the first few months of the year. This latter difference was reduced by the data assimilation, as expected, within a few days of the dates of observations.

For more complete spatial information, model-observation comparisons have been made of the monthly-mean geographic structure, during a series of months spanning the seasonal cycle, of near-surface and near-bottom temperature (Figure 4-3a,b) and salinity (Figure 4-4a,b). The observed fields in these figures are computed using measurements from all stations (black dots) sampled during each month-long period. For most months there was a one-day survey in Massachusetts Bay and Cape Cod Bay, and Boston Harbor stations were sampled weekly or biweekly (for more detail on harbor station locations see, e.g., Taylor, 2015). The model fields in these figures are computed using the subset of model outputs from the dates and locations corresponding to the associated set of observations. (Consequently they are not expected to match exactly the monthly-means of all modeled times, which are shown in Figure 4-6 and Figure 4-7 below.)

The seasonal cycle and general spatial structure of the model fields is in reasonably good agreement with the observations. The most notable model-observation differences for shallow temperatures (Figure 4-3a) were that model results were typically more spatially uniform than the observations; relative to observations the model results were also notably warmer in June and October. For deep temperatures (Figure 4-3b) the agreement was better, with the most notable differences being a different spatial structure in June and higher temperatures in October. The model shallow salinities (Figure 4-4a) have less spatial structure during April, and are notably fresher during August and October, compared to observations. The model deep salinities (Figure 4-4b) were not as spatially uniform as observations during April and June. The model captured the general spatial pattern of onshore freshening throughout the year.

Comparisons between modeled and observed 2015 non-tidal currents are shown in Figure 4-5a,b at the Mooring A01 site in northeastern Massachusetts Bay off Cape Ann, the only location where time series observations are available. (Tidal currents, while important in controlling vertical mixing and dispersal of materials, are not examined in this report. Tidal currents in these simulations are very similar to tidal currents in other similarly-configured FVCOM simulations spanning the Gulf of Maine, and have been shown—e.g., see Appendix of Chen et al., 2011—to be in very good agreement with observed tidal currents.) The model-observation comparisons of non-tidal currents include time variations and vertical structure, with wind forcing included for context.

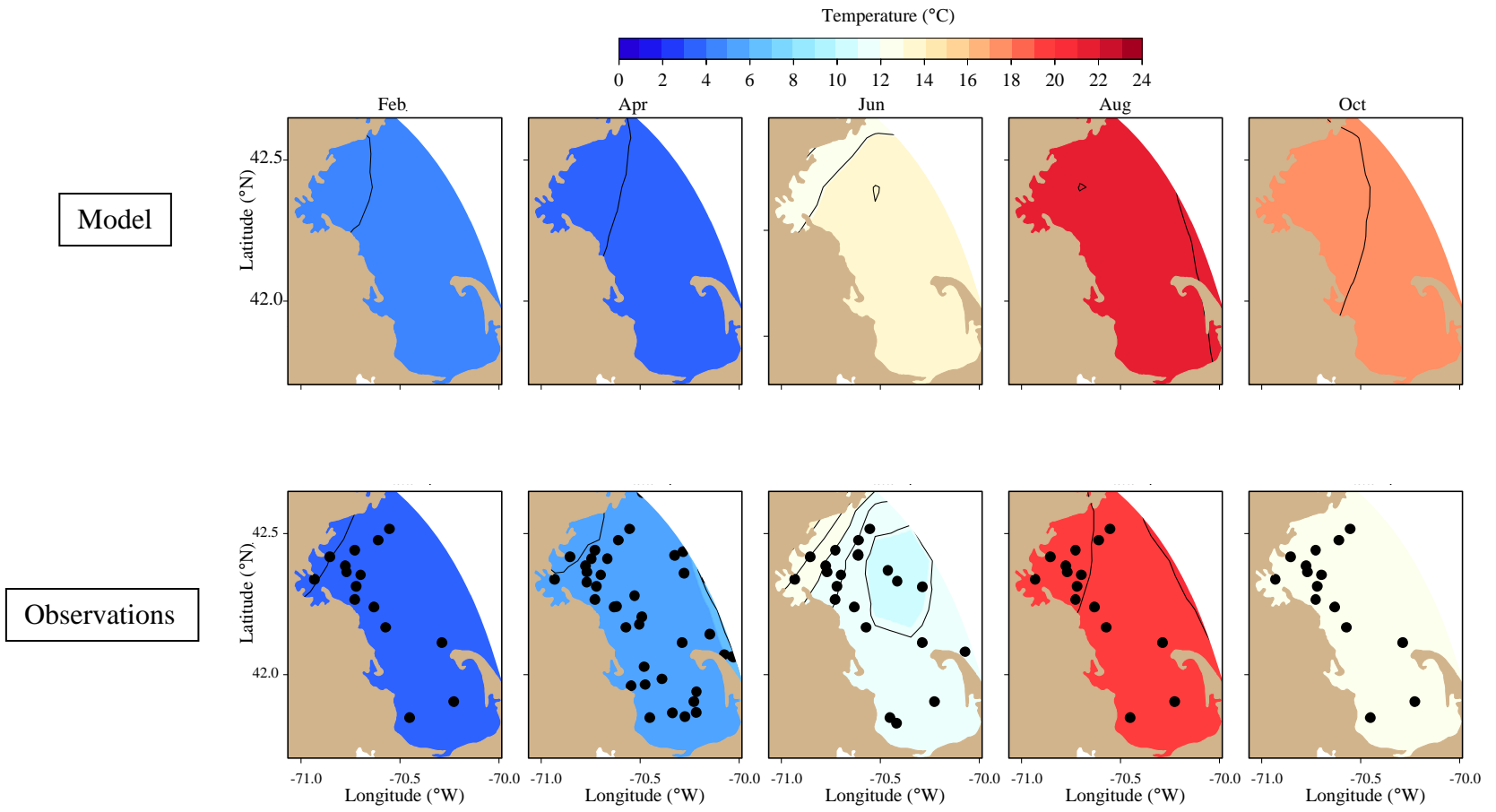


**Figure 4-3a.** Temperature spatial structure, at/near sea surface, model-observation comparison.

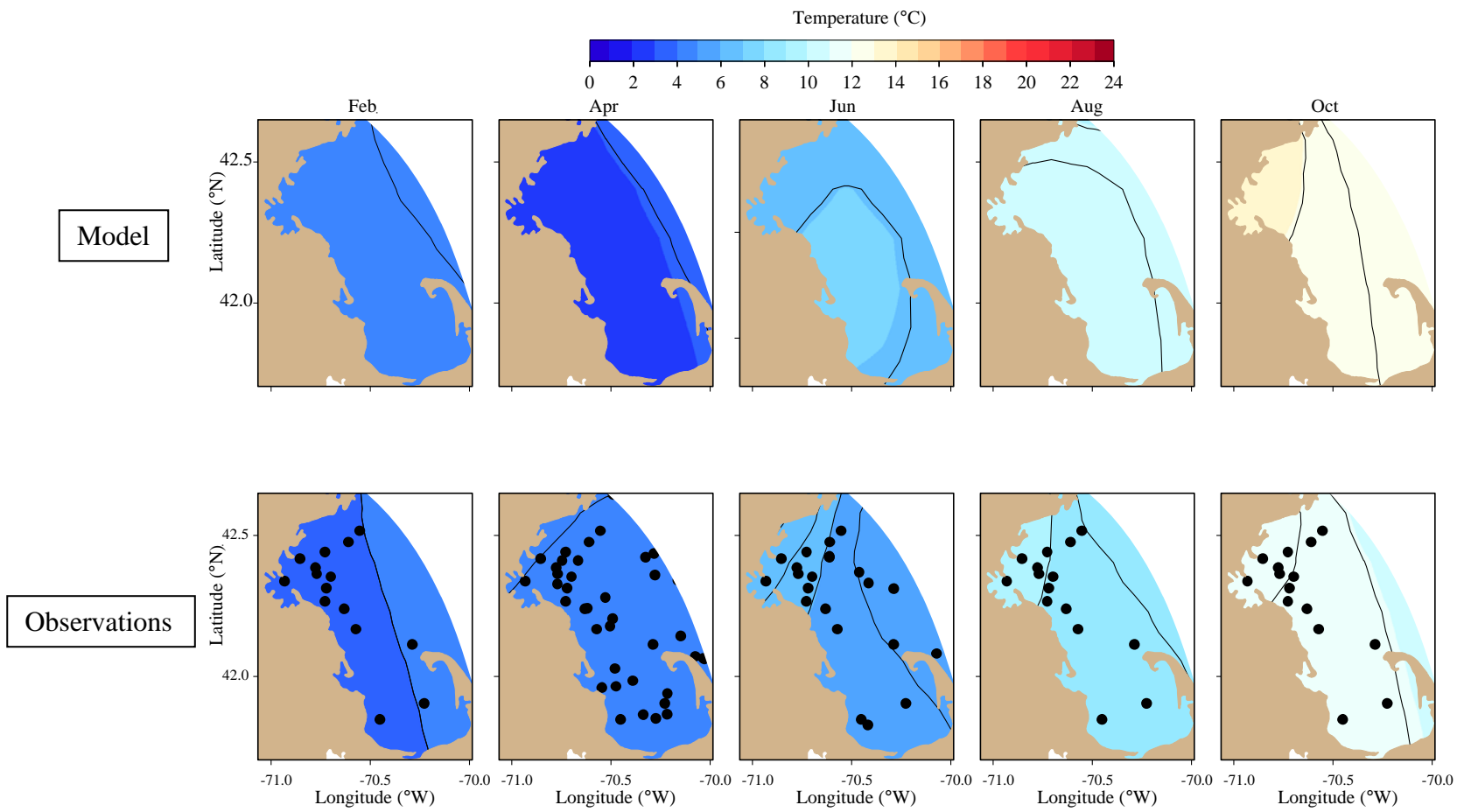


**Figure 4-3b.** Temperature spatial structure, at/near seafloor, model-observation comparison.

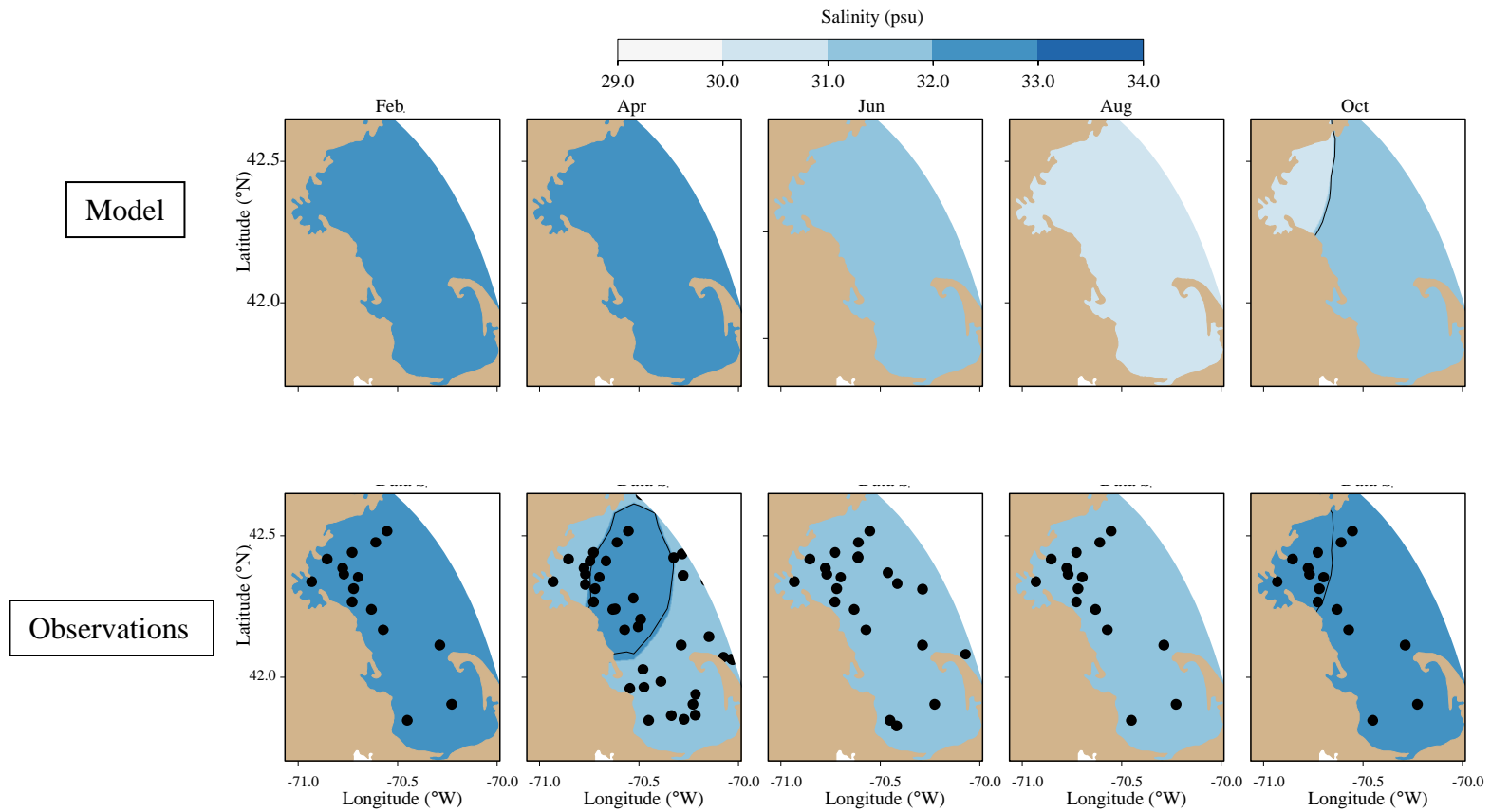


**Figure 4-4a.** Salinity spatial structure, at/near sea surface, model-observation comparison.

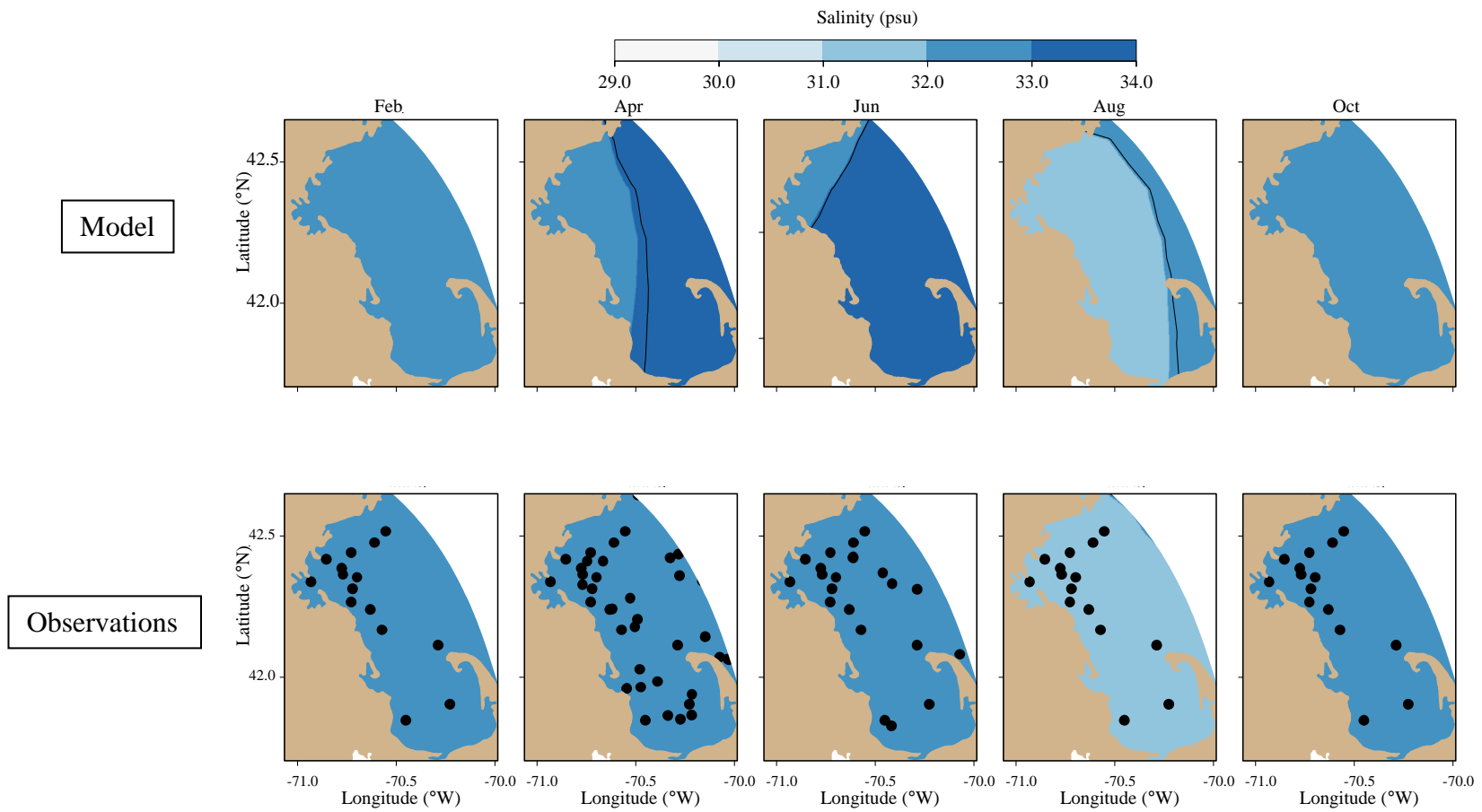


**Figure 4-4b.** Salinity spatial structure, at/near seafloor, model-observation comparison.

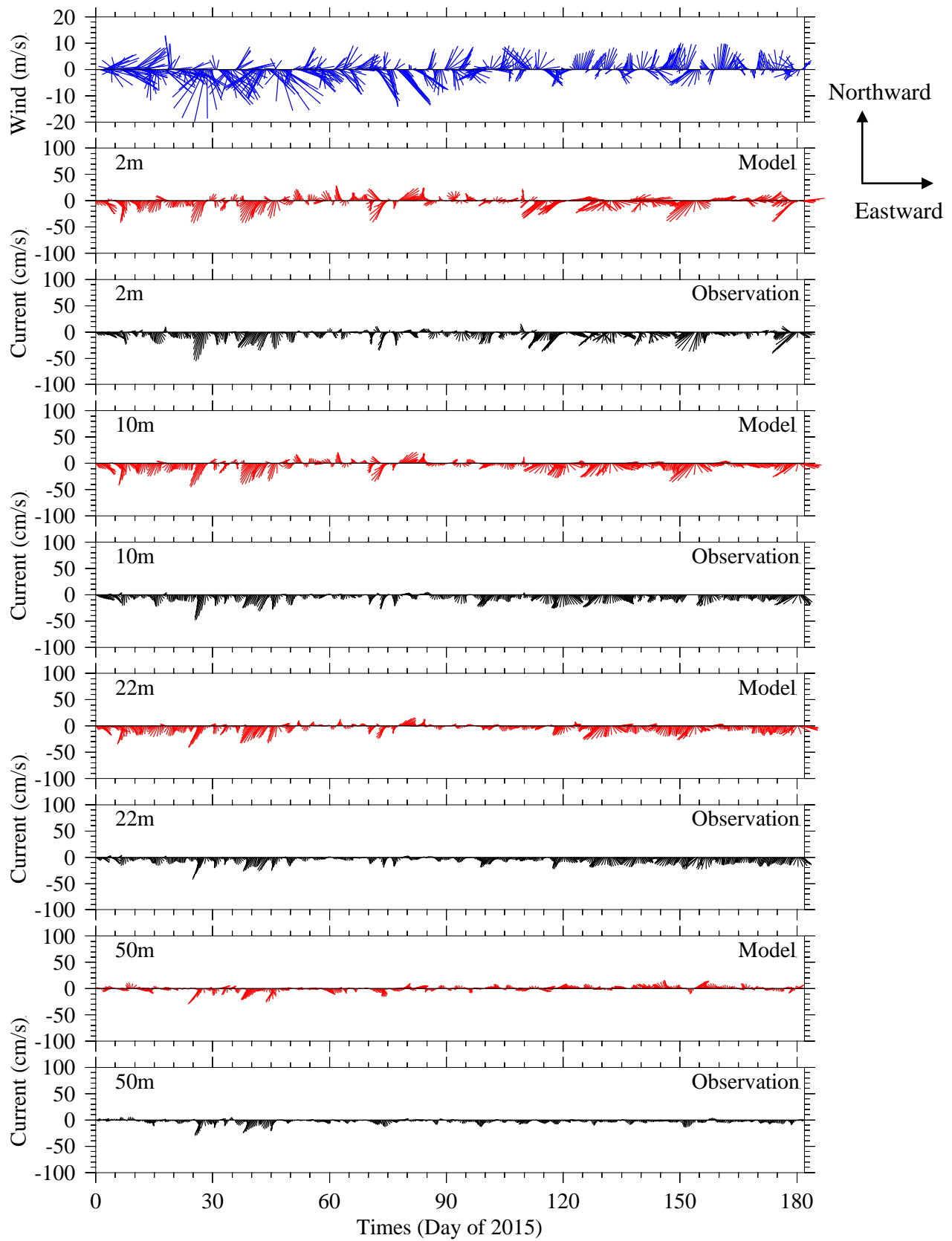


**Figure 4-5a.** Currents time series model-observation comparison, Jan – Jun. Winds top frame. Sticks point in the direction of flow, away from zero line; north/eastward flow up/rightward.

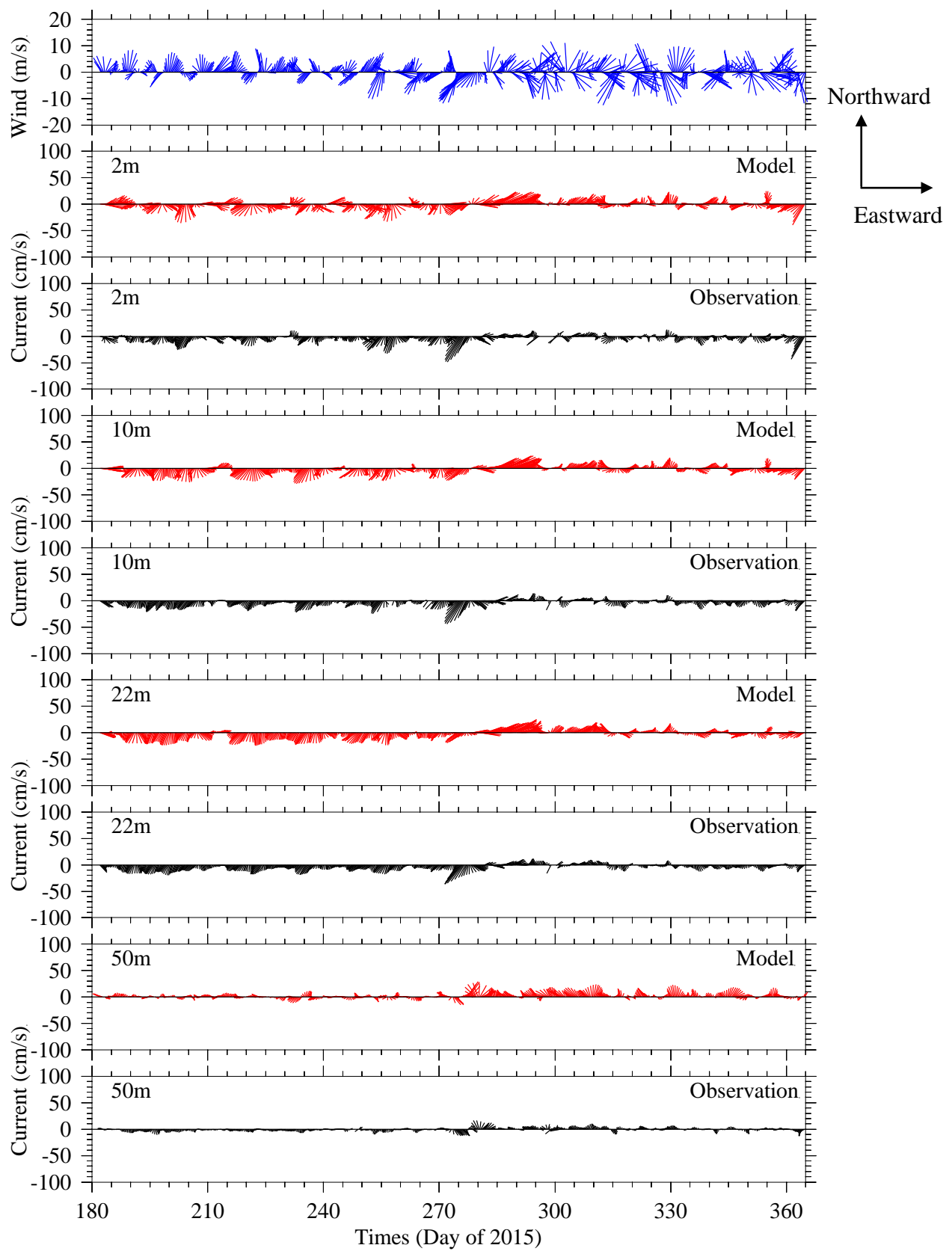


**Figure 4-5b.** Currents time series model-observation comparison, Jul - Dec.

In order to isolate the non-tidal variability of interest, consisting mainly of weather-related and seasonal changes, the tidal variability has been removed using a low-pass filter (38-hr half-power period, PL66TN; e.g., Limeburner 1985) and the results subsampled to 6 hour resolution.

As expected, the main features of the winds (from the WRF model) are weather-band changes on timescales of about 3-10 days. These features include: wind directions spanning the full compass range; generally weaker magnitudes in the summer; and a tendency for longer-term (monthly or longer) average winds to be weaker than weather-band changes, and directed towards the east year round, southward in winter, and northward in summer.

Observed currents are generally toward the south and west at this location (see Figure 1-1) and the model adequately captures this feature. The most prominent model-observation difference is that the model currents tend to have slightly larger magnitudes than observed. Most of the individual storm events seen in the observed currents occur in the model currents, and for most events the timing and direction of the flow is similar in the model and observations. These detailed comparisons of the time variations and vertical structure of currents in the model to direct observations at a particular site form a challenging test of the hydrodynamic simulation performance. Agreement is sufficient to conclude that the hydrodynamic model represents observed processes adequately to support the water quality modeling.

## **4.2 *Model monthly-mean temperature, salinity, and circulation***

Based on the above comparisons having demonstrated a level of agreement between the 2015 simulation and available observations, this subsection presents a more complete view of the monthly-averaged simulation temperature, salinity, and circulation throughout the year.

Model temperatures followed the expected seasonal cycle (Figure 4-6a,b) with peak values in summer and early fall and minima in late winter. Horizontal gradients are notable, with inshore temperatures generally colder during winter and spring and warmer during summer and fall. From about April/May to October/November the surface temperatures (Figure 4-6a) are markedly higher than bottom temperatures (Figure 4-6b). Model salinities (Figure 4-7a,b) have a weaker seasonal cycle than temperature, particularly at depth. Water near the coastlines is generally fresher year-round, both at the surface (Figure 4-7a) and the seafloor (Figure 4-7b). At the surface, from April to June the offshore extent of relatively fresh water increased, first in the southern Gulf of Maine and then in Massachusetts Bay, where it then decreased from July to September.

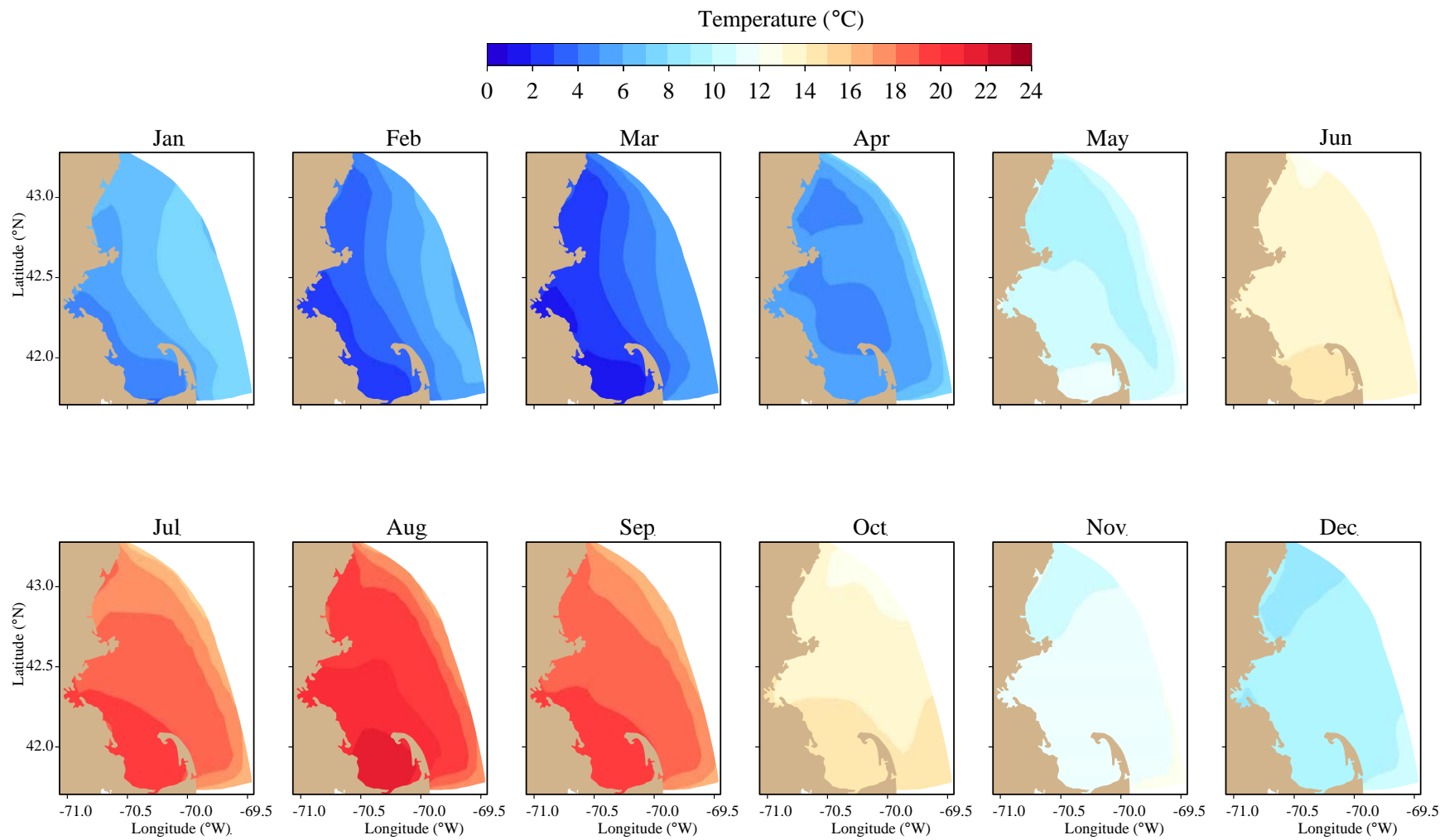


**Figure 4-6a.** Model temperature, monthly-mean spatial structure, at sea surface.

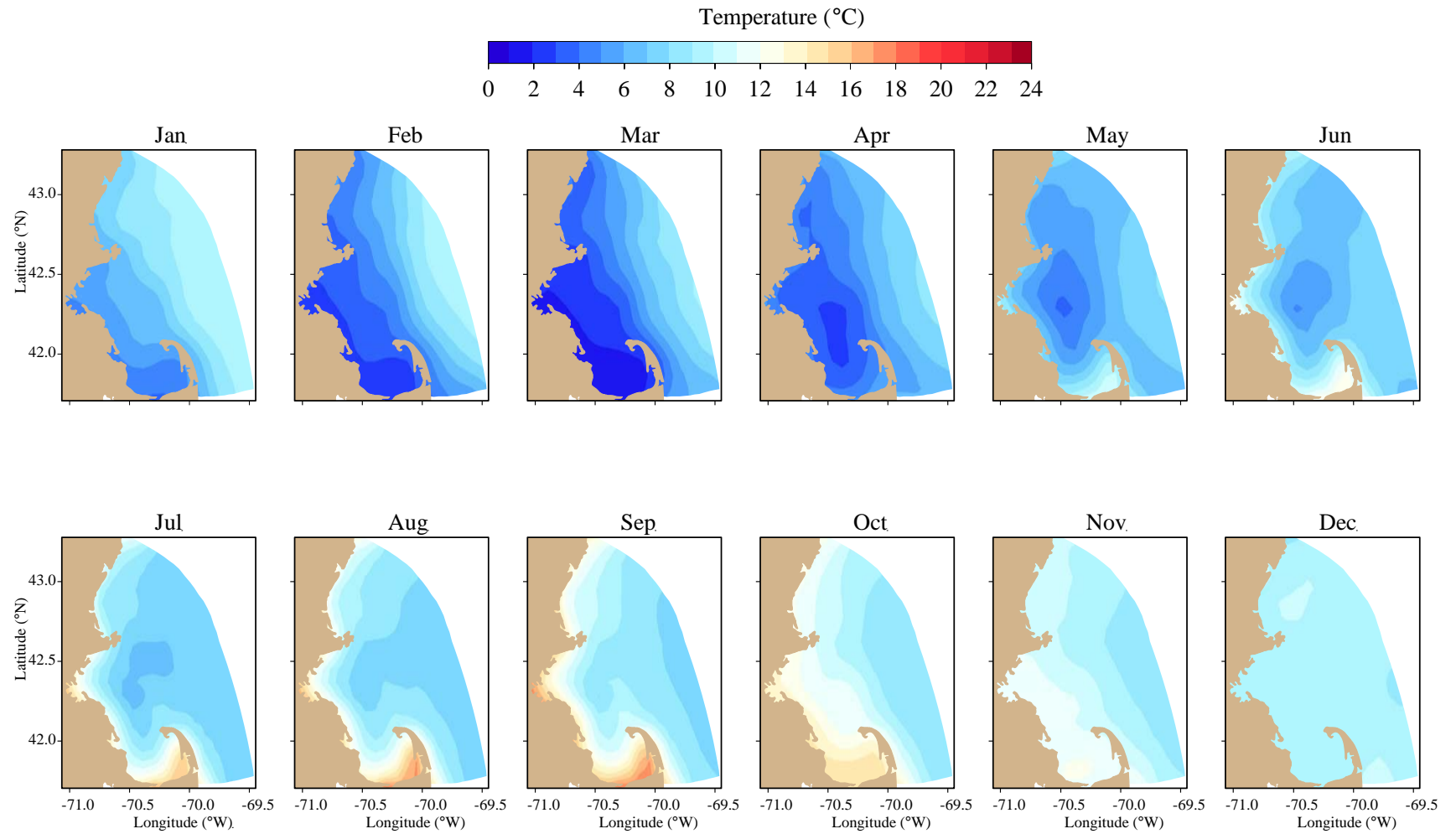


**Figure 4-6b.** Model temperature, monthly-mean spatial structure, at seafloor.

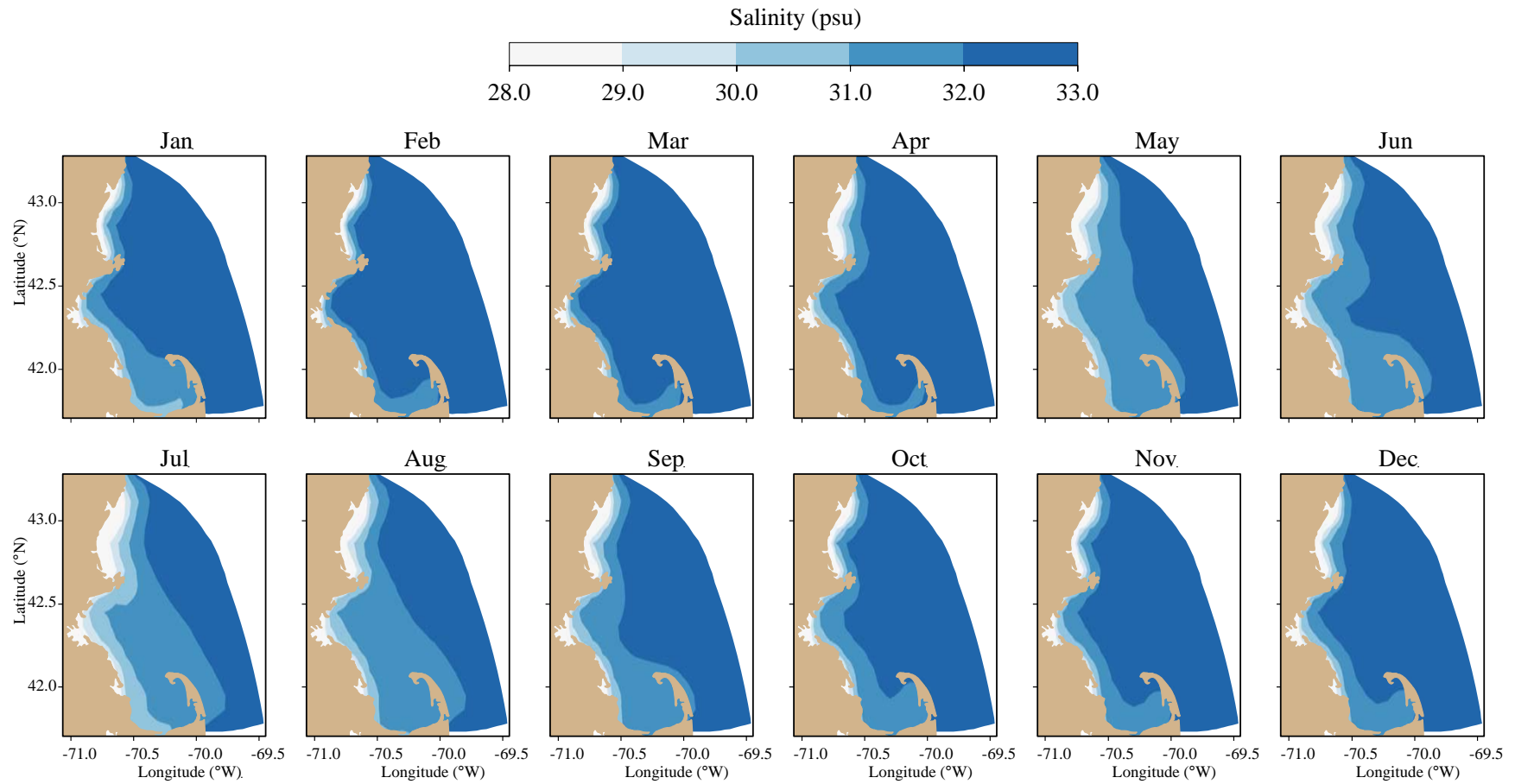


**Figure 4-7a.** Model salinity, monthly-mean spatial structure, at sea surface.

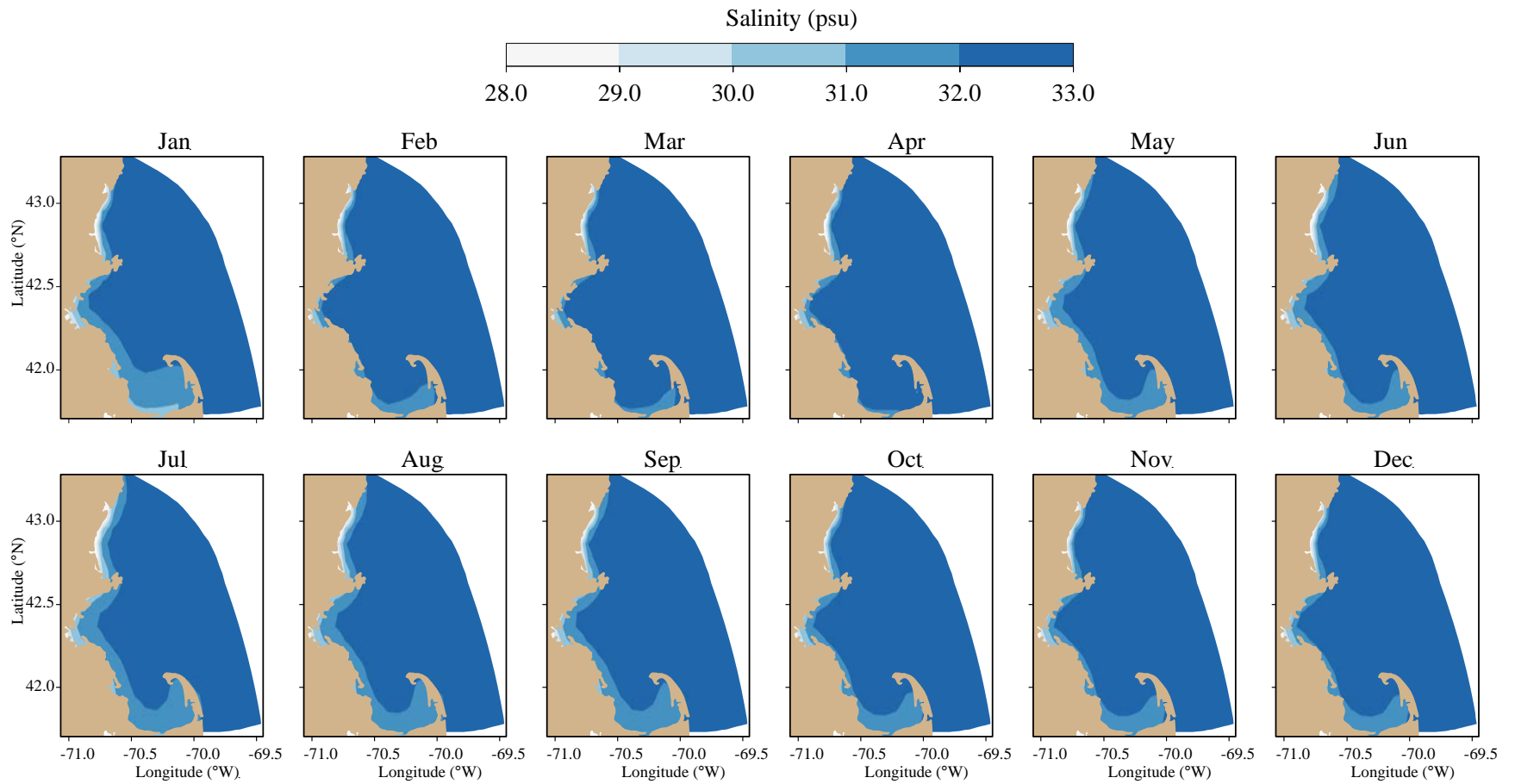


**Figure 4-7b.** Model salinity, monthly-mean spatial structure, at seafloor.

The temporal progression of the geographic pattern of 2015 monthly-mean currents at the surface (Figure 4-8a) and at 15 m deep (Figure 4-8b) is consistent with the schematic in Figure 1-1 and characterized by the following main features. At the surface (Figure 4-8a), in January and October-December currents within the bays were generally weak. Southward flow within about 10-20 km of the western coast of Massachusetts and Cape Cod Bays was strongest in January and February, reaching about  $20 \text{ cm s}^{-1}$ , associated with the unusually strong winds discussed above (Section 3.1). Flow into Massachusetts Bay south of Cape Ann was strongest in April. From May through October a counterclockwise flow occupied Massachusetts Bay with water moving eastward just north of the northern tip of Cape Cod. For most of the year currents were strongest, reaching up to  $30\text{-}40 \text{ cm s}^{-1}$ , along the area offshore extending from Cape Ann to Cape Cod, having originated in the Western Maine Coastal Current north of Cape Ann.

At 15 m deep (Figure 4-8b) the flow patterns are generally similar to the surface, with the main difference being that currents are generally not stronger than about  $10\text{-}15 \text{ cm/s}$ , and are thus substantially weaker than currents at the surface. At this depth, the flow into Massachusetts Bay south of Cape Ann occurred throughout most of the summer months.

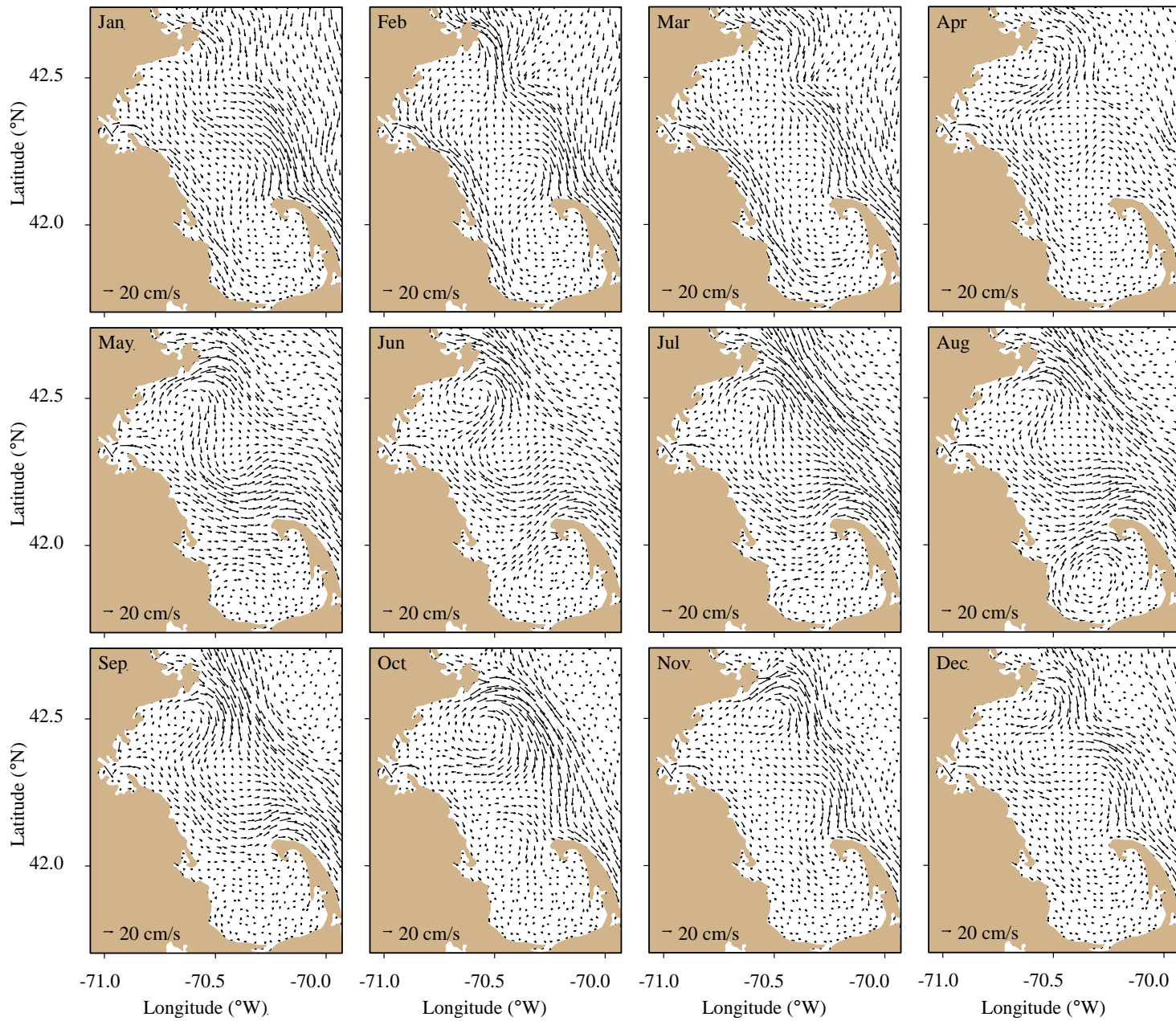


**Figure 4-8a.** Model currents, monthly-mean spatial structure, at sea surface.

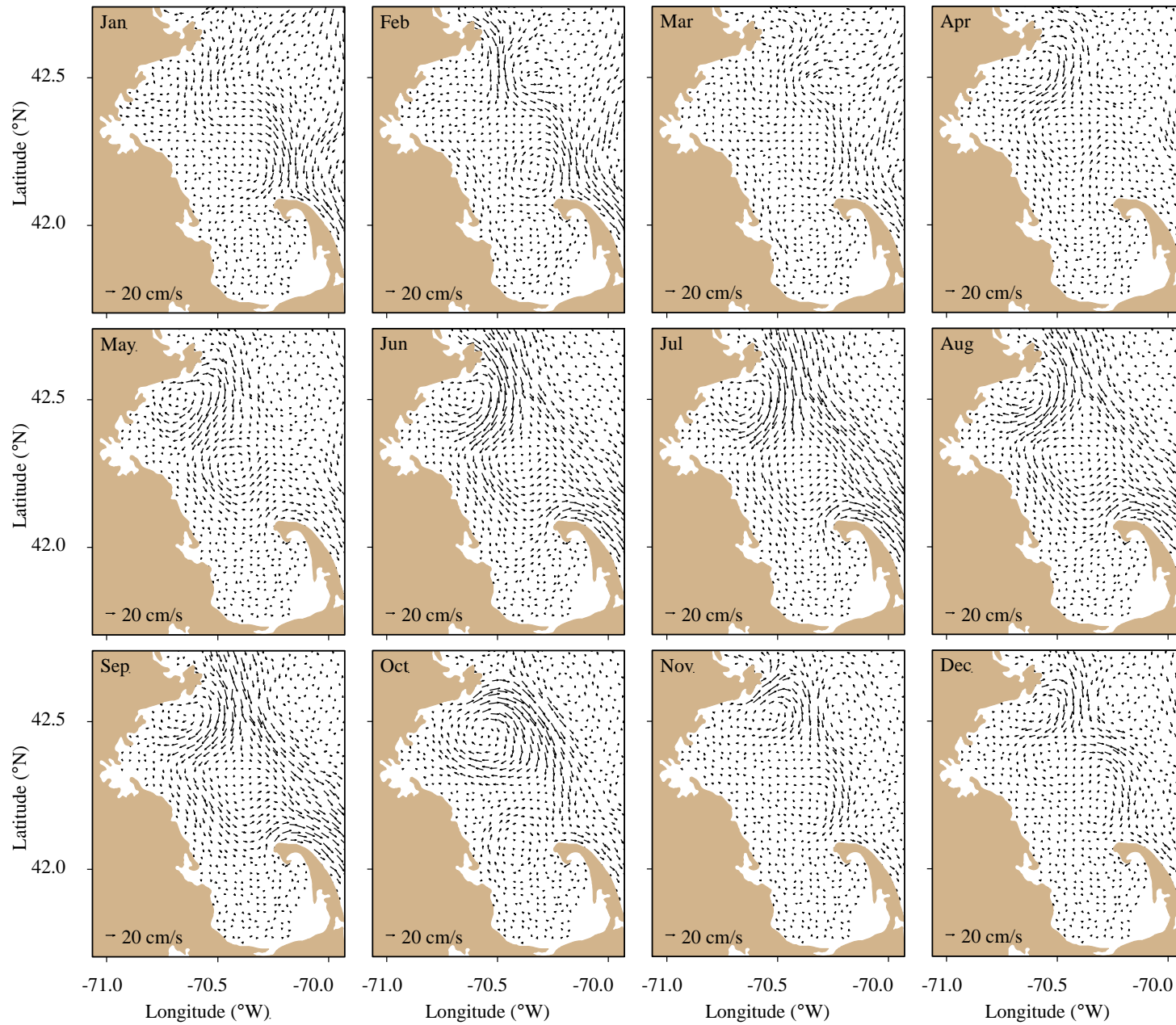


**Figure 4-8b.** Model currents, monthly-mean spatial structure, 15 m deep

## 5. Water quality

Model-observation correlation and regression analyses of key water quality variables from the 2015 simulation are presented in Figure 5-1, including surface chlorophyll, surface inorganic nutrients (nitrate  $\text{NO}_3^-$ , ammonium  $\text{NH}_4^+$ , and silicate  $\text{SiO}_3^{2-}$ ), bottom dissolved oxygen (DO) concentration ( $\text{mg L}^{-1}$ ) and DO saturation (%). These comparisons use observations from all Massachusetts Bay and Cape Cod Bay sites sampled by MWRA during 2015, comprising a total of 14 stations (see, for example, Figure 3-1 on page 8 of Werme et al. 2016). (For clarity of presentation, as noted above, figures in the remainder of this section use a subset of 10 such stations, as shown in Figure 3-6.) In 2015 there was no meaningful correlation for near-surface chlorophyll, silicate, or ammonium. The model significantly underestimated chlorophyll when its concentration was higher than about  $2 \mu\text{g L}^{-1}$ . For surface  $\text{NO}_3^-$  the correlation of 0.92 is comparable to values near 0.9 in past years. For DO concentration the correlation coefficient is 0.94. The DO saturation was not directly modeled, rather it was calculated based on temperature, salinity and DO concentration using the approximate relation given in equation 2.3 of Zhao et al. (2012); biases in the simulation for these parameters could be factors that contribute to the lower correlation coefficient for DO percent saturation than for DO concentration.

The remainder of this section describes the 2015 annual progressions of a representative set of water quality model variables from representative locations. Individual figures generally show results of model-observation comparisons for stations from one of the three groups in Figure 3-6 (northern, southern, and harbor), or monthly-mean model output along an east-west transect (shown in Figure 3-6) that originates at the coast, passes through the outfall site, and extends offshore across the Stellwagen Basin depression and the shoaling Stellwagen Bank.

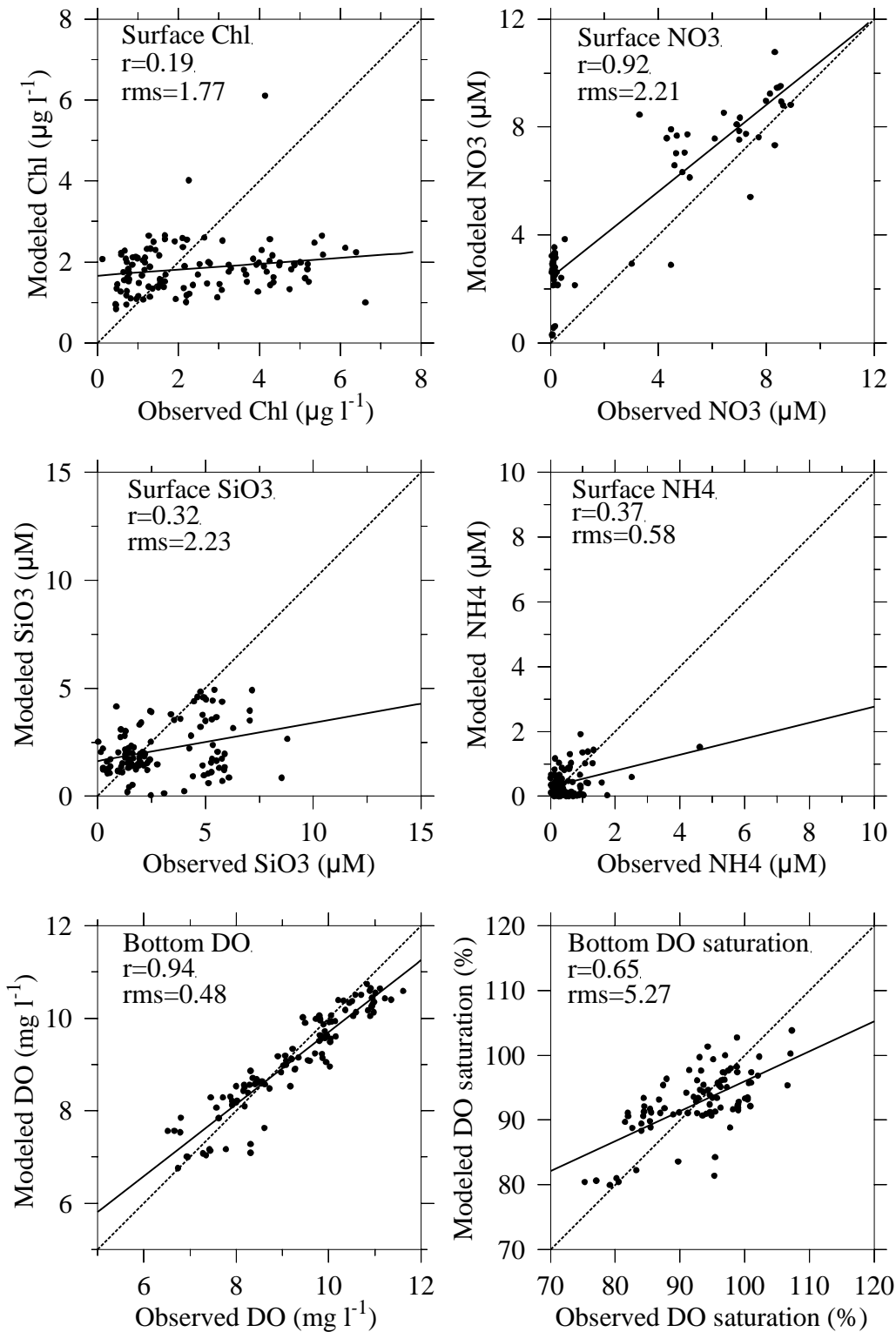


**Figure 5-1.** Model-observation correlations/regressions for key water quality parameters.

All stations outside Boston Harbor; regressions are solid lines, dashed lines indicate equality between observed and modeled results.

## 5.1 *Light*

For light, model-observation comparisons use extinction coefficients for attenuation of photosynthetically active radiation (PAR) in the water column, as described in Section 2.2 of Zhao et al. 2016. At stations in the northern group (Figure 5-2a) and southern group (Figure 5-2b) spanning Massachusetts Bay and Cape Cod Bay, the model extinction coefficient results include annual-average values that differ modestly from site to site. Temporal variations during the year are minor, and the late-spring peak associated with chlorophyll self-shading (Hydroqual, 2001) typical in other years (e.g., see Zhao et al., 2016) is modest or absent, consistent with the lack of an observed 2015 spring phytoplankton bloom. At all stations the range of temporal variability in the model is much lower than that in the observations. The modeled values are generally within the range of observations and model-observation bias is generally not pronounced.

The extinction coefficient results for the harbor group of stations (Figure 5-2c) are similar to those in the bays, with respect to site-to-site variations in the model being modest, and annual-average levels generally consistent with the observations. As expected, extinction is much more rapid in the harbor than in the bay. At sites in the harbor (station 140, and to a lesser extent station 124) where the temporal variability of observations is more pronounced, this leads to larger model-observation differences. At the other sites (024, 142, 139) there is evidence of modest positive bias in the model extinction coefficient relative to the observations.

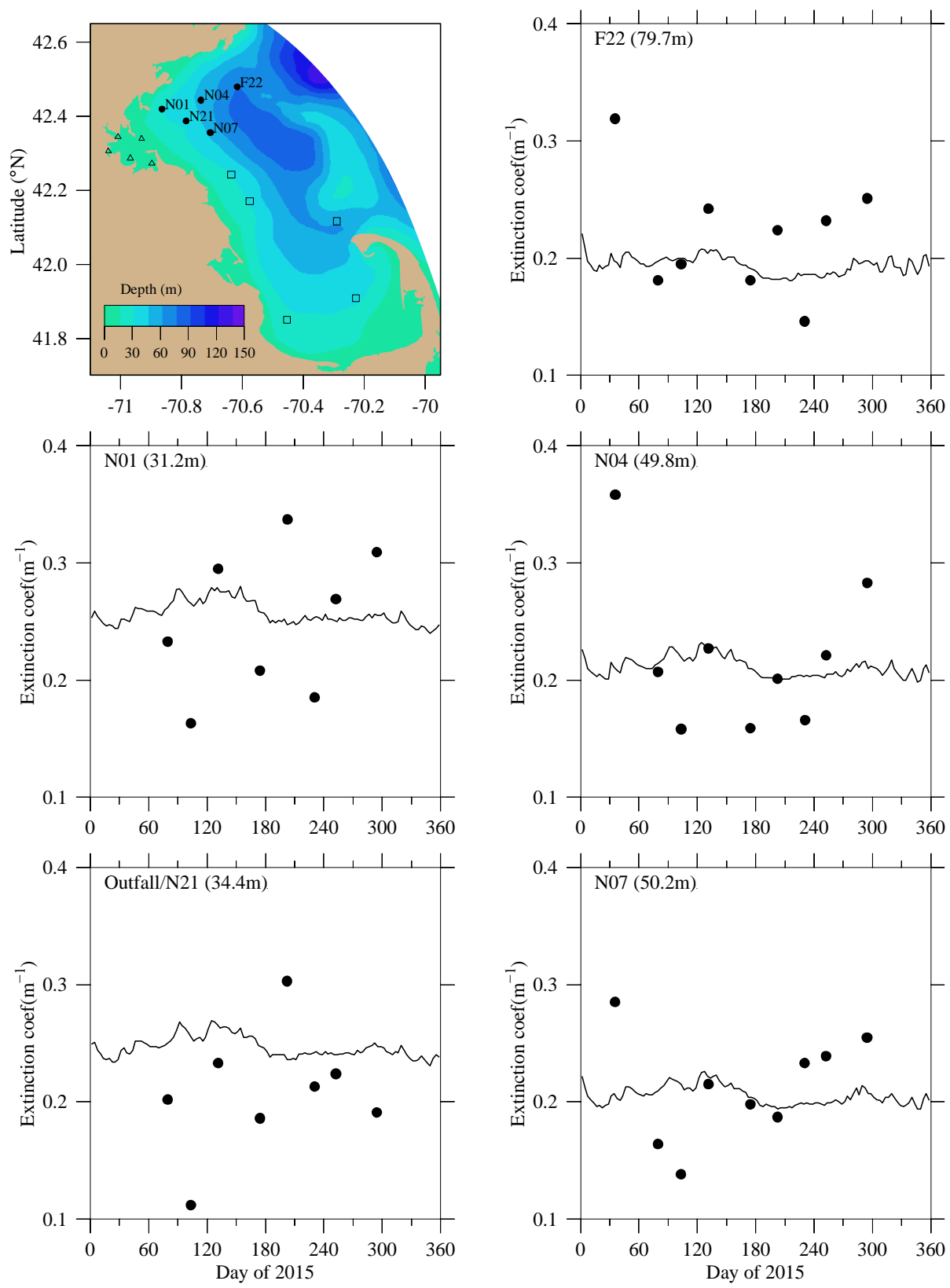


**Figure 5-2a.** Light extinction. Northern stations. Line: Model. Symbols: Observations. In this and all similar plots to follow, upper left of frame shows “station name (bathymetric depth)”.

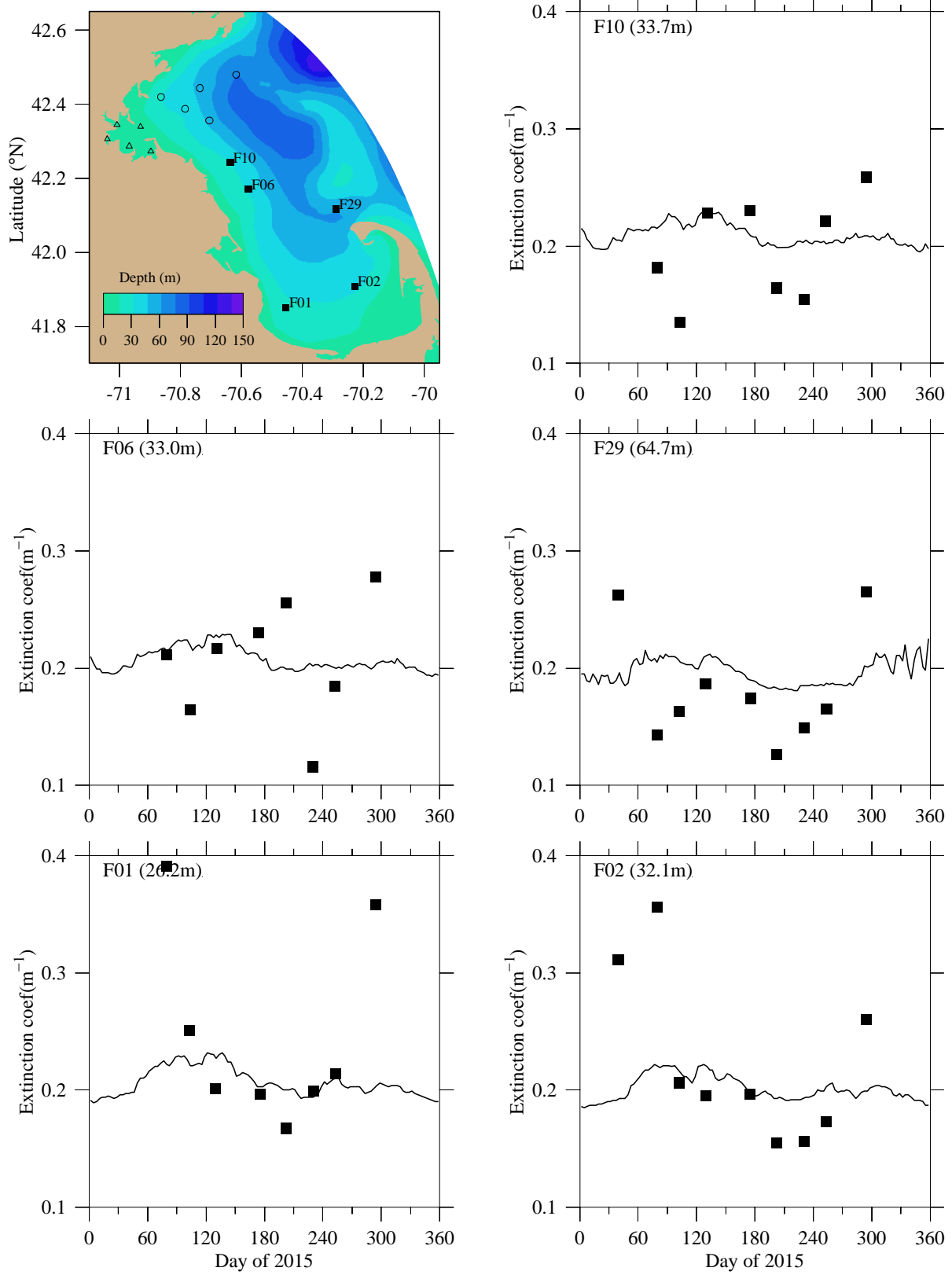


**Figure 5-2b.** Light extinction. Southern stations. Line: Model. Symbols: Observations.

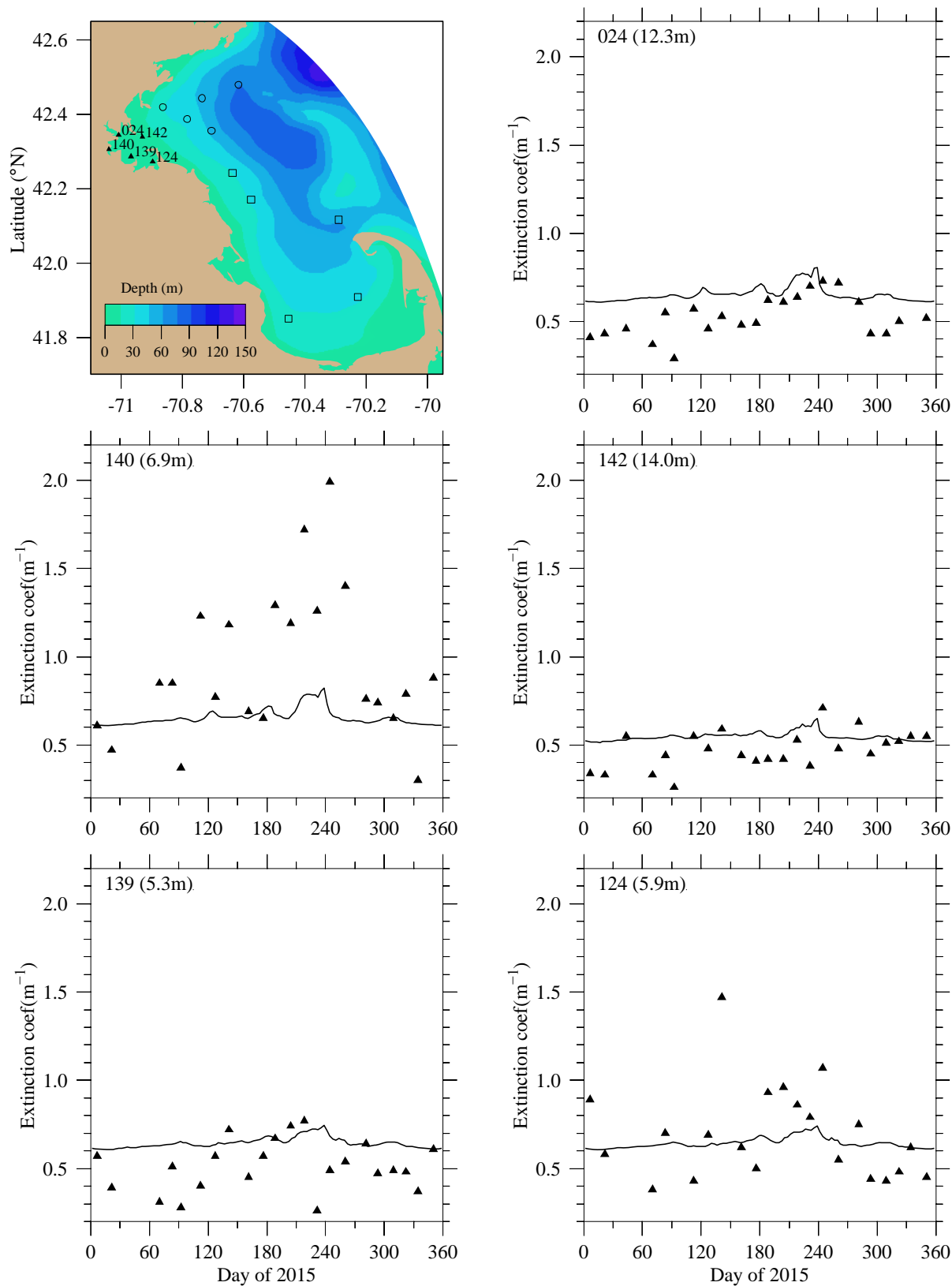


**Figure 5-2c.** Light extinction. Harbor stations. Line: Model. Symbols: Observations.

Note different y-axis scale than for bay stations in Figure 5-2a and Figure 5-2b.

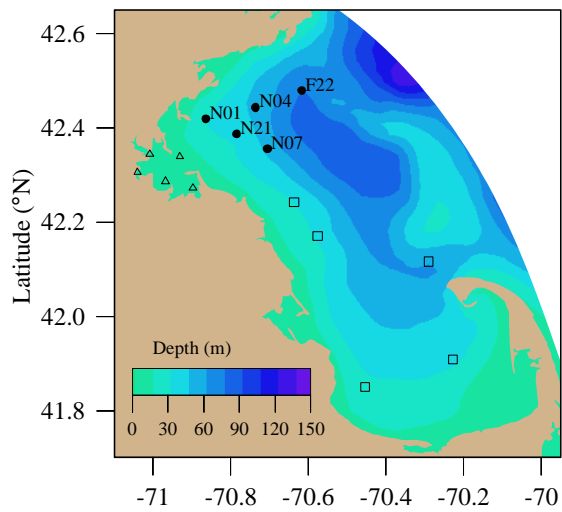
## 5.2 *Dissolved inorganic nitrogen*

Dissolved inorganic nitrogen (DIN) is the sum of the nitrogen in ammonium ( $\text{NH}_4$ ), nitrate ( $\text{NO}_3$ ), and nitrite ( $\text{NO}_2$ ). Seasonal variations in modeled and observed DIN during 2015 at the northern and southern station groups were mostly typical (Figure 5-3a,b). At the start of the year the shallow and deep DIN concentrations were comparable. By May the shallow values were drawn down to nearly zero by phytoplankton consumption, and remained low through summer. Deep concentrations were also reduced in the summer, though by a much smaller amount. Unlike 2014, in 2015 at the outfall/N21 site some observations (notably Feb, Mar, Nov) had higher concentrations near the surface, in contrast to other stations; the simulation did not capture this feature. At stations in and near Cape Cod Bay (F29, F01, F02; Figure 5-3b) the measured early-year concentrations (until at least late April) were very low both near the surface and near the seafloor, which the model did not capture; in addition the model concentrations at depth became substantially lower than observed at stations F22 and N04.

At many stations, in particular the offshore station F22, the near-seafloor concentrations in the model underestimated the observed values. An exception occurs at the outfall/N21 station, where the model concentrations substantially exceeded measured for most of the year.

For harbor stations the magnitudes and seasonal cycles of DIN in the model were generally similar to observations (Figure 5-3c). At most stations the observed differences between shallow and deep concentrations were minor and surface-bottom differences in the model were very small. At station 140 the observations had a more pronounced difference between shallow and deep, while the model results had no shallow-deep difference and were notably lower than nearly all the observations.

The modeled signature of the outfall in DIN is made clear by monthly-mean concentrations on the east-west transect (Figure 5-3d). The highest DIN levels generally occur near the seafloor, and within about 10 km of the outfall, year-round. High concentrations occurred within 5-10 km of the coast during January and, to a lesser extent, February and October. Away from the outfall, during winter conditions (Jan-Apr and Oct-Dec) vertical gradients are weak in association with more vigorous vertical mixing and reduced plankton uptake, while for the rest of the year concentrations in the upper water column are substantially lower than at depth due to uptake when stratification impedes vertical exchange. These patterns in 2015 were generally similar to simulations of prior years.



**Black:** Observations near-surface, model at surface  
**Red:** Observations near-seafloor, model at seafloor

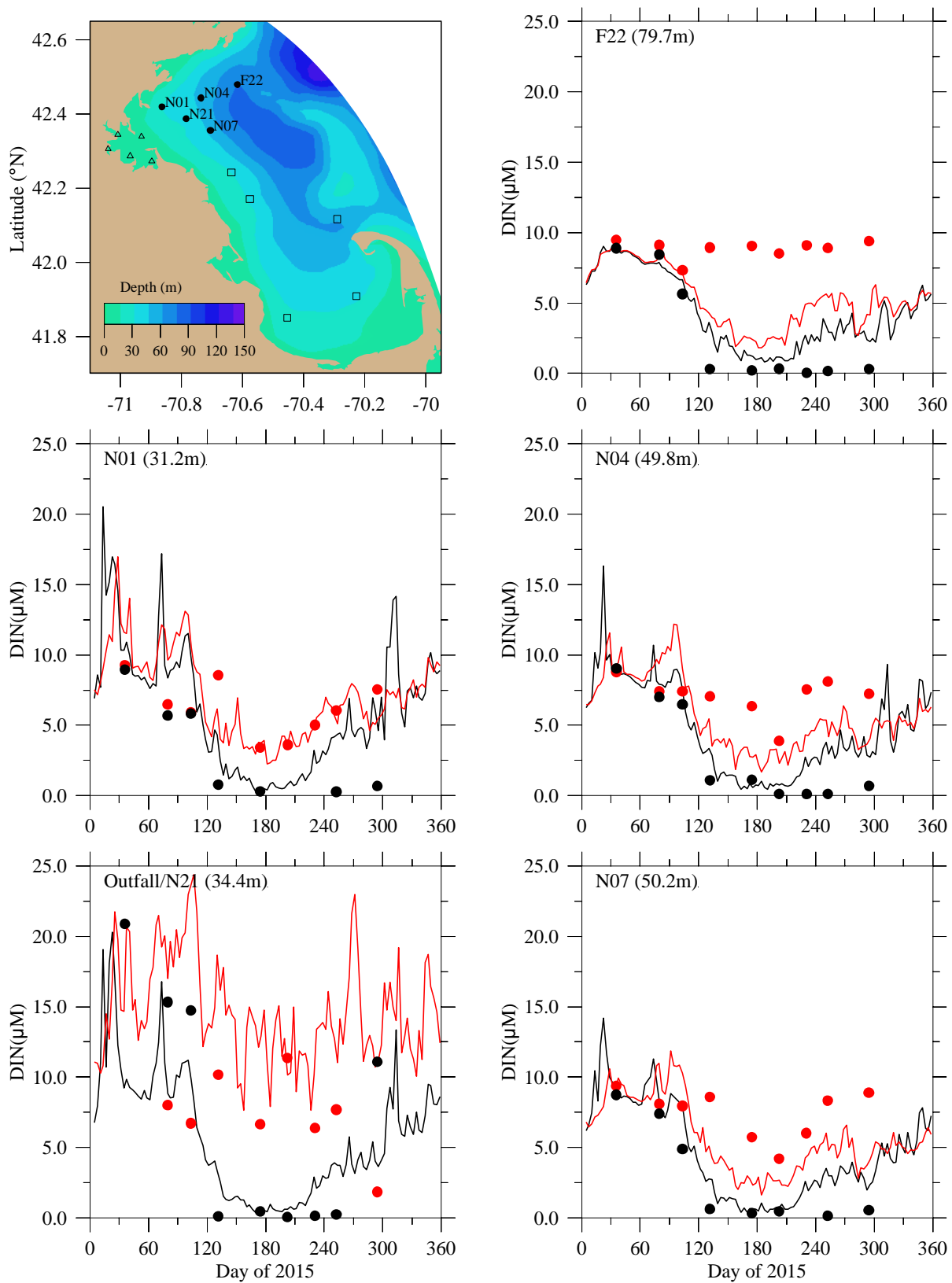
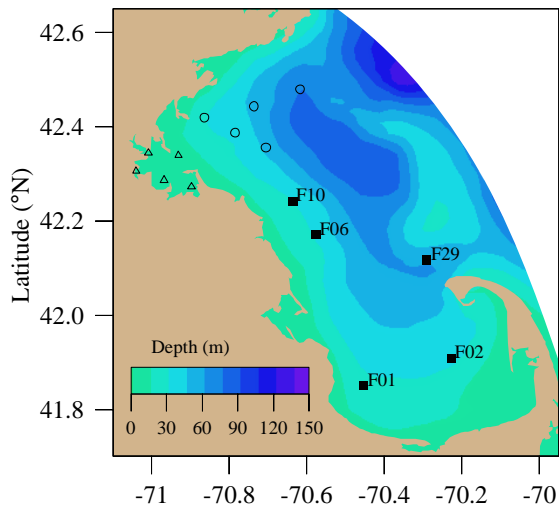


**Figure 5-3a.** Dissolved inorganic nitrogen. Northern stations. Model-observation comparisons.



**Black:** Observations near-surface, model at surface  
**Red:** Observations near-seafloor, model at seafloor

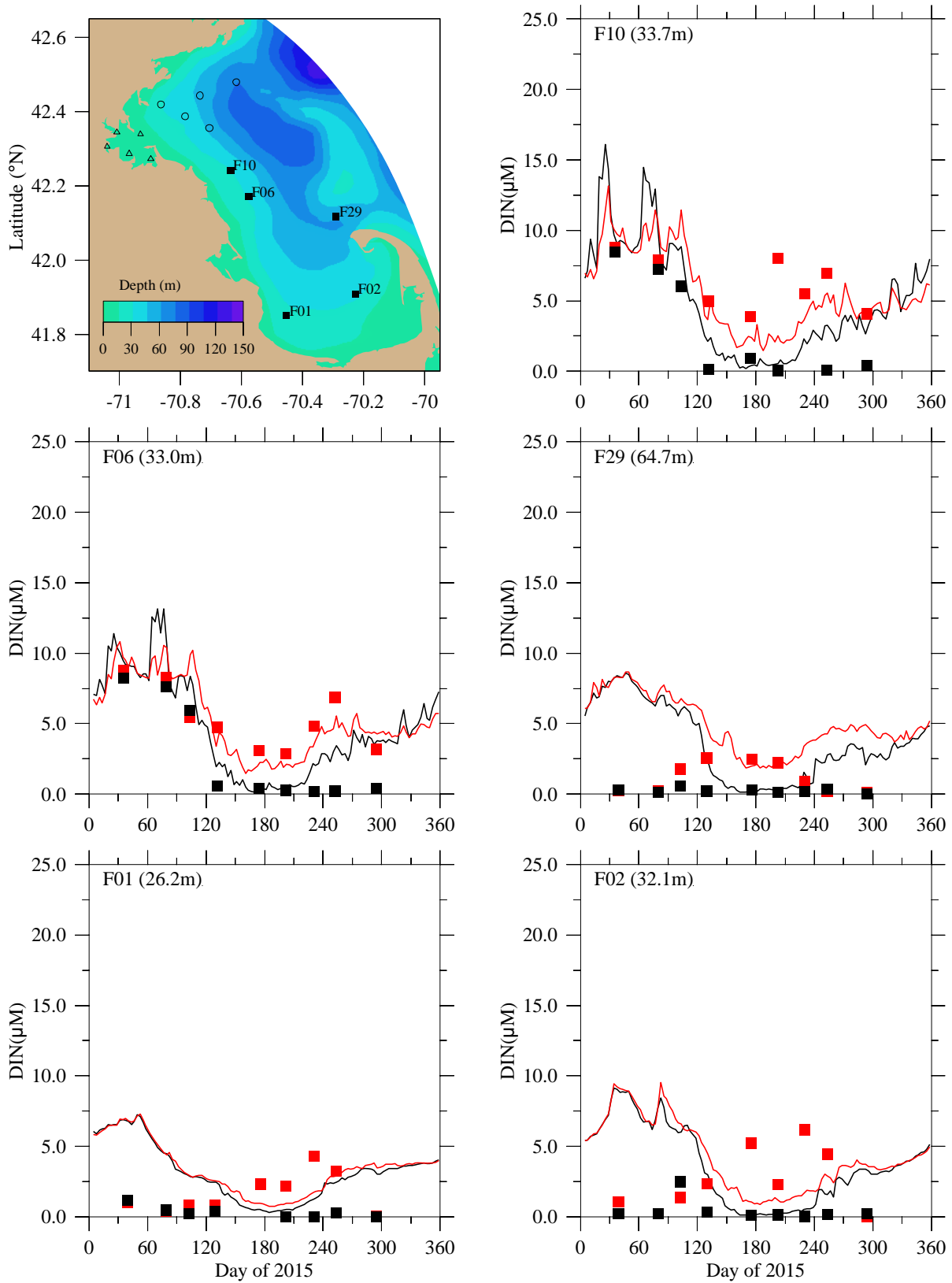


**Figure 5-3b.** Dissolved inorganic nitrogen. Southern stations. Model-observation comparisons.

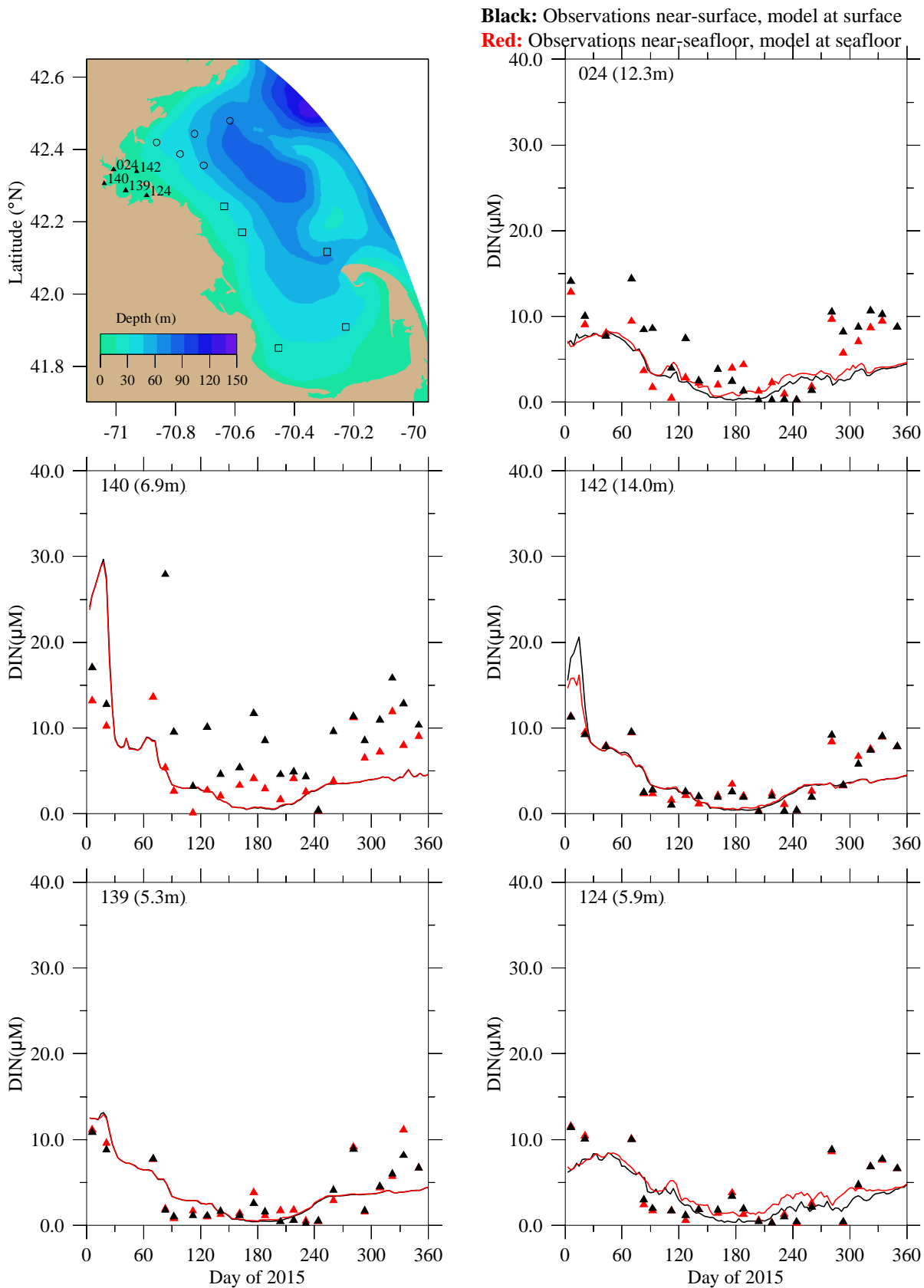


**Figure 5-3c.** Dissolved inorganic nitrogen. Harbor stations. Model-observation comparisons. Note different y-axis scale than for bay stations in Figure 5-3a and Figure 5-3b.

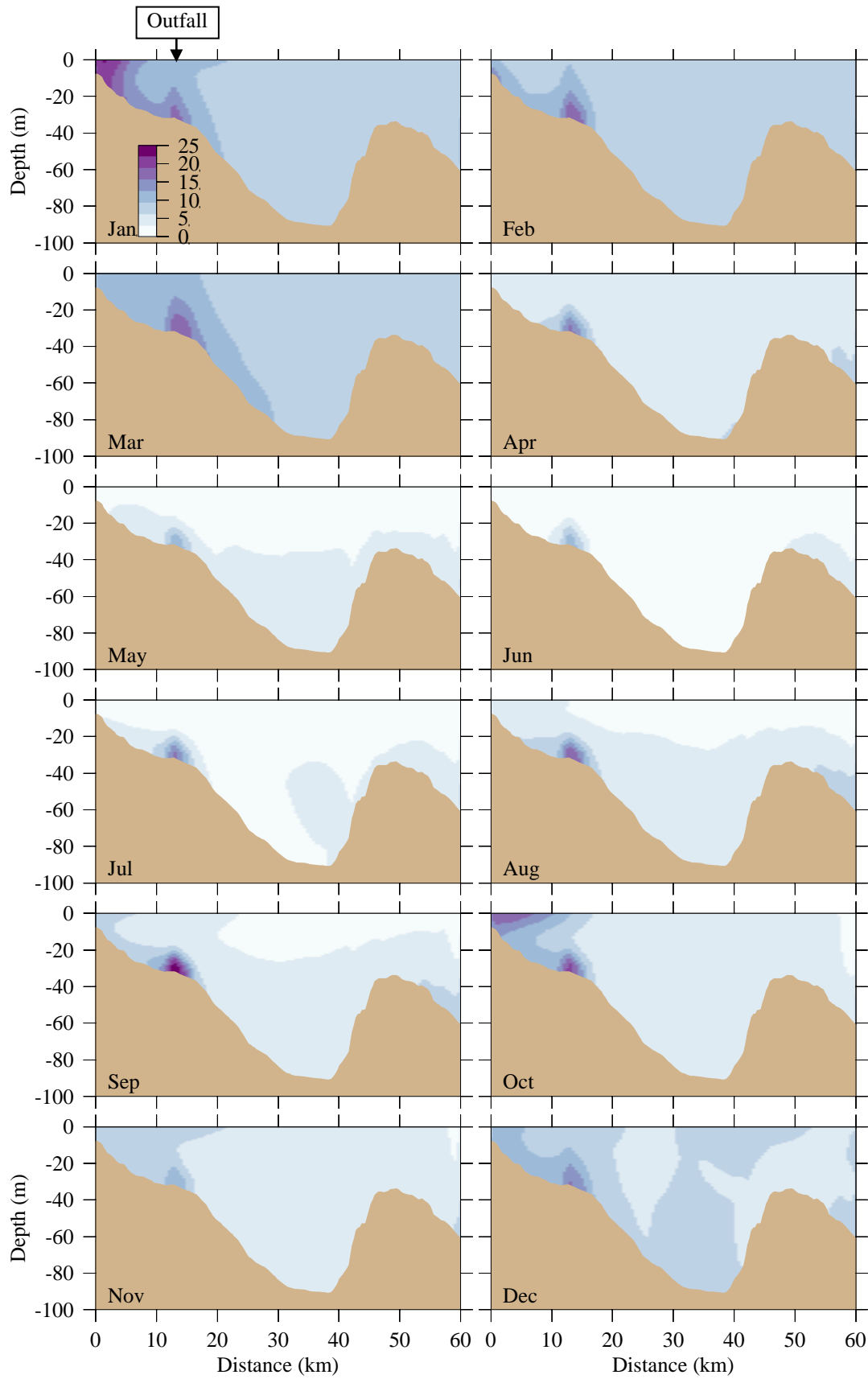


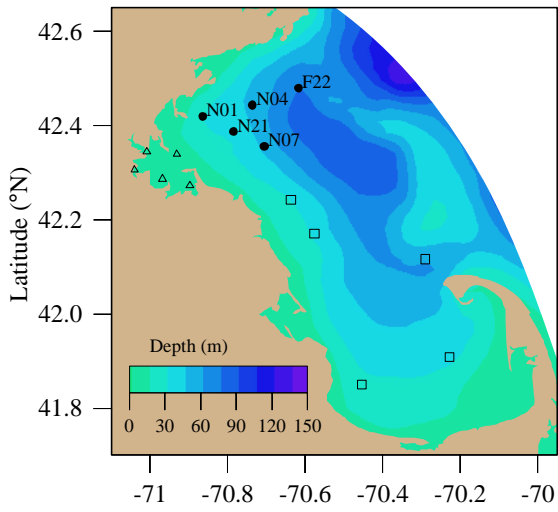
**Figure 5-3d.** Dissolved inorganic nitrogen ( $\mu\text{M}$ ). Model results, east-west transect (Fig. 3-7). Horizontal axis is distance eastward from coast; outfall is on seafloor at approximately 13 km.

### **5.3 Chlorophyll**

Model chlorophyll concentrations at Massachusetts Bay and Cape Cod Bay stations in 2015 (Figure 5-4a,b) showed modest temporal variations through the year. The model was generally within the observed ranges. However, at most stations the model did not capture certain features of the observations well: the observations were notably higher near the surface than near the seafloor throughout most of the year, and both shallow and deep observed concentrations were reduced from the spring through the summer.

At some harbor stations (Figure 5-4c; 140, 142, 139) the seasonal cycle of chlorophyll in the model featured increased levels during the summer, in particular the late summer. At 140 and 139 the deep concentrations were notably higher than shallow concentrations in the model, which was not observed. At 024 and 124 the observed late summer increase in concentrations was not captured by the model.

Model chlorophyll on the east-west transect (Figure 5-4d) had relatively low and vertically uniform concentrations early in the year. They increased weakly in March, April, and May. Concentrations were relatively low, with modest spatial variations, through the summer and fall. From October to December there were high concentrations at the far offshore end of the transect. In contrast to DIN, in model chlorophyll there was no signature of the outfall plume.



**Black:** Observations near-surface, model at surface  
**Red:** Observations near-seafloor, model at seafloor

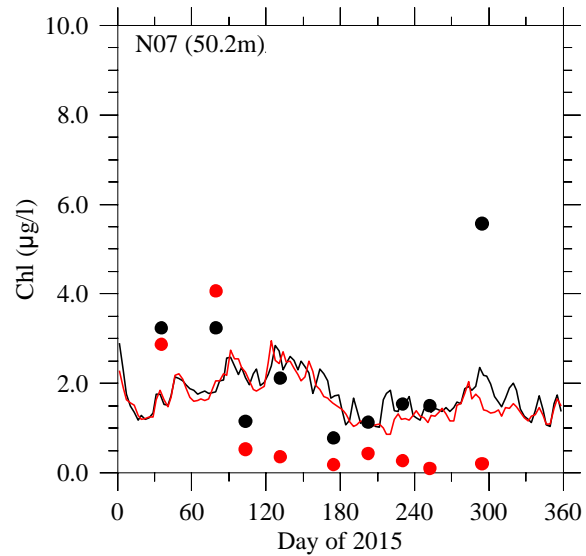
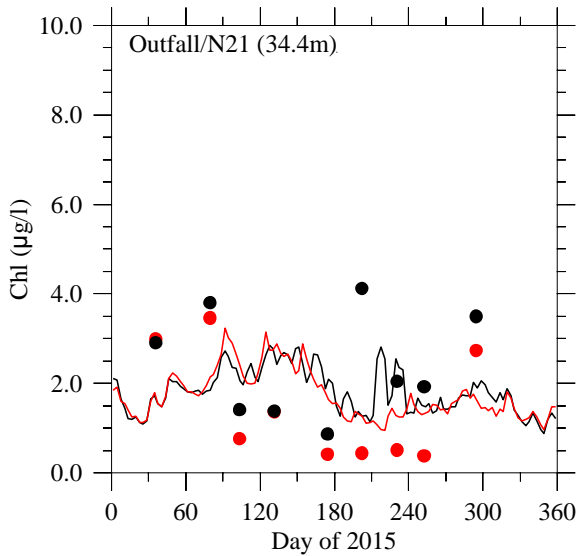
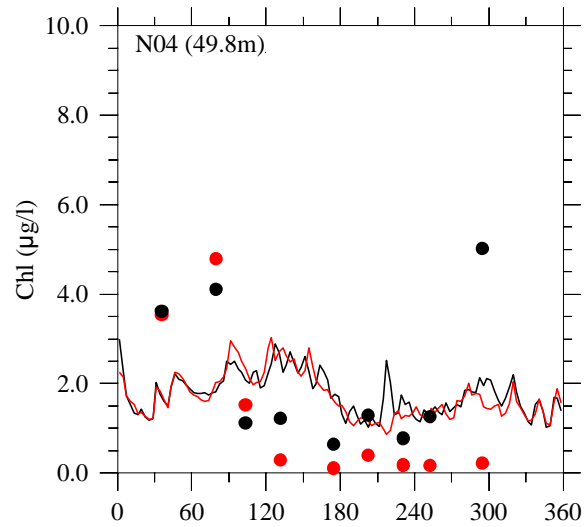
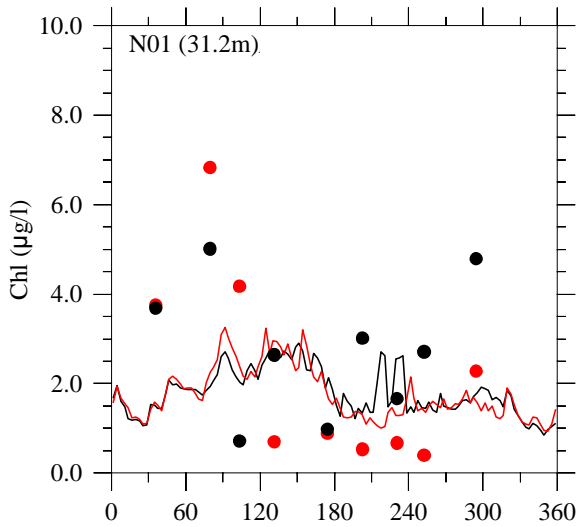
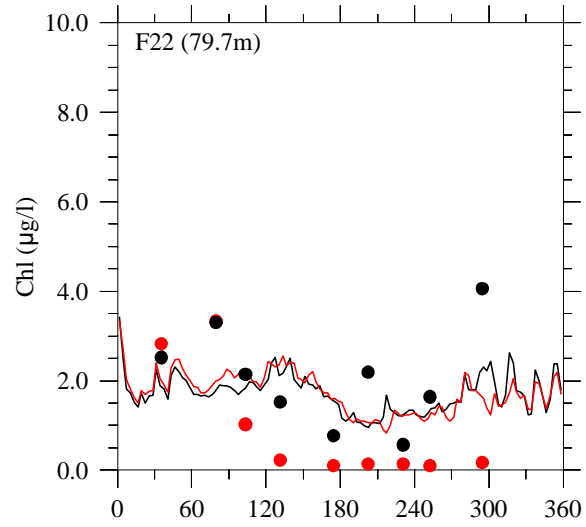


**Figure 5-4a.** Chlorophyll. Northern stations. Model-observation comparisons.

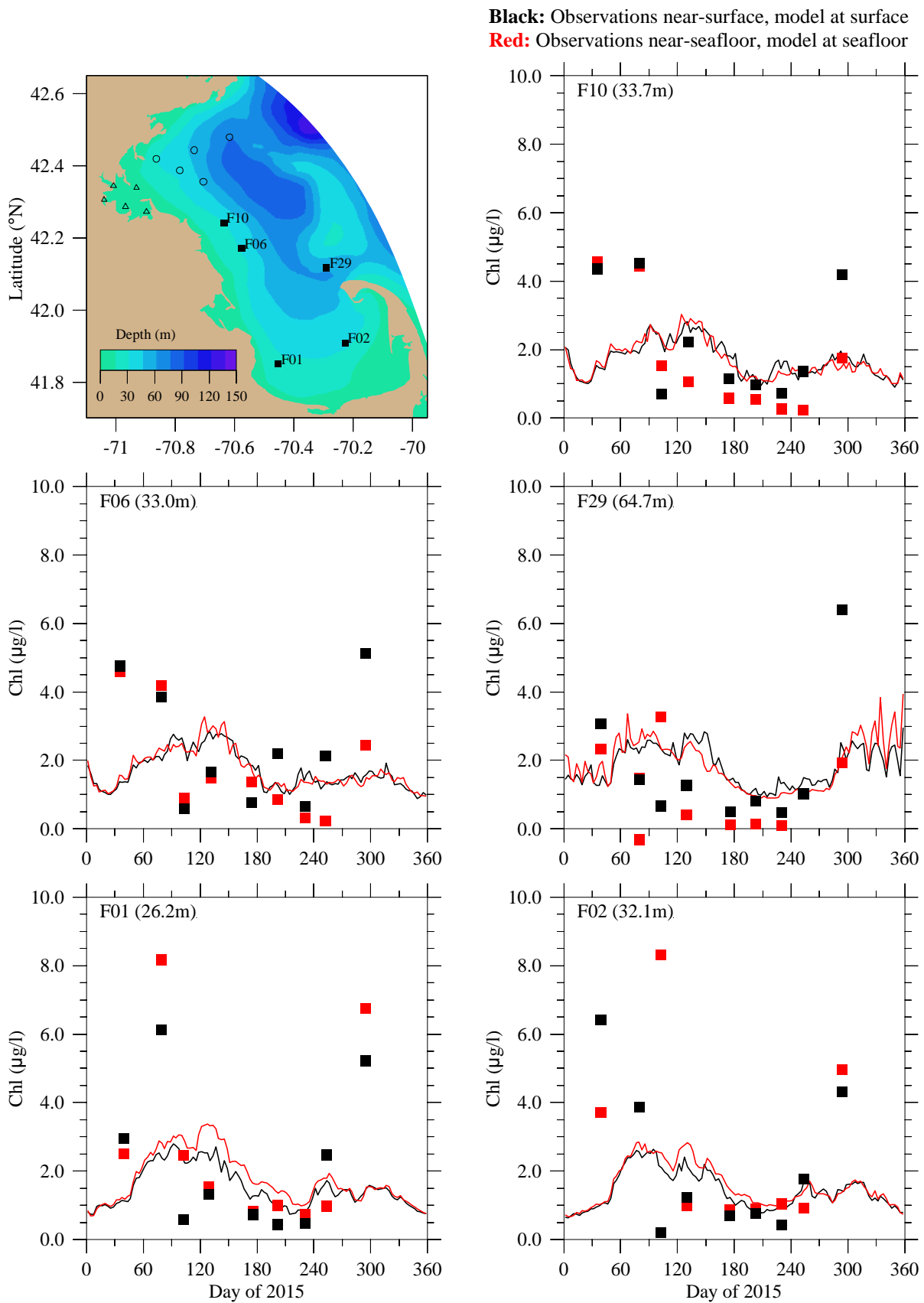


**Figure 5-4b.** Chlorophyll. Southern stations. Model-observation comparisons.

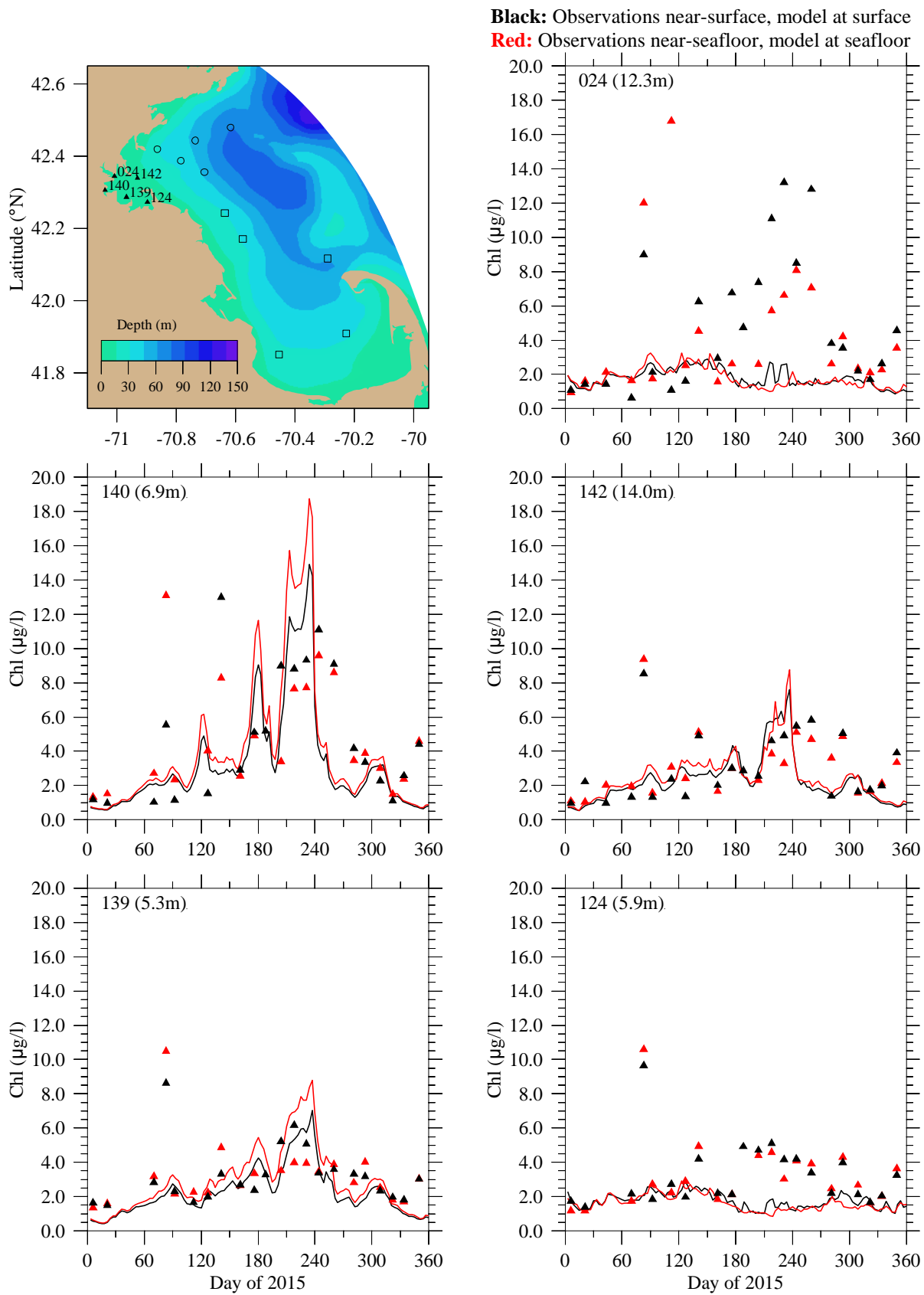


**Figure 5-4c.** Chlorophyll. Harbor stations. Model-observation comparisons.

Note different y-axis scale than for bay stations in Figure 5-4a and Figure 5-4b.

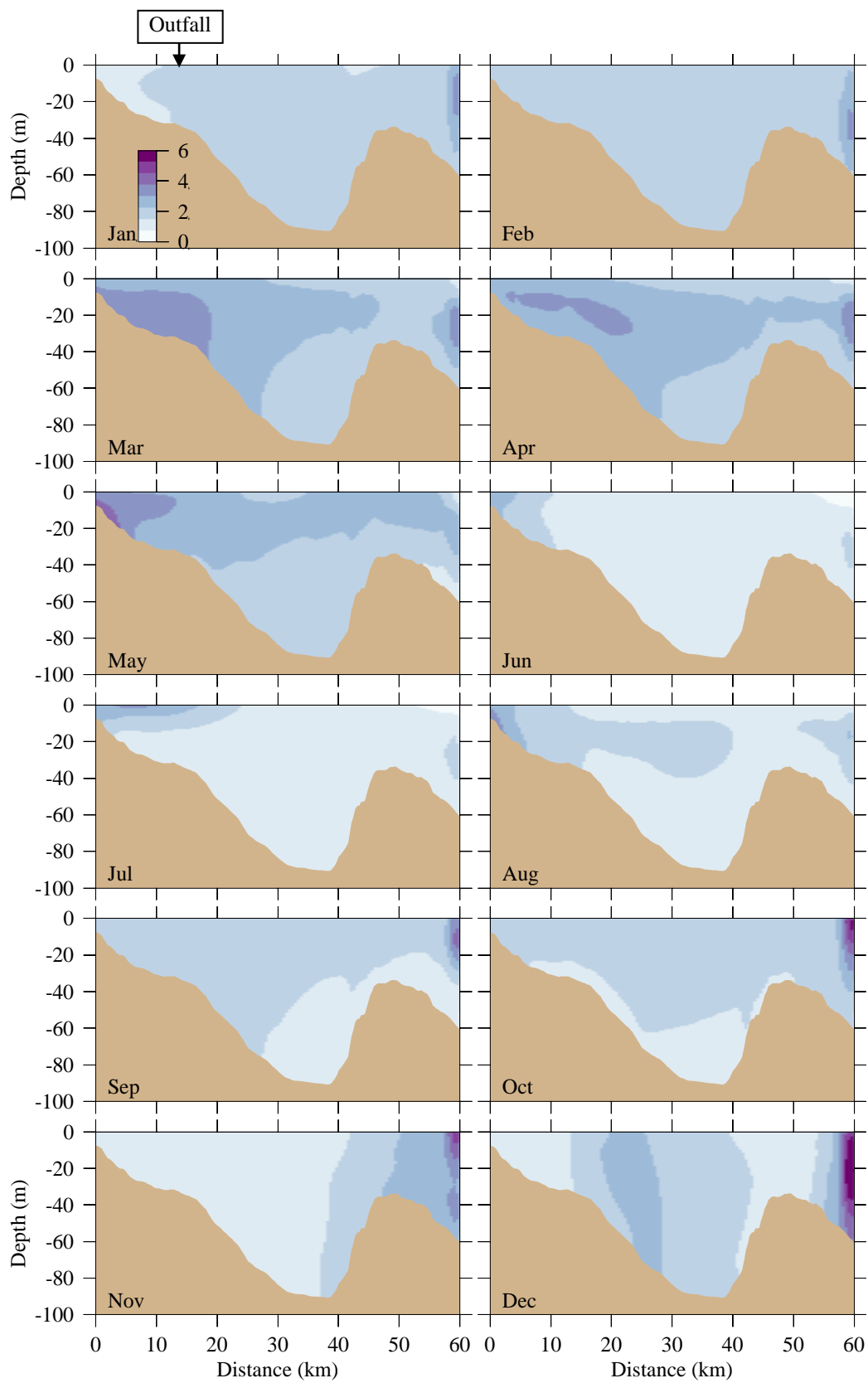


**Figure 5-4d.** Chlorophyll ( $\mu\text{g L}^{-1}$ ). Model results, east-west transect (Fig. 3-7).

Horizontal axis is distance eastward from coast; outfall is on seafloor at approximately 13 km.

#### **5.4 *Primary productivity***

Primary productivity in the 2015 model run is shown in Figure 5-5 at three monitoring stations (F23 at the mouth of BH; N04 to the northeast of the outfall; and N18 nearest to the outfall) where observations of primary productivity had been made in past years. Ongoing field sampling no longer includes primary productivity measurements, but for context the observations from 1995-2010 are superimposed as box-whisker plots on the model outputs (a review of the field results is included as part of Keay et al., 2012; methods are described in Appendix C of Libby et al., 2005). The box-whisker plots consist of a box with the 25<sup>th</sup> and 75<sup>th</sup> percentiles at its lower and upper bounds and a horizontal line bisecting the box at the median (50<sup>th</sup> percentile), with whiskers that extend to the 9<sup>th</sup> and 91<sup>st</sup> percentiles. For most of the year, 2015 modeled primary productivity was within ranges of historic observations. At F23 there was a pronounced increase in late summer. The springtime increase was modest, occurred somewhat later than observed in past years, and increased levels were sustained at N04 and N18 through about mid-summer. In fall, the modeled primary productivity decreased to low levels earlier than was observed in many past years. These features are all within similar ranges of results from model simulations of past years.

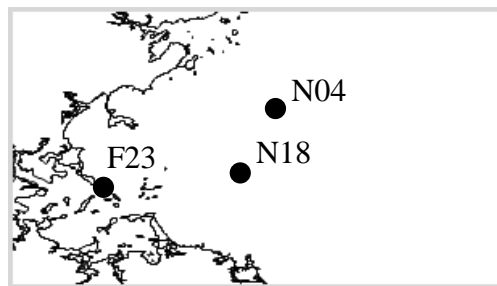
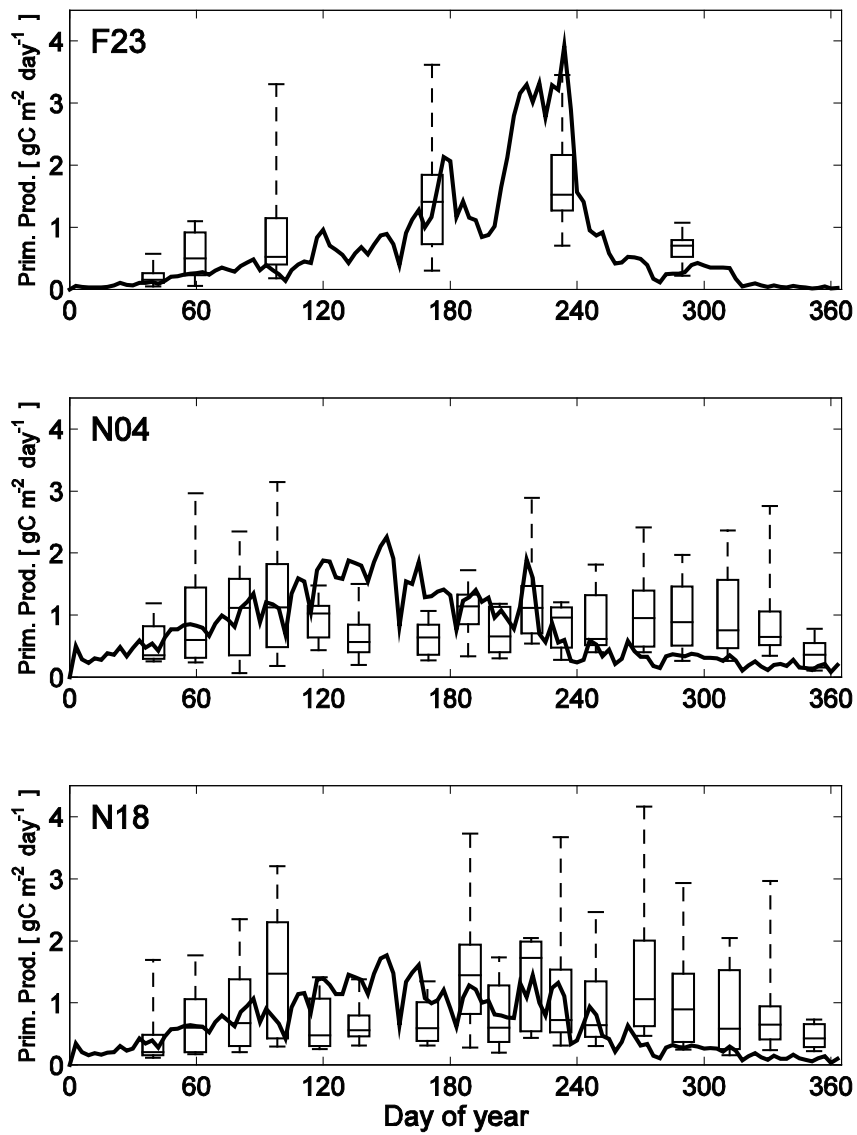


**Figure 5-5.** Primary production, vertically integrated, model-observation comparison.

Line is 2015 model result. Box-whiskers are 1995-2010 observations; box shows 25<sup>th</sup>, 50<sup>th</sup>, and 75<sup>th</sup> percentiles and whiskers are 9<sup>th</sup> and 91<sup>st</sup> percentiles.

## **5.5 *Dissolved and particulate organic nitrogen***

Model dissolved organic nitrogen (DON) levels during 2015 were generally within the range of variability of observations (Figure 5-6a,b). Temporal variations in the model were somewhat weaker than observations, and neither model nor observations included a strong seasonal signal. Vertical difference in model DON were modest, with surface values slightly higher, particularly in the late summer, as evidenced in the east-west transect results (Figure 5-6).

Model particulate organic nitrogen (PON) during 2015 showed a stronger seasonal cycle than in DON, with low concentrations in winter, then elevated levels in spring and summer that slowly decreased through fall (Figure 5-7a,b); at most stations, deep concentrations were modestly less than shallow concentrations. The range of temporal variability in the model was less than in observations, and at most stations the deep observed values remained markedly lower than shallow values for all or most of the year, a feature the model did not capture. The east-west transect results for PON (Figure 5-7c) demonstrate that the seasonal changes and vertical structure just described generally occurred regionwide.

As noted for chlorophyll above, in both model and observations there was not a persistent anomalous signal near the outfall in either DON or PON. This is evidence supporting the conclusion that these variables are not detectably influenced by outfall effluent.

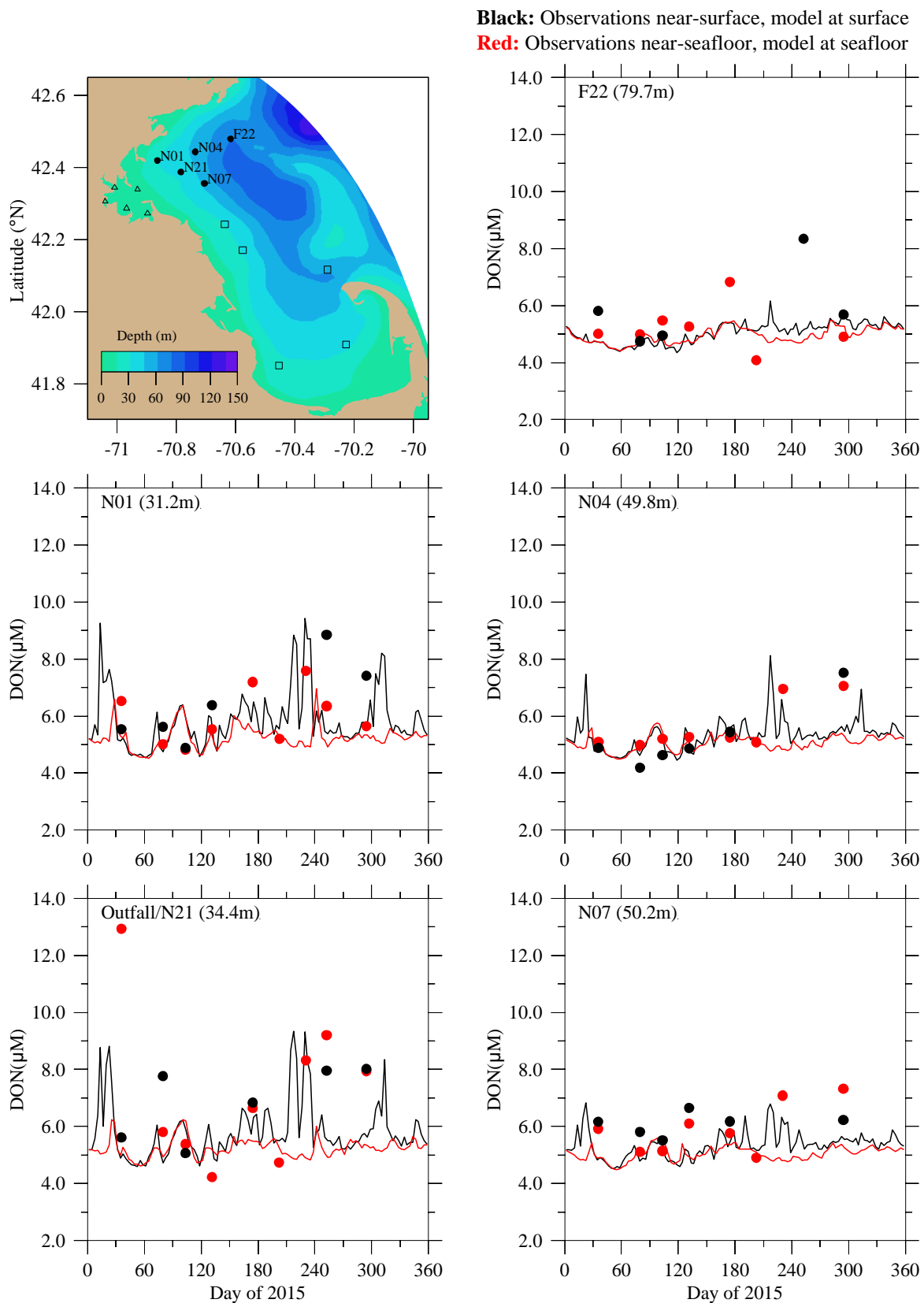


**Figure 5-6a.** Dissolved organic nitrogen. Northern stations. Model-observation comparisons.

Because observed DON is computed using measurements of TDN (total dissolved nitrogen), NO<sub>2</sub>, NO<sub>3</sub>, and NH<sub>4</sub>, if any of those four measurements was unavailable the observed DON does not appear on these plots. This was the case for many near-surface samples during the summer months.

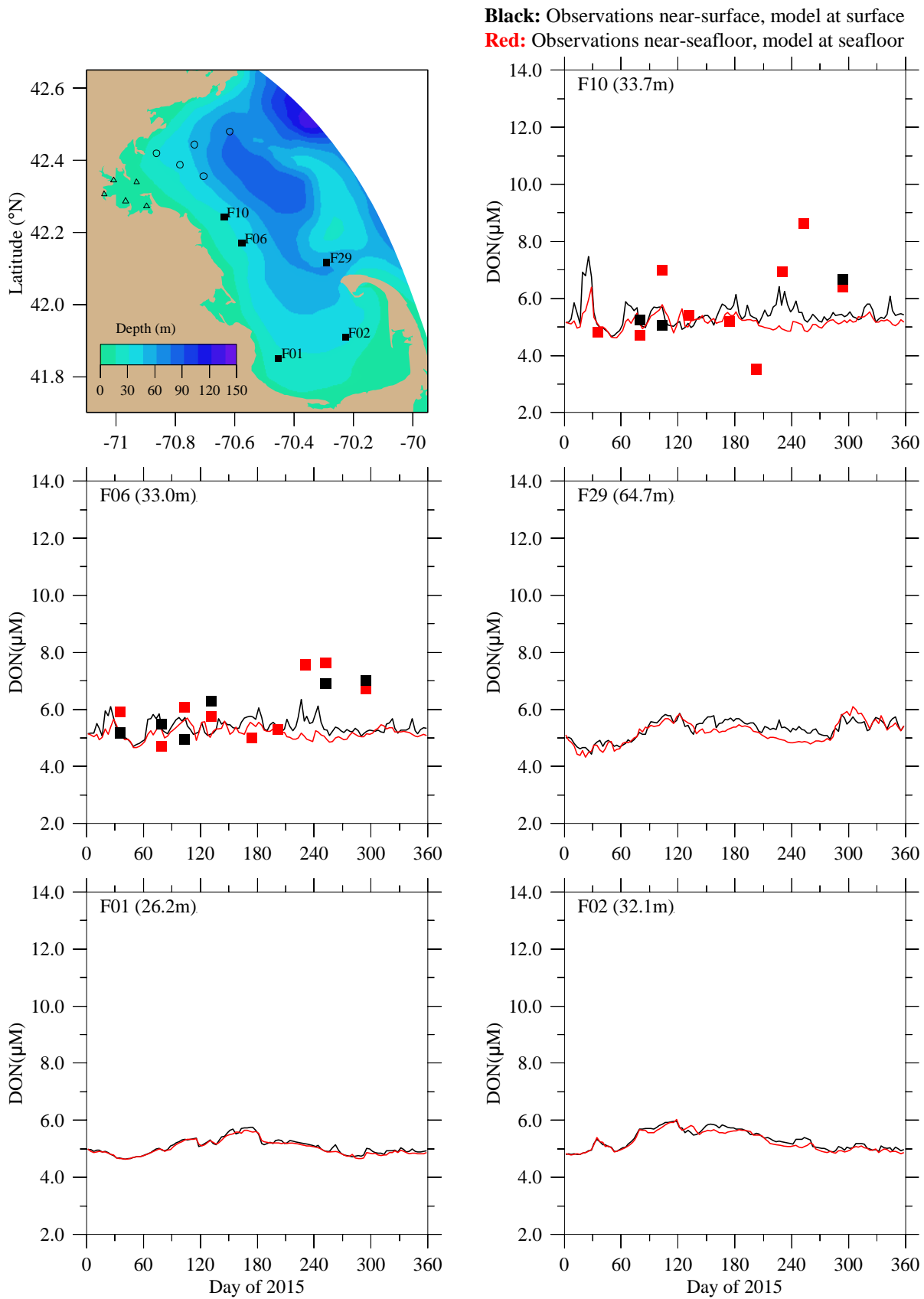


**Figure 5-6b.** Dissolved organic nitrogen. Southern stations. Model-observation comparisons. No observations were collected at stations F29, F01, or F02.

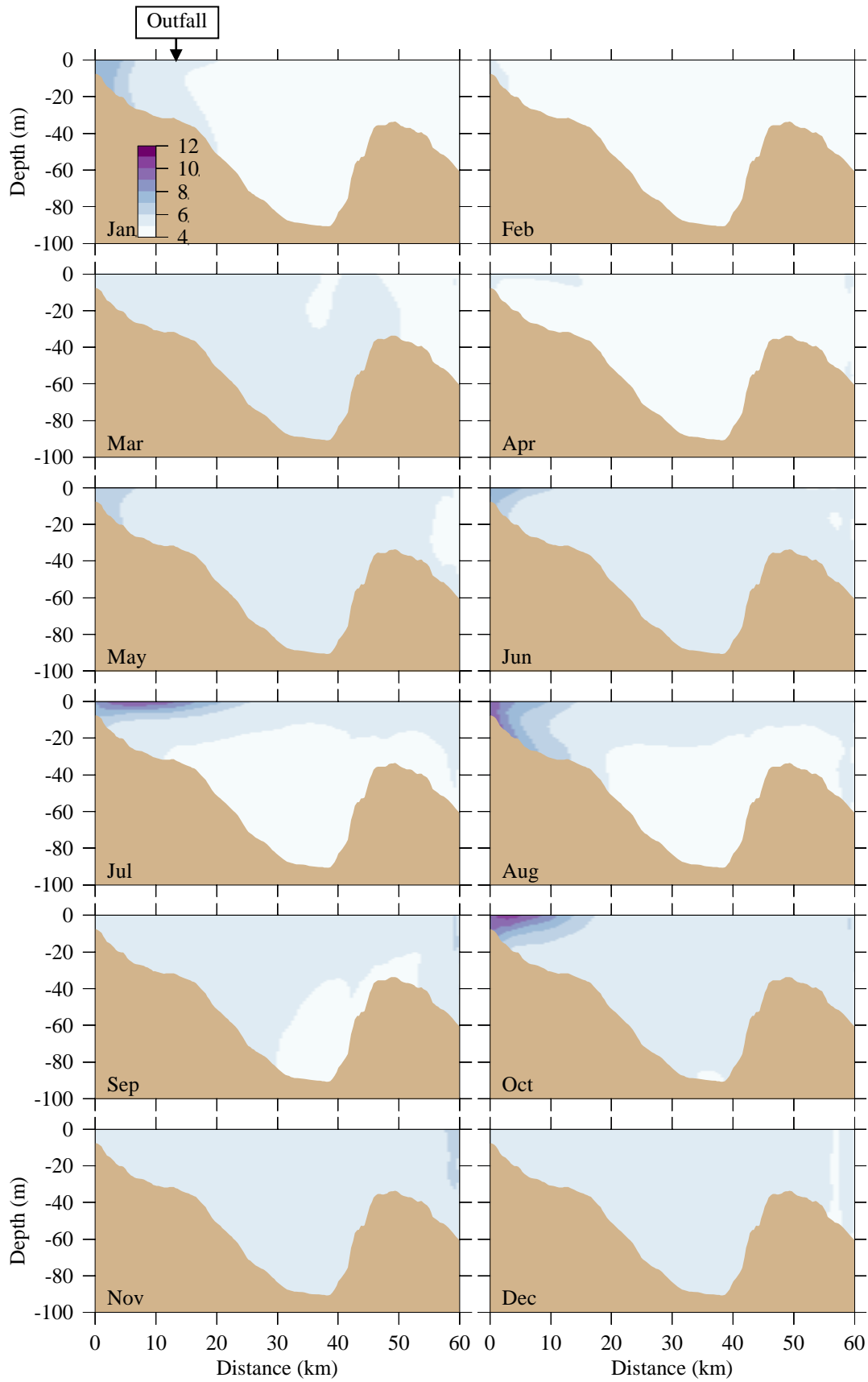


**Figure 5-6c.** Dissolved organic nitrogen ( $\mu\text{M}$ ). Model results, east-west transect (Fig. 3-7). Horizontal axis is distance eastward from coast; outfall is on seafloor at approximately 13 km.

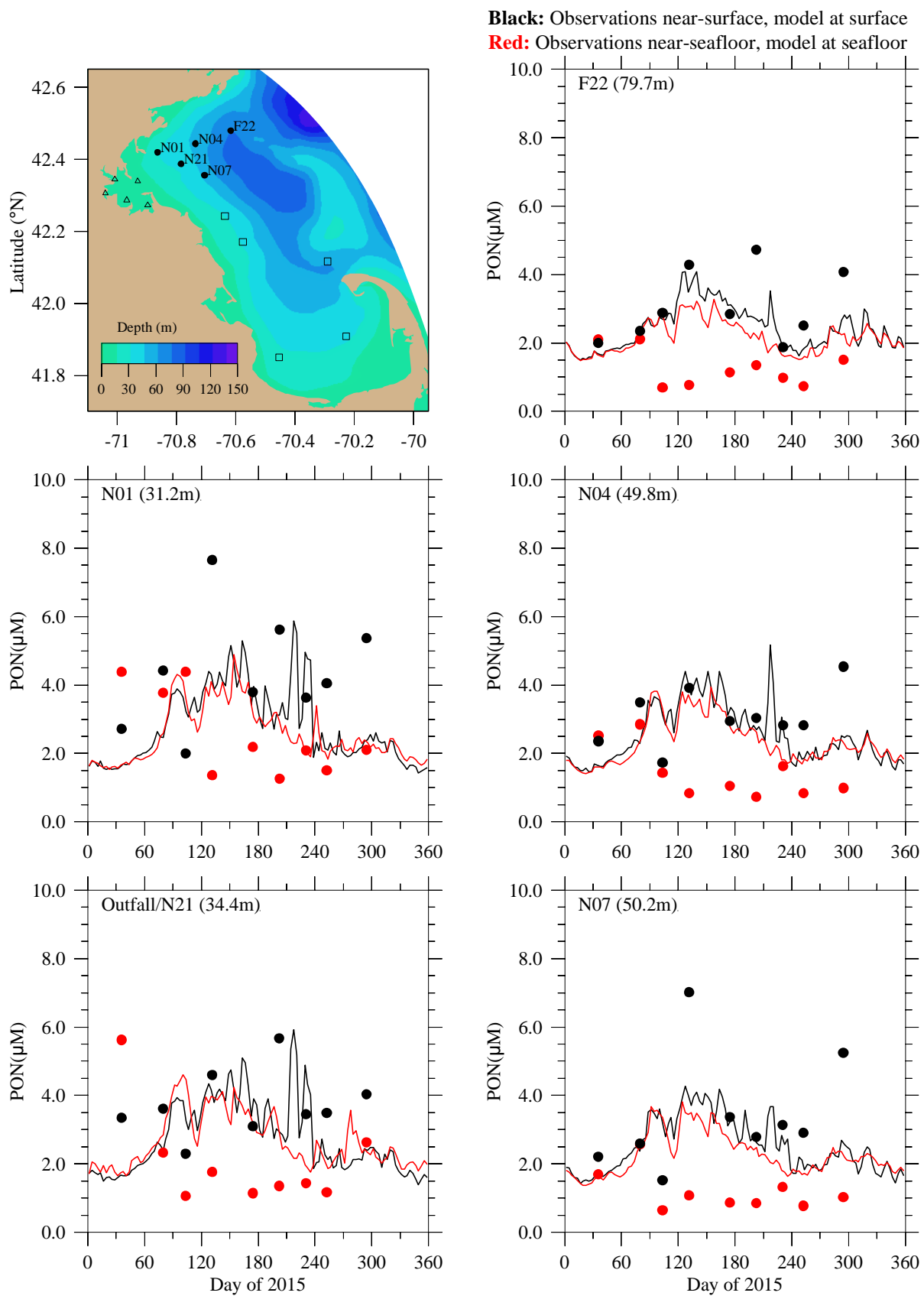


**Figure 5-7a.** Particulate organic nitrogen. Northern stations. Model-observation comparisons.

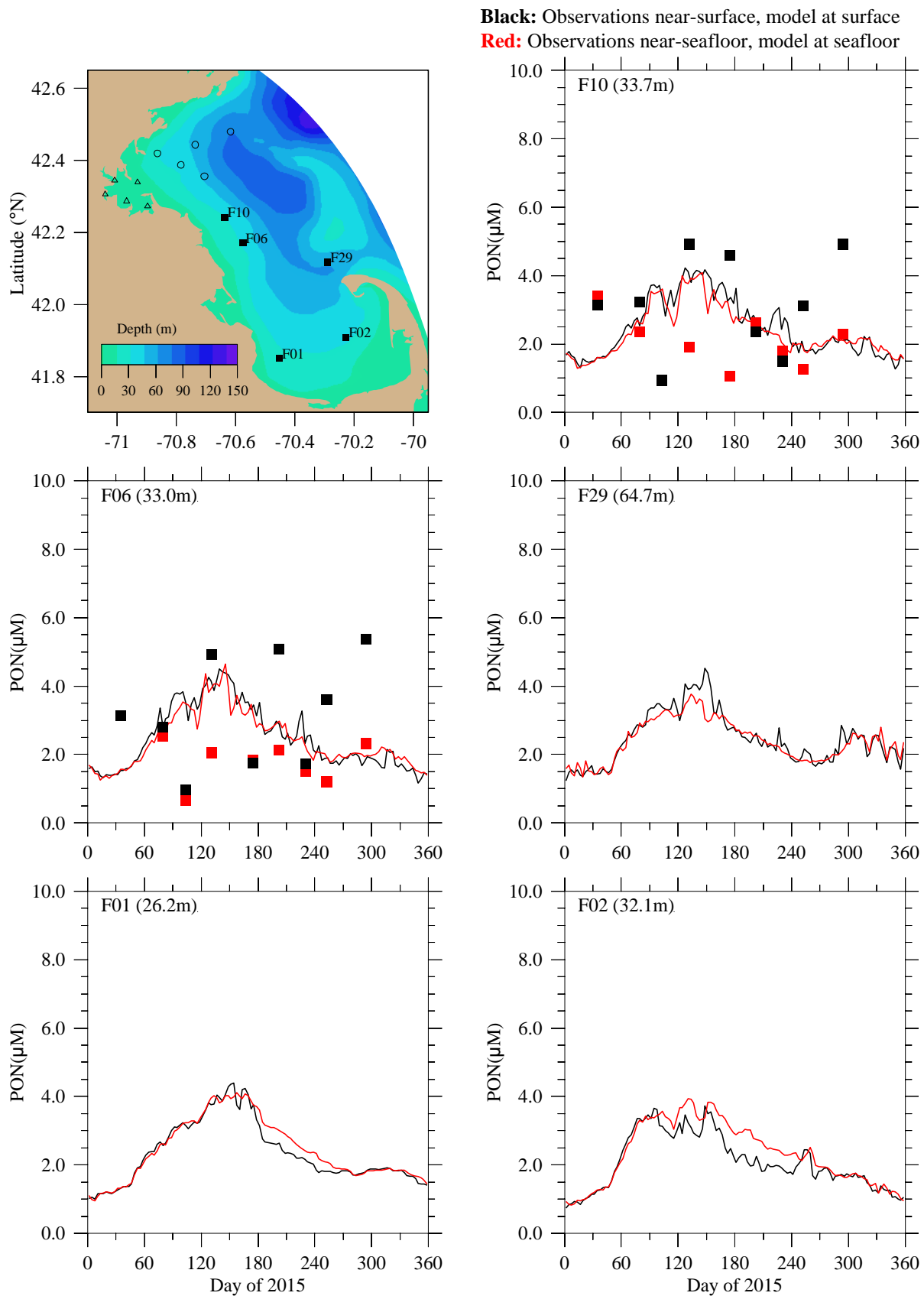


**Figure 5-7b.** Particulate organic nitrogen. Southern stations. Model-observation comparisons. No observations were collected at stations F29, F01, or F02.

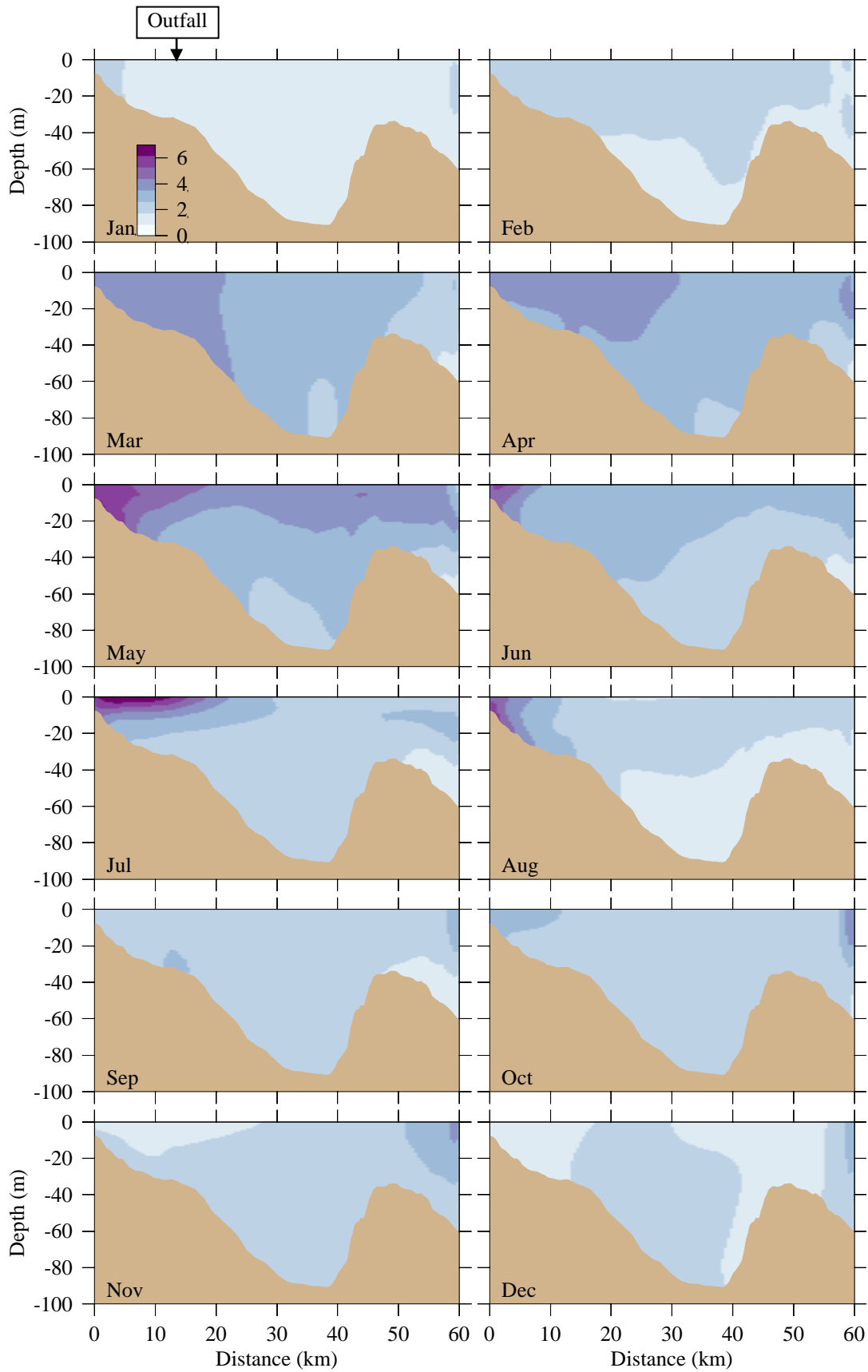


**Figure 5-7c.** Particulate organic nitrogen ( $\mu\text{M}$ ). Model results, east-west transect (Fig. 3-7). Horizontal axis is distance eastward from coast; outfall is on seafloor at approximately 13 km.

## 5.6 *Particulate organic carbon*

The seasonal cycle in model particulate organic carbon (POC) during 2015 at Massachusetts Bay stations was modest (Figure 5-8a,b) and included low values January through March or April, then higher levels for the remainder of the year. The ranges of model values were generally near the range of observed values, but at many stations the model results were biased higher than observations. In the observations, deep concentrations were almost all substantially lower than shallow values, while the opposite was true for much of the year at many stations in the model. This mismatch between the vertical structure of POC in the model and observations is apparently due to parameterization of biogeochemical processes in UG-RCA, given that the hydrodynamic model is capturing observed variations of vertical structure (stratification) well, as described above.

Model POC on the east-west transect in 2015 (Figure 5-8c) showed generally higher concentrations from April to December, consistent with Figure 5-8a,b. Highest concentrations occurred at the surface or at mid-depth. There were also high concentrations at the far offshore end of the transect.

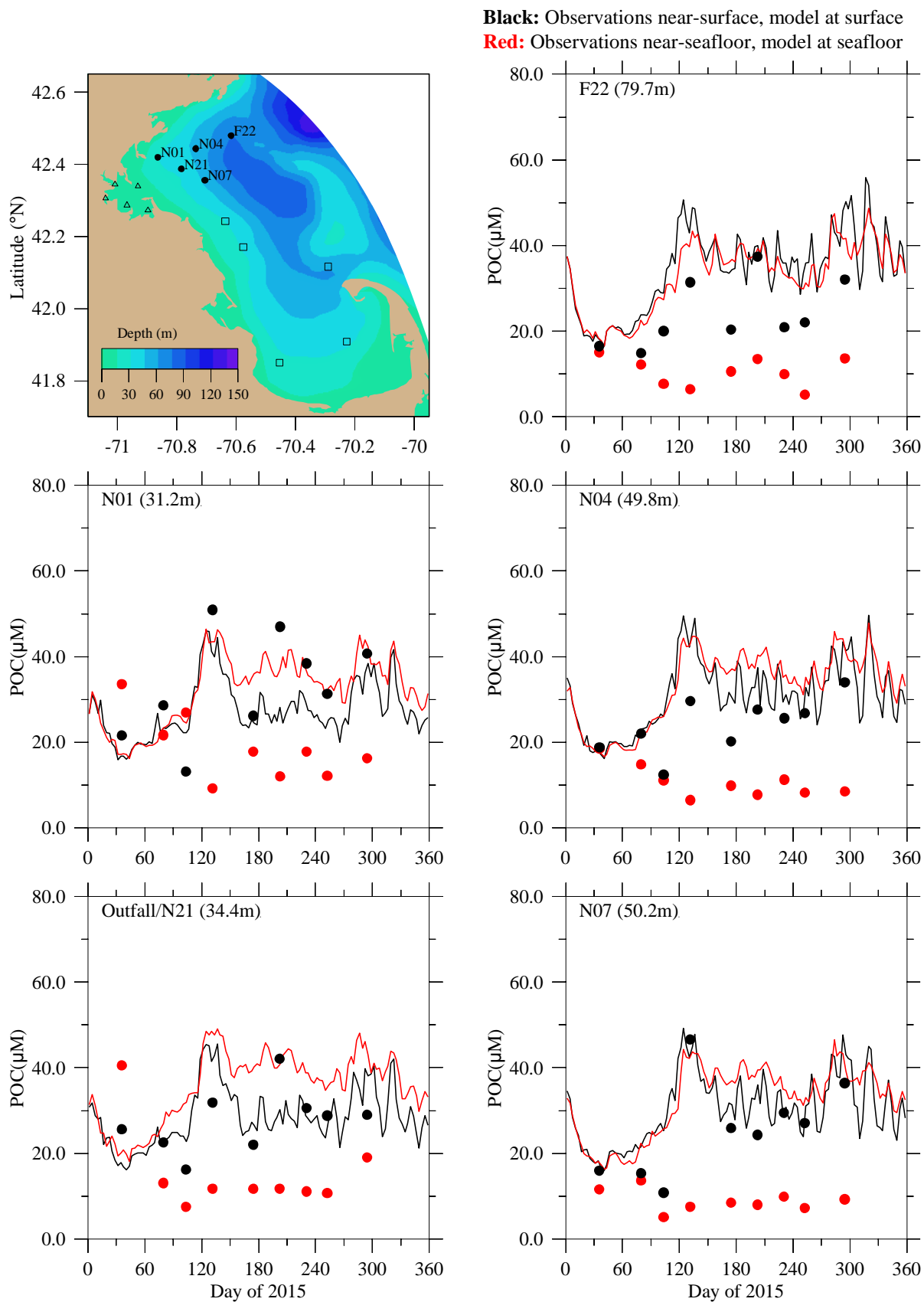


**Figure 5-8a.** Particulate organic carbon. Northern stations. Model-observation comparisons.

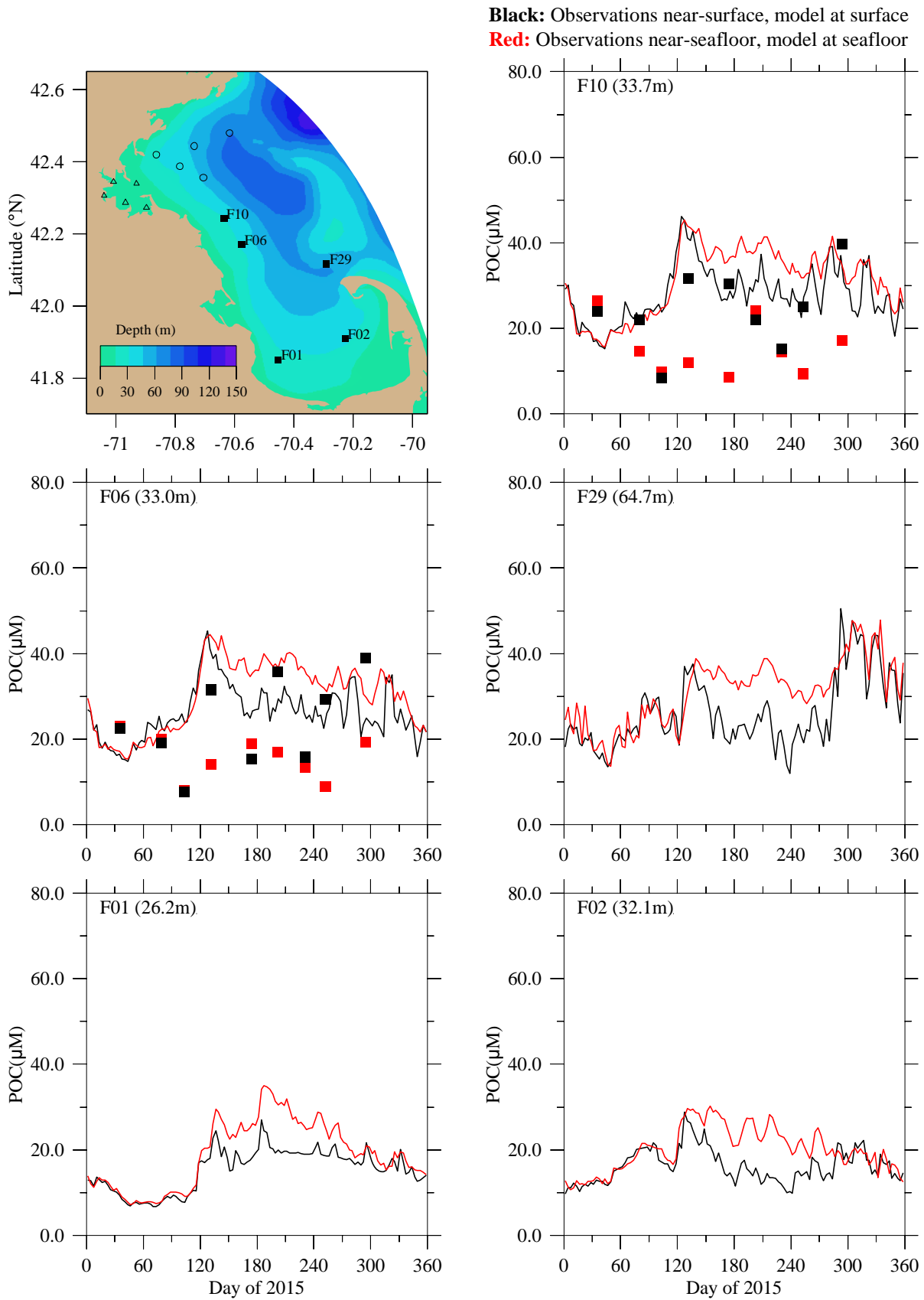


**Figure 5-8b.** Particulate organic carbon. Southern stations. Model-observation comparisons. No observations were collected at stations F29, F01, or F02.

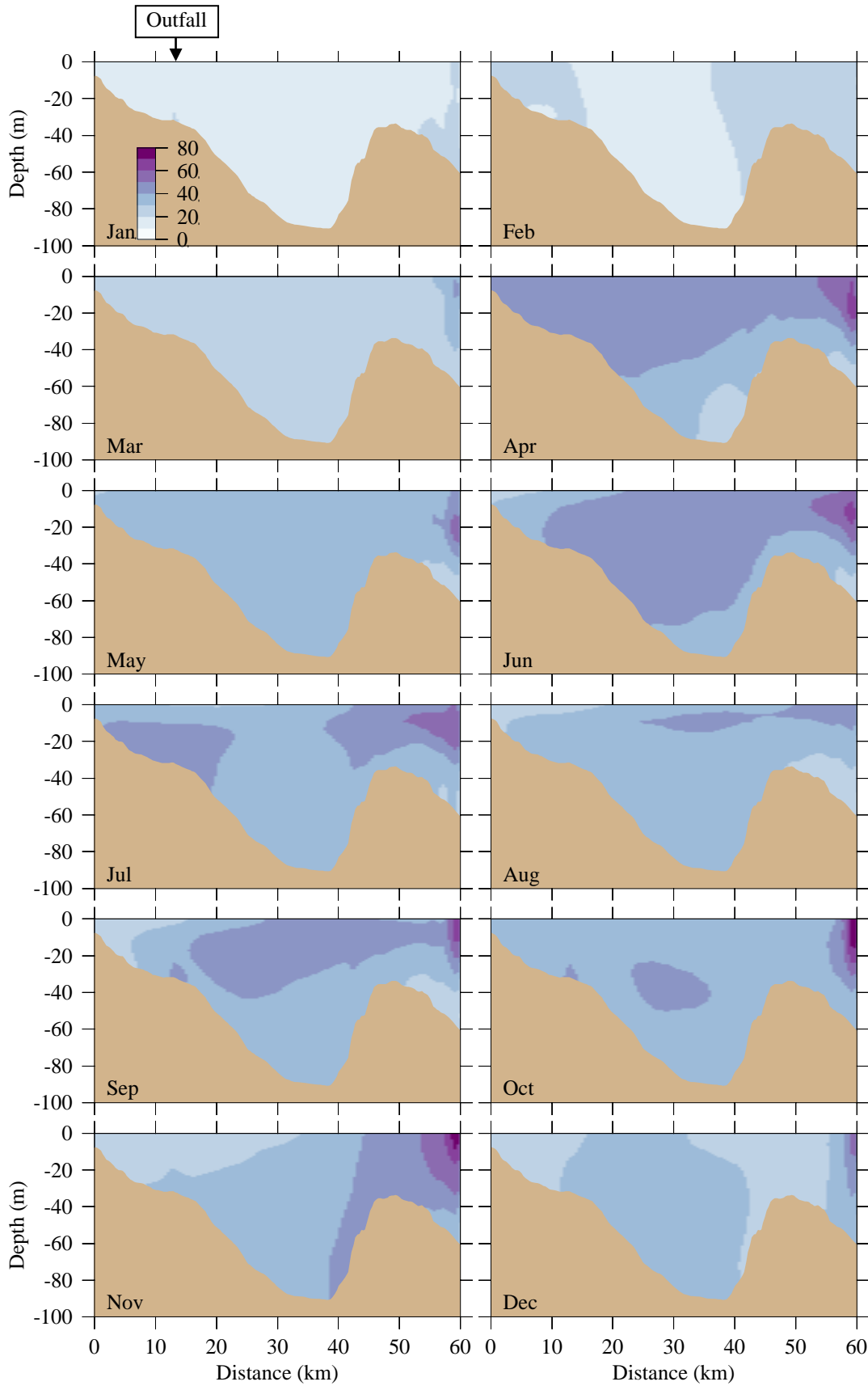


**Figure 5-8c.** Particulate organic carbon ( $\mu\text{M}$ ). Model results, east-west transect (Fig. 3-7). Horizontal axis is distance eastward from coast; outfall is on seafloor at approximately 13 km.

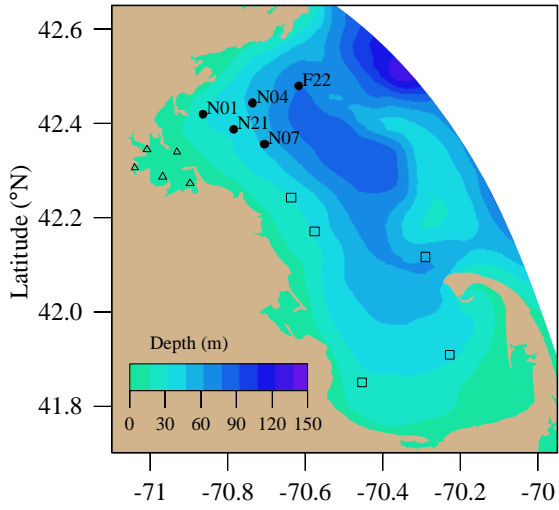
## 5.7 *Dissolved oxygen*

The observed seasonal cycle in dissolved oxygen concentration (peak in spring, decrease through summer to minimum in late fall, then increase) in 2015 was reproduced well by the model at Massachusetts Bay and Cape Cod Bay stations (Figure 5-9a,b). As noted above (Figure 5-1) the correlation between modeled and observed DO concentrations was 0.94 near the bottom, with root-mean square (RMS) error of  $0.48 \text{ mg L}^{-1}$ . Concentrations are highest in spring and lowest in late summer, with values near the surface generally higher than near the bottom. The late summer and fall observed values at F02 and, to a lesser extent, F01 were substantially lower than at other stations, a feature the model did not capture. The model-observation differences in the 2015 simulation were similar in magnitude to those of previous years. Model DO concentration on the west-east transect (Figure 5-9c) showed the same general patterns as those found in previous years but with somewhat less-pronounced vertical structure, which could be due to the weak or absent spring phytoplankton bloom which would further increase near-surface concentrations.

DO percent saturation depends on temperature and salinity as well as oxygen concentration, and is a useful quantity to help understand the relative influence of temperature and photosynthesis on DO. Percent saturation above 100% can result from photosynthetic production. We computed DO saturation from observations of DO concentration, temperature, and salinity using the approximate relation given in equation 2.3 of Zhao et al. (2012). Comparisons between this result and observed DO saturation (Figure 5-10a, b) reveal reasonable agreement. The pattern is similar at most stations, and on the east-west transect (Figure 5-10c), with reaeration due to exchange between atmosphere and ocean playing a dominant role as described by Xue et al. (2014). In winter, DO saturation levels are modest due to weaker reaeration, and vertical mixing keeps them nearly vertically uniform; in spring, photosynthesis helps increase surface values, which remain higher through summer when reaeration is most active, while levels in deeper water steadily decrease because they are isolated by stratification. The deep minimum is reached in late summer, after which the fall overturn returns the system to winter conditions.

Finally, model DO concentration and percent saturation have also been compared (Figure 5-11) directly to the only available time series observations of DO, from near the surface (2 m deep) and 51 m deep at the Mooring A01 site (see Figure 1-1) in northeastern Massachusetts Bay. In order to minimize the influence of intermittent sensor noise due to bubble sweepdown, daily medians of the raw hourly near-surface measurements are used. The daily medians are averaged over 3 day

intervals to match the temporal resolution of the model output. The general patterns of seasonal variations in the model, as described above, are similar to the observations. However, the model oxygen concentration (upper frame, Figure 5-11) near the surface is systematically lower than observed; it is recognized that the observations can require calibration offsets at least as large as these differences, and the process of ground-truthing and correcting the observations for these offsets is still underway as of the time of publication of this report. Due to the high winds during the early months of 2015 (discussed above), vertical mixing can be expected to have been vigorous such that the observations from near the surface and near the bottom should be nearly the same, as occurs in the model results. Presuming that a constant calibration offset was present in the observations, this implies that a negative offset correction is applicable to the shallow sensor, such that corrected results from both sensors would align with the shallow and deep model outputs (nearly equal to each other) during that time of the year. For DO percent saturation (lower frame, Figure 5-11) the relationships between model results and observations are similar to those for DO concentration. These model results, for both DO concentration and DO percent saturation, and for both annual-mean levels and seasonal variations about them, are similar to model simulations of past years.



**Black:** Observations near-surface, model at surface  
**Red:** Observations near-seafloor, model at seafloor

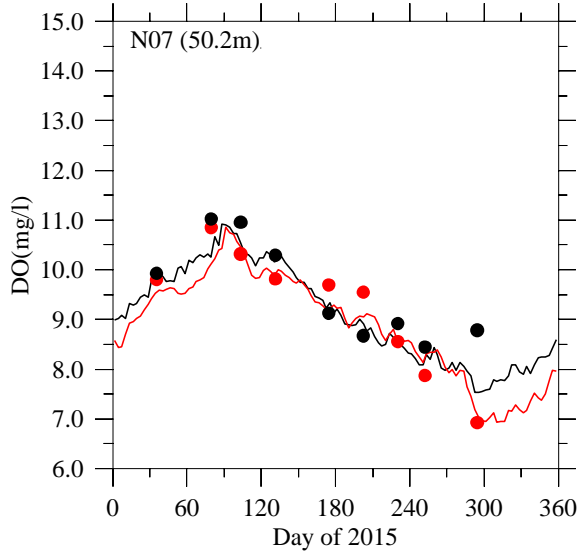
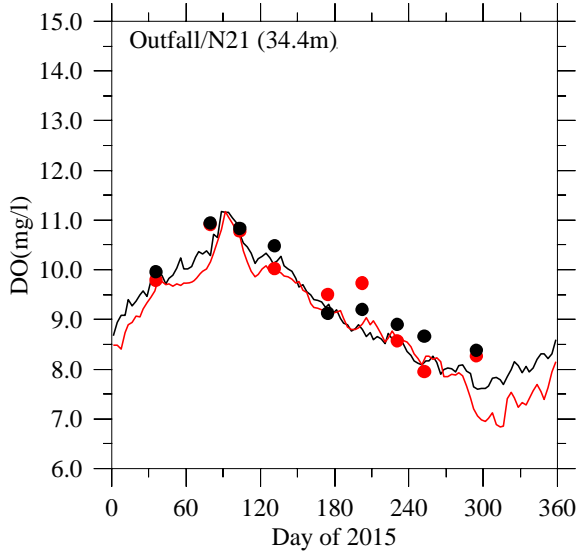
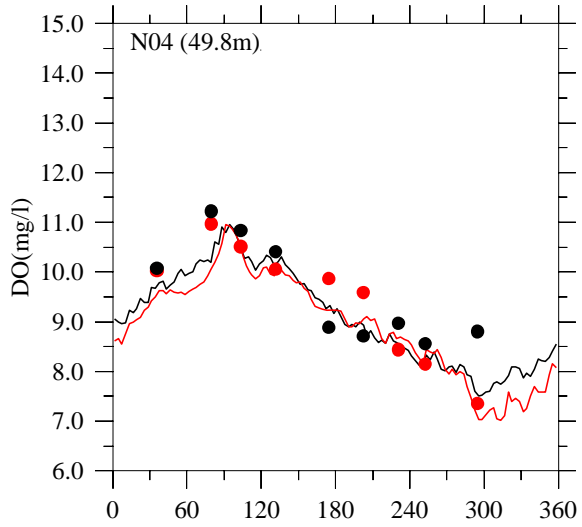
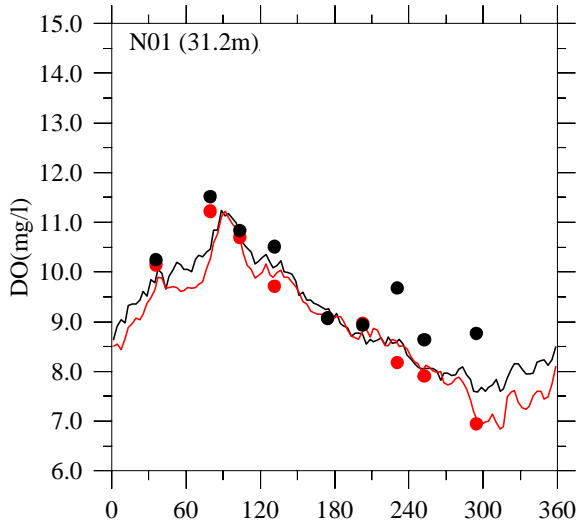
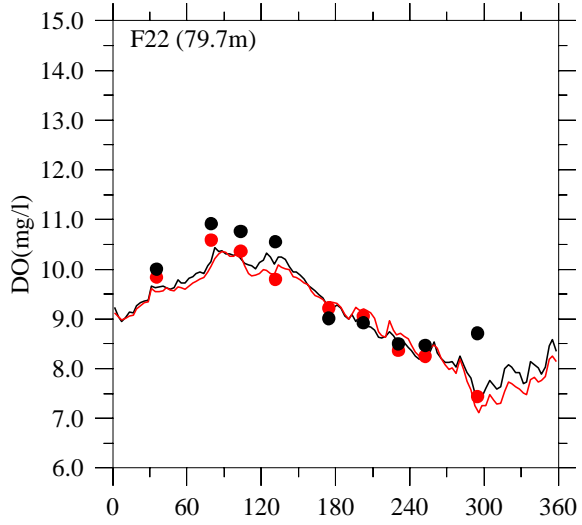
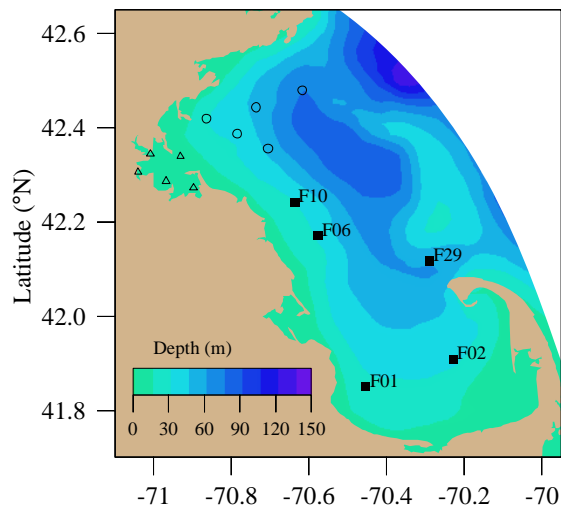


**Figure 5-9a.** Oxygen concentration. Northern stations. Model-observation comparisons.



**Black:** Observations near-surface, model at surface  
**Red:** Observations near-seafloor, model at seafloor

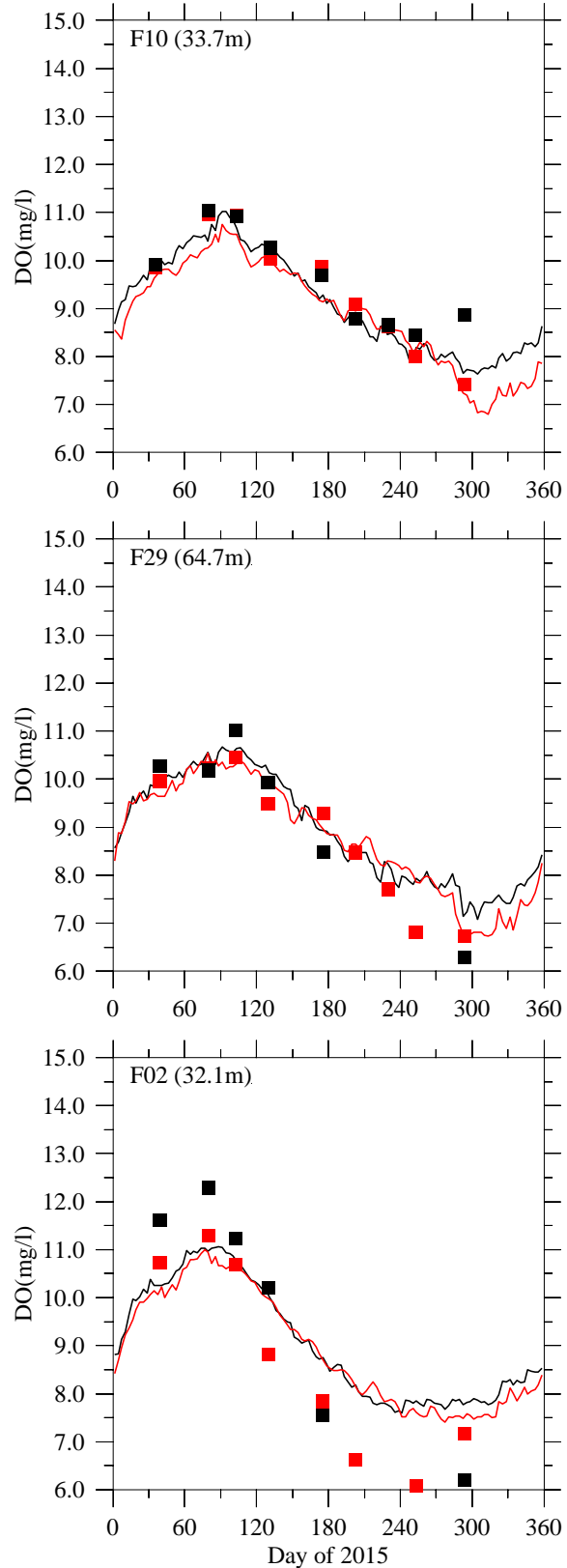
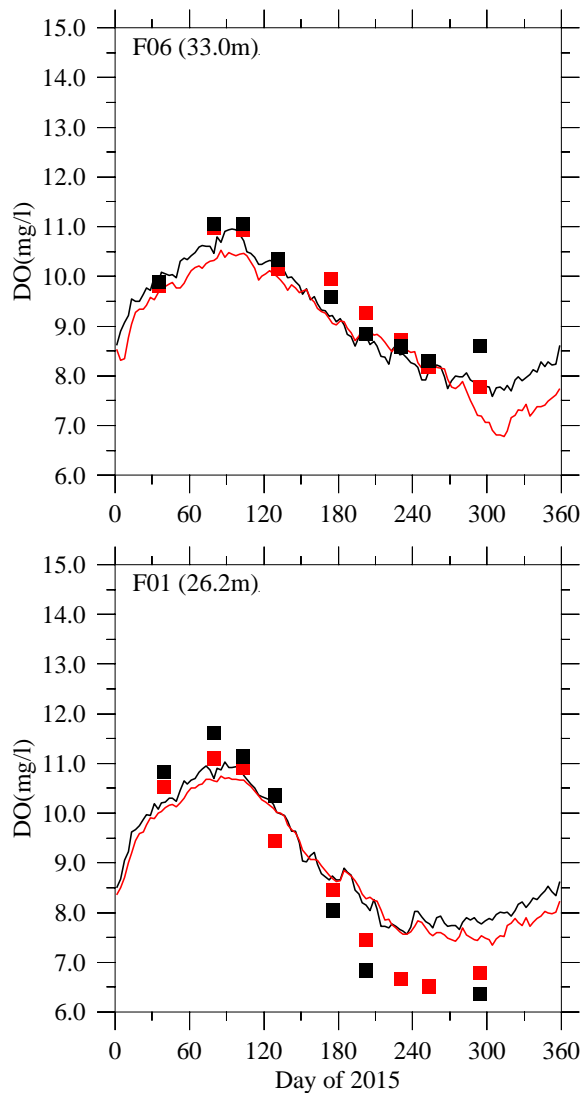


**Figure 5-9b.** Oxygen concentration. Southern stations. Model-observation comparisons.

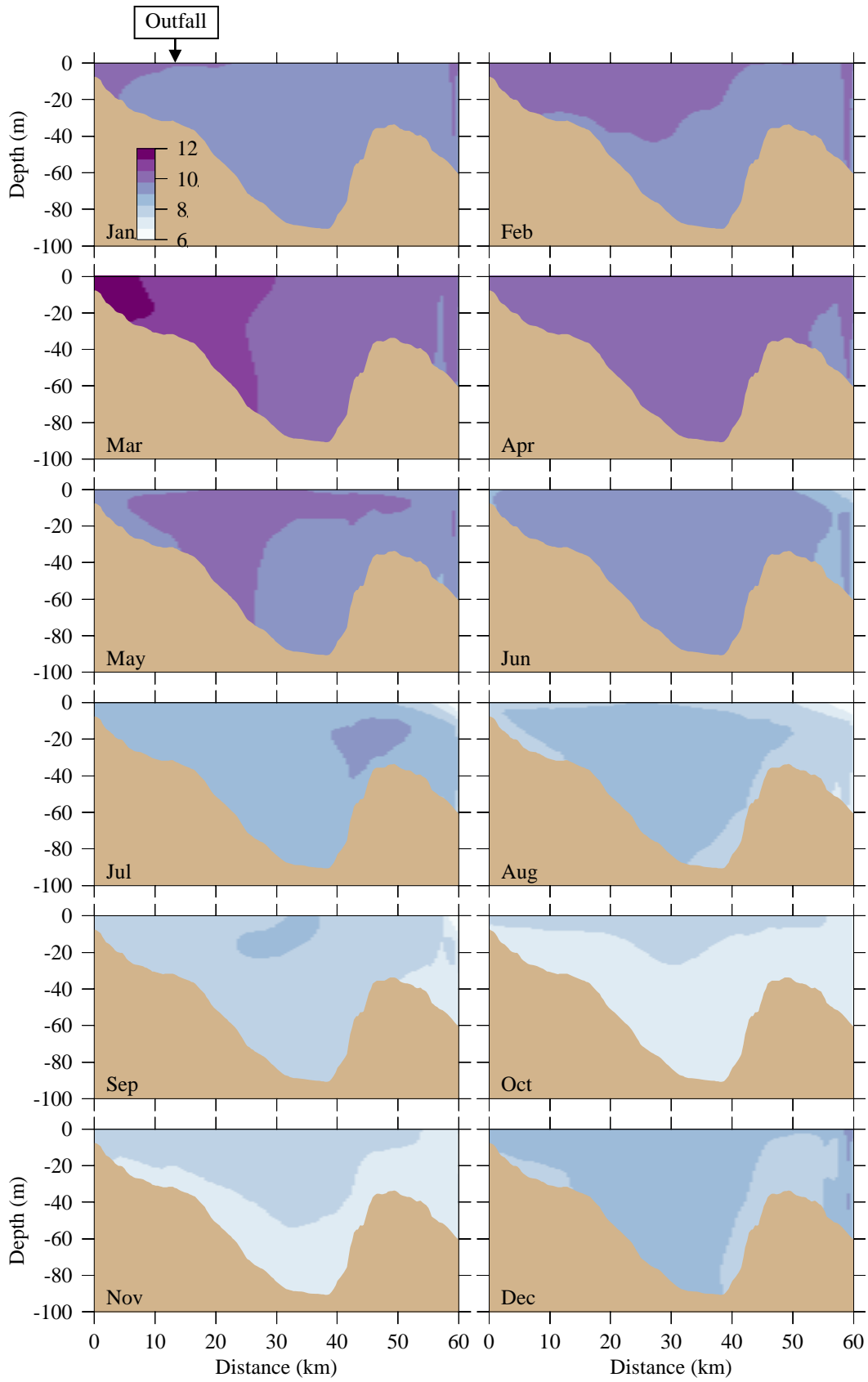


**Figure 5-9c.** Oxygen concentration ( $\text{mg L}^{-1}$ ). Model results, east-west transect (Fig. 3-7). Horizontal axis is distance eastward from coast; outfall is on seafloor at approximately 13 km.

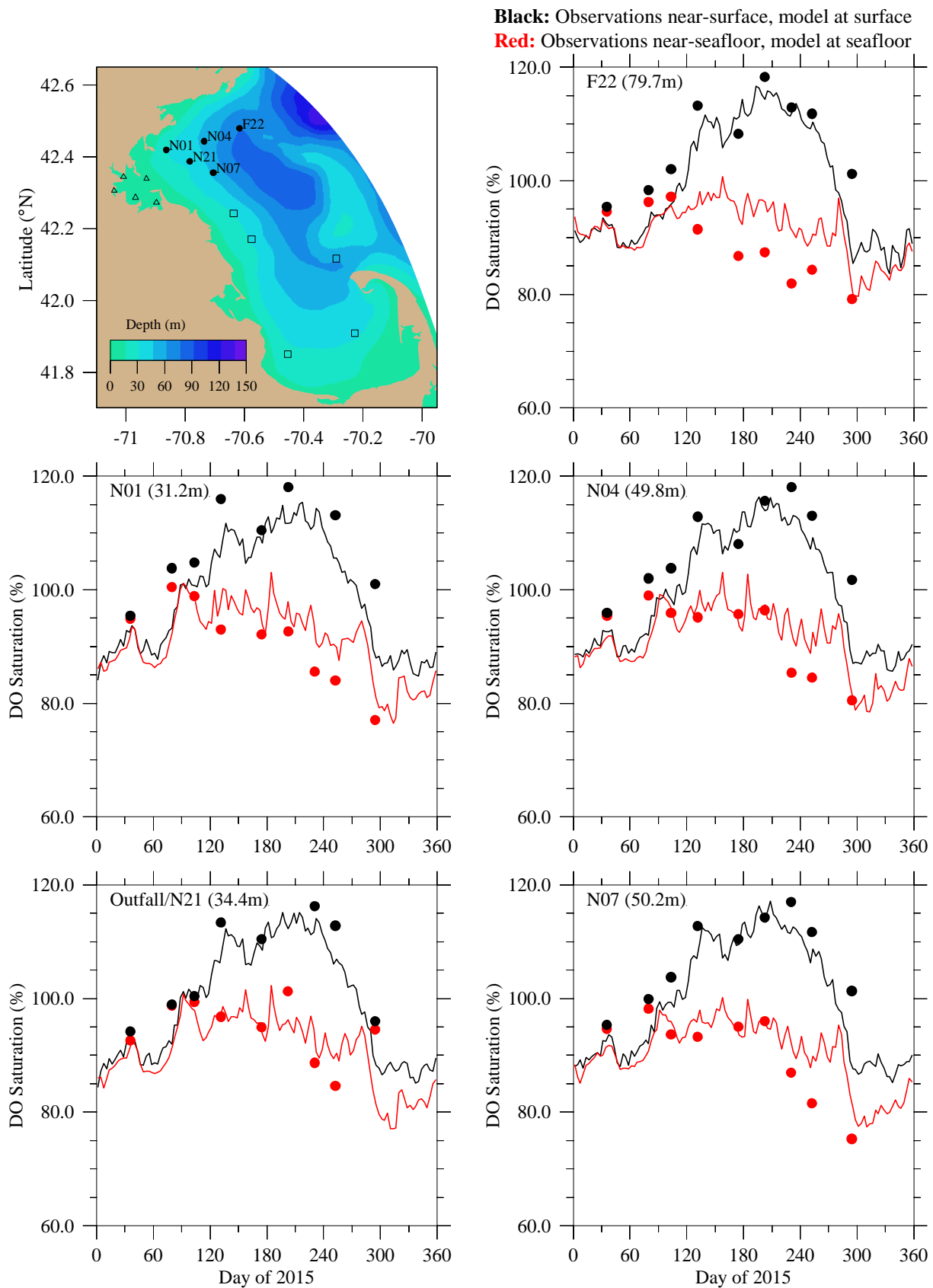
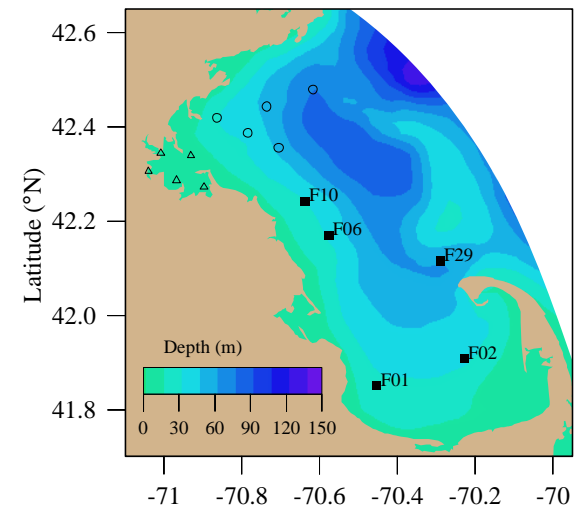


**Figure 5-10a.** Oxygen percent saturation. Northern stations. Model-observation comparisons.



**Black:** Observations near-surface, model at surface  
**Red:** Observations near-seafloor, model at seafloor

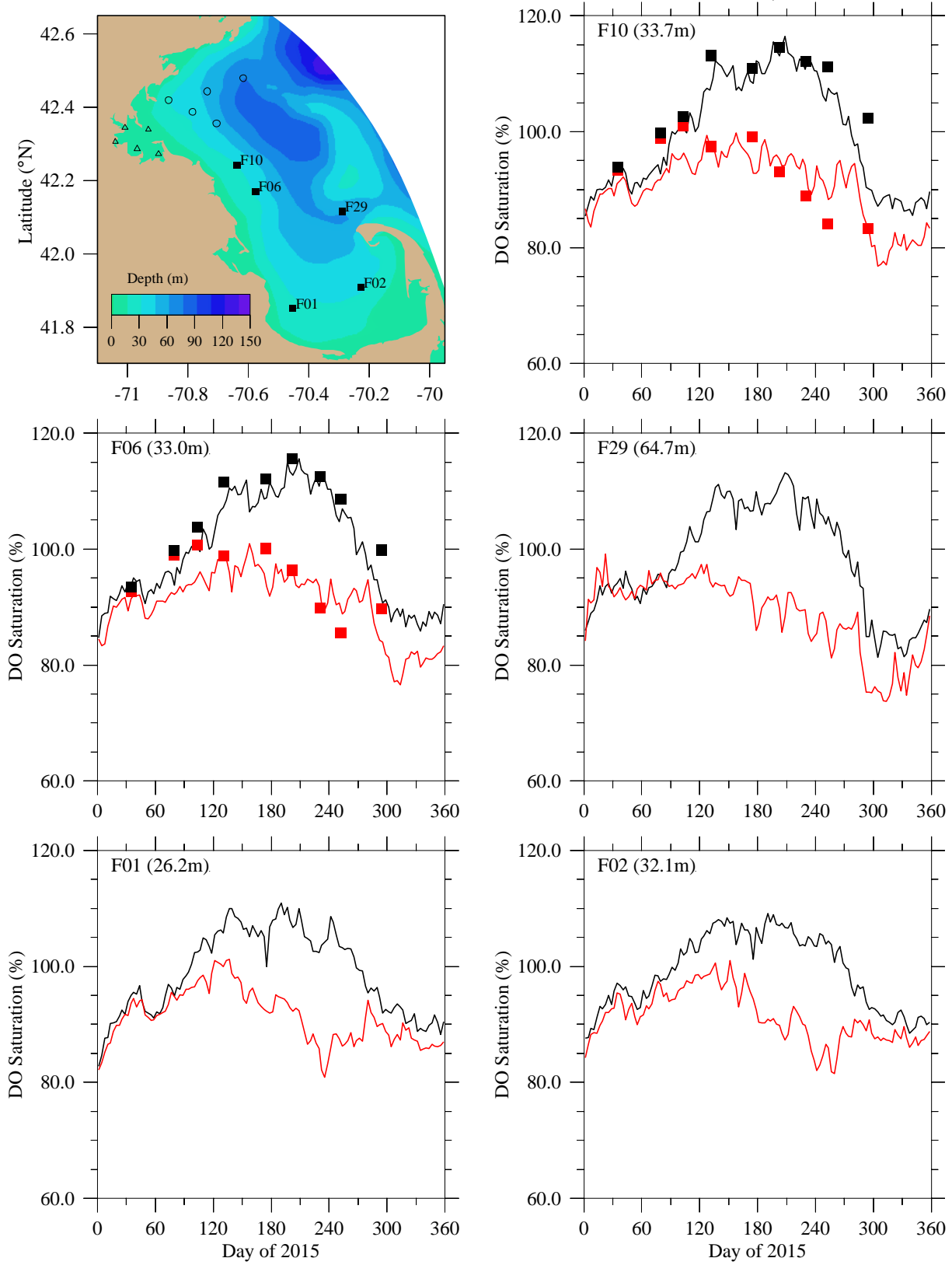


**Figure 5-10b.** Oxygen percent saturation. Southern stations. Model-observation comparisons.

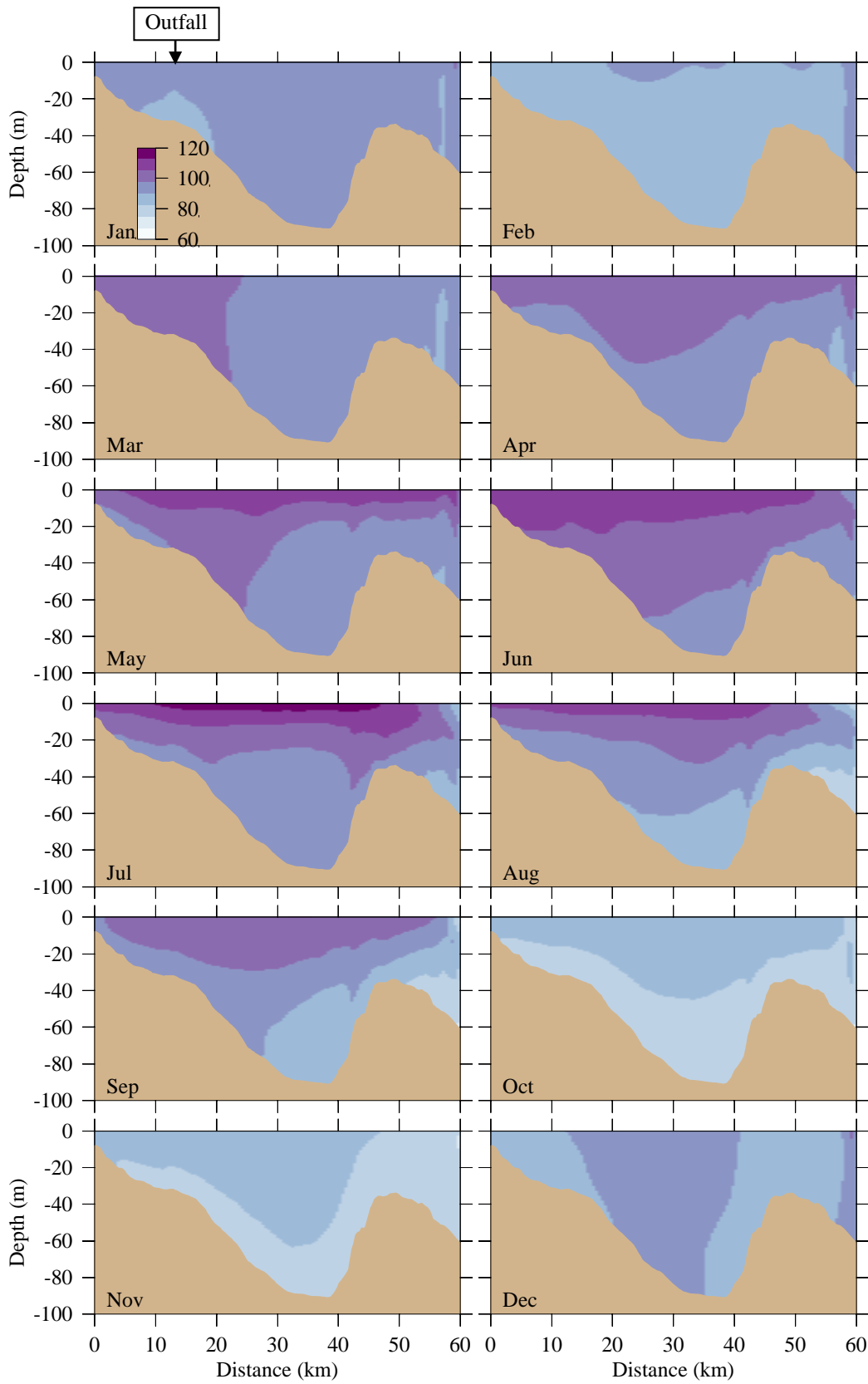


**Figure 5-10c.** Oxygen percent saturation. Model results, east-west transect (Fig. 3-7). Horizontal axis is distance eastward from coast; outfall is on seafloor at approximately 13 km.

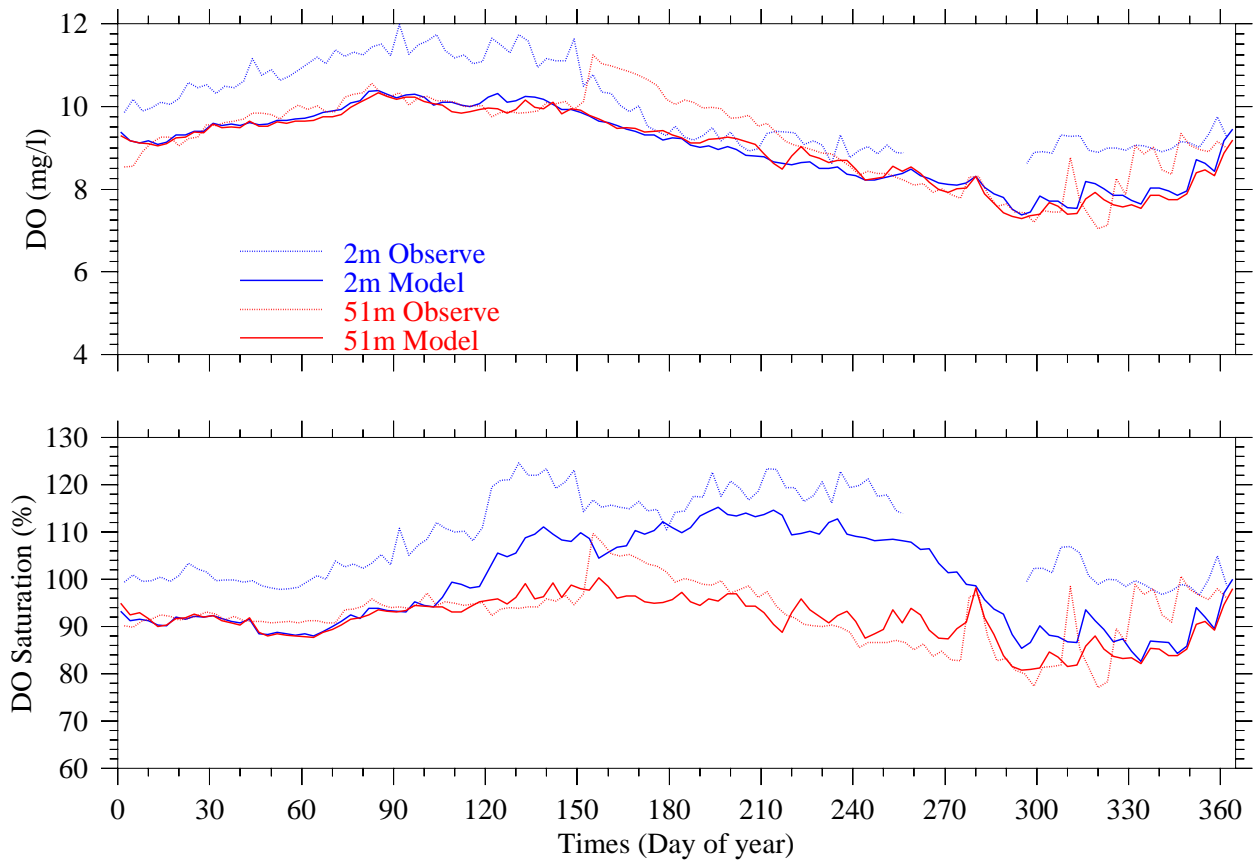


**Figure 5-11.** Oxygen time series, Mooring A01 site, model-observation comparison.

## 5.8 *Sediment fluxes*

Sediment  $\text{NH}_4^+$  fluxes and sediment oxygen demand (SOD) from the 2015 simulation are shown in Figure 5-12 and Figure 5-13, for the Massachusetts Bay and Boston Harbor stations where flux measurements had been made most consistently in earlier years to best facilitate model-observation comparisons. Ongoing field sampling no longer includes these benthic fluxes, but to provide context the observations from 2000-2010 are superimposed as box-whisker plots (as described in Section 5.4) on the model results (the field program and its results are described in MWRA technical reports, for example Tucker et al., 2010). Observations from prior to 2001 were not included, because diversion of the outfall to its current location occurred in 2000. At harbor stations the model  $\text{NH}_4^+$  flux in 2015 was nearly zero except during about 5 months from summer to early fall, when it was systematically lower than the central range of observed values except at BH03 during summer and early fall. At bay stations it was nearly zero except between May and December, when model values were generally within the range of historic observations, though they were higher than observations at stations MB03 and MB05 in the fall. Model SOD at harbor stations exhibited seasonality, and low bias relative to observations, similar to the  $\text{NH}_4^+$  flux there. At bay stations, model SOD had similar seasonality to the  $\text{NH}_4^+$  flux there; relative to the range of observations, model values were low in the spring and early summer, near the lower end of the range in summer, and within or nearer to the range in fall. These characteristics and relationships to observations for the 2015 simulation are similar to those of simulations from earlier years.

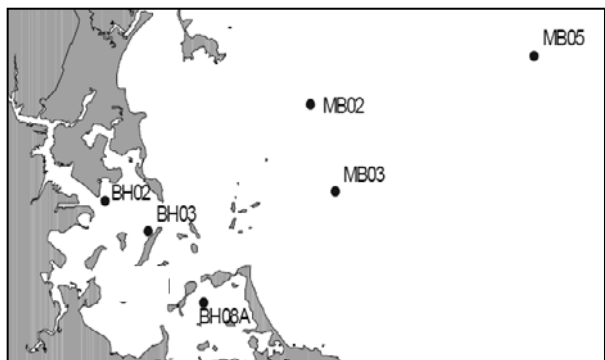
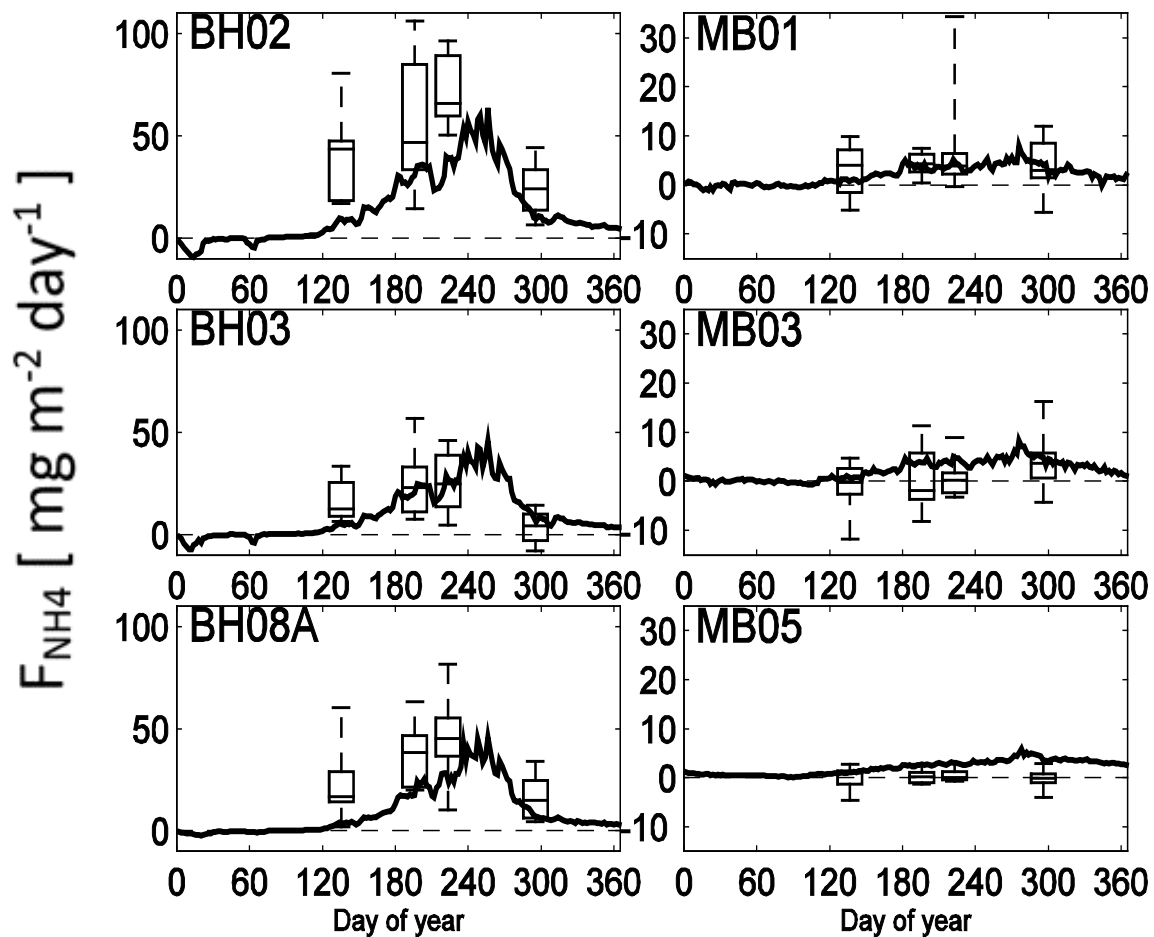


**Figure 5-12.** Sediment NH<sub>4</sub><sup>+</sup> flux. Model 2015 (line), observed 2001-2010 (box-whiskers). Select Boston Harbor stations (left column) and Massachusetts Bay stations (right column).

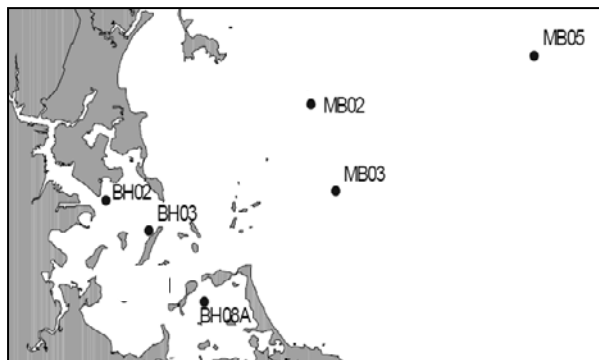
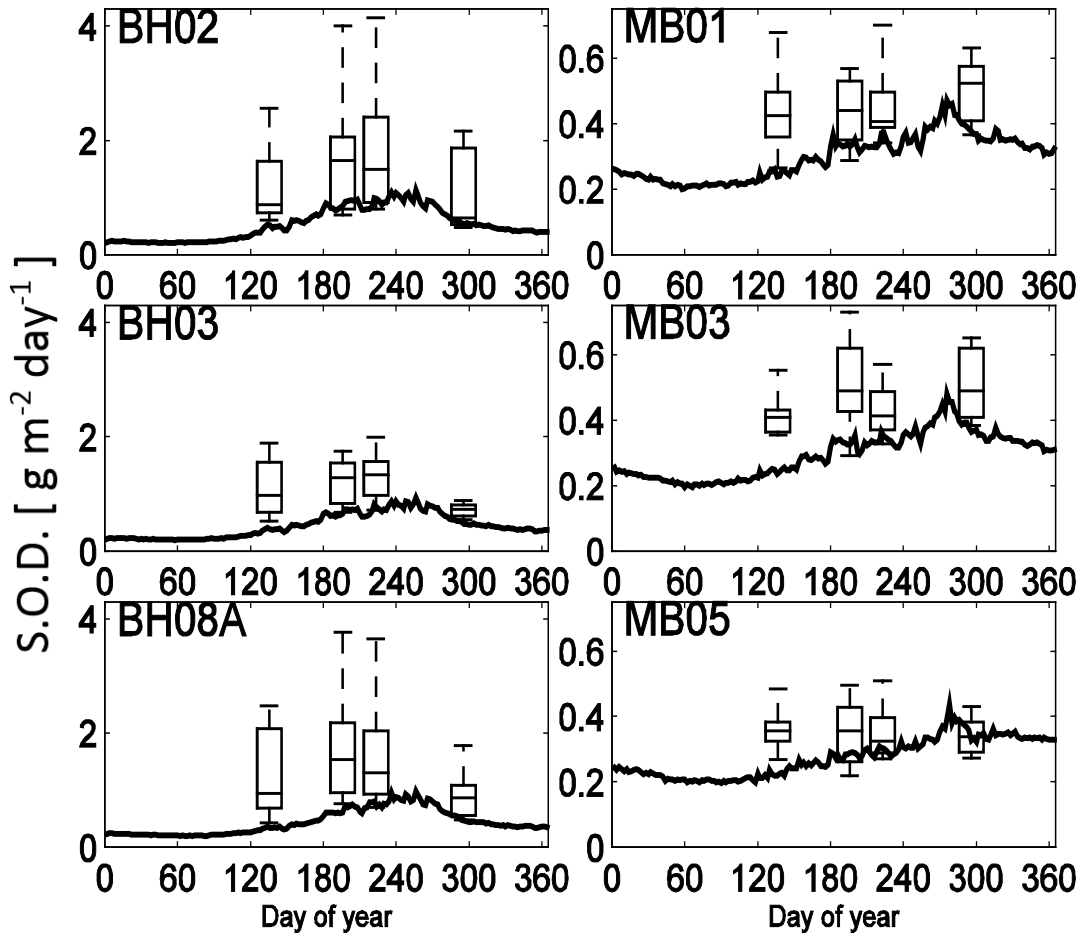


**Figure 5-13.** Sediment oxygen demand. Model 2015 (line), observed 2001-2010 (box-whiskers). Select Boston Harbor stations (left column) and Massachusetts Bay stations (right column).

## **5.9** *Summary*

In summary, the UG-RCA 2015 simulation captured many of the observed seasonal and vertical variations of an array of key water quality parameters examined here. Among them, agreement of the model with observations was generally strongest for DIN and DO, was modest for light, DON, and PON, and was weakest for POC and chlorophyll. Temporal and spatial variability in the model is typically less than observed, and at most stations surface-bottom differences in the model are smaller than observed. These results are typical of model-observation comparisons for the water quality parameters in BEM.

## 6. **Synthesis: Preliminary study of bay oxygen and chlorophyll variations in relation to inflow from offshore**

This section describes results of a preliminary investigation of the potential relationship between temporal variations in the water inflow on the northern boundary of Massachusetts Bay with variations of DO and chlorophyll concentrations within the bay. The hypothesis explored is that the major influence on DO and chlorophyll variability within the bay is variability of the inflowing current from offshore, and its associated physical transport of DO and chlorophyll—referred to as horizontal advection—as opposed to variability in biological processes local to the bay, in which the outfall may play a role. Advection was inferred by Geyer et al. (2002) to play a role in inter-annual variations of near-bottom DO at the outfall, based on correlations between inter-annual variations in observed near-bottom DO and temperature and salinity. In addition, analysis of observations and simulations by Xue et al. (2014) concluded that advection is important to seasonal variability of DO in northern Massachusetts Bay. This investigation uses the 21-year time series of the UG-RCA output over the period 1995-2015, for which UG-RCA results are available with 3-day time resolution. Temporal variability is examined on timescales from 3 days to inter-annual.

The transect used for the model net volume transport computation extends from Cape Ann about 18 km to the south and east (green line, Figure 1-1). The inflow to Massachusetts Bay typically occurs as a current flowing southward and westward south of Cape Ann, with a width that extends some distance from the coast. Because this distance varies but is generally not farther than 18 km offshore, computing the transport through this transect is considered to capture the inflow well. Volume transport is computed using the component of velocity perpendicular to the transect, with negative transport values corresponding to flow through the transect toward the south and west. Over the 21-year hindcast simulation the long-term mean (1995-2015) transport across the transect was  $-7.6 \times 10^4 \text{ m}^3 \text{ s}^{-1}$  directed in to Massachusetts Bay.

The 3-day, monthly-mean and annual-mean volume transport through the transect were computed, and the anomalies from the long-term mean transport are shown in the top frames of Figure 6-1, Figure 6-2, and Figure 6-3 respectively. Seasonal and inter-annual changes in transport anomaly are appreciable. Larger-magnitude anomalies, both positive and negative, tend to occur in the fall-winter seasons. Northeasterly winds are prevalent during that time of year, but anomalies of either sign can occur, for example depending on whether the frequency of nor'easter storms in each year is higher or lower than typical. Negative anomaly peaks (stronger flow in to Massachusetts

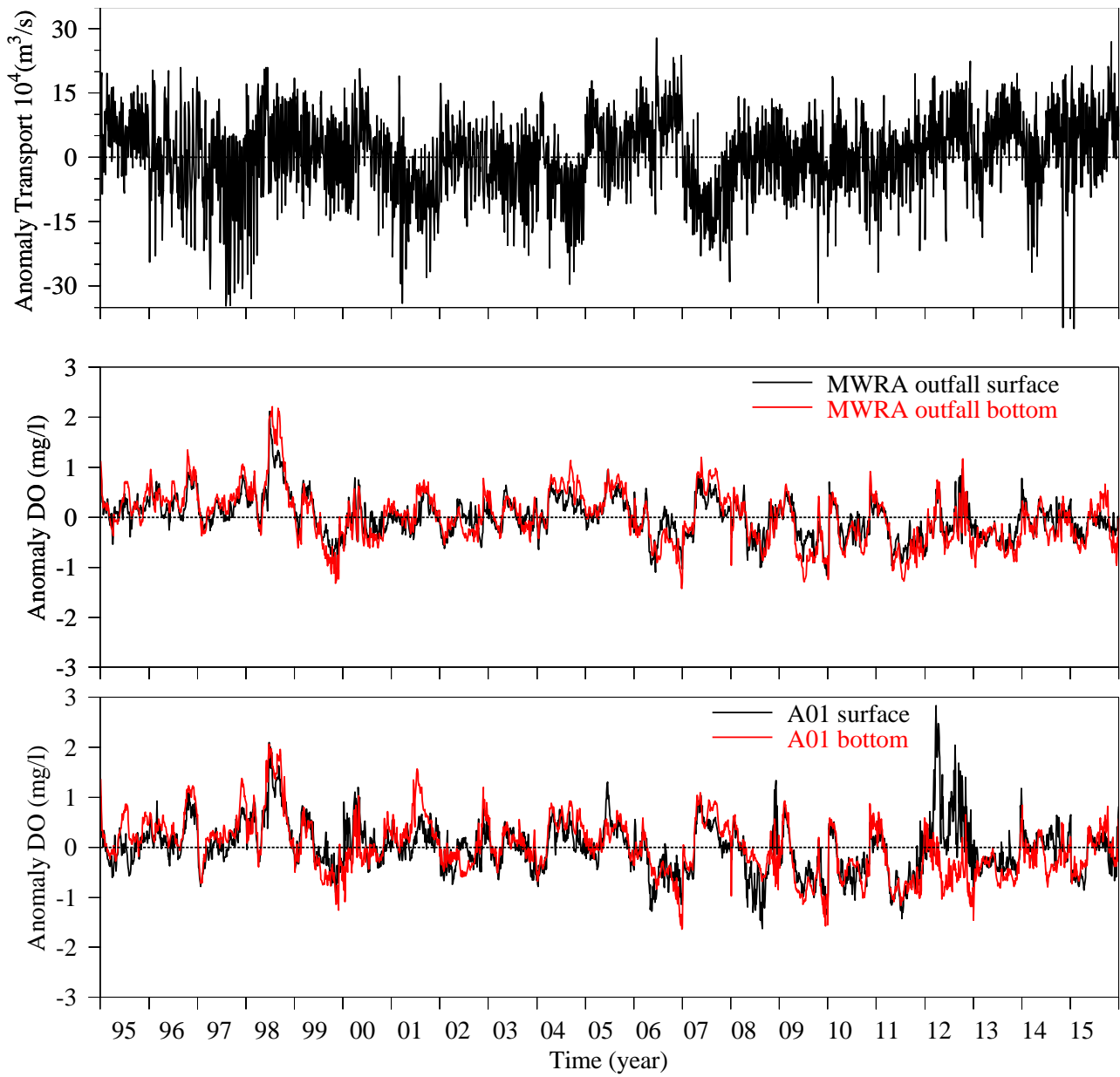


**Figure 6-1.** Transport anomaly and DO concentration anomalies, 3-day resolution.

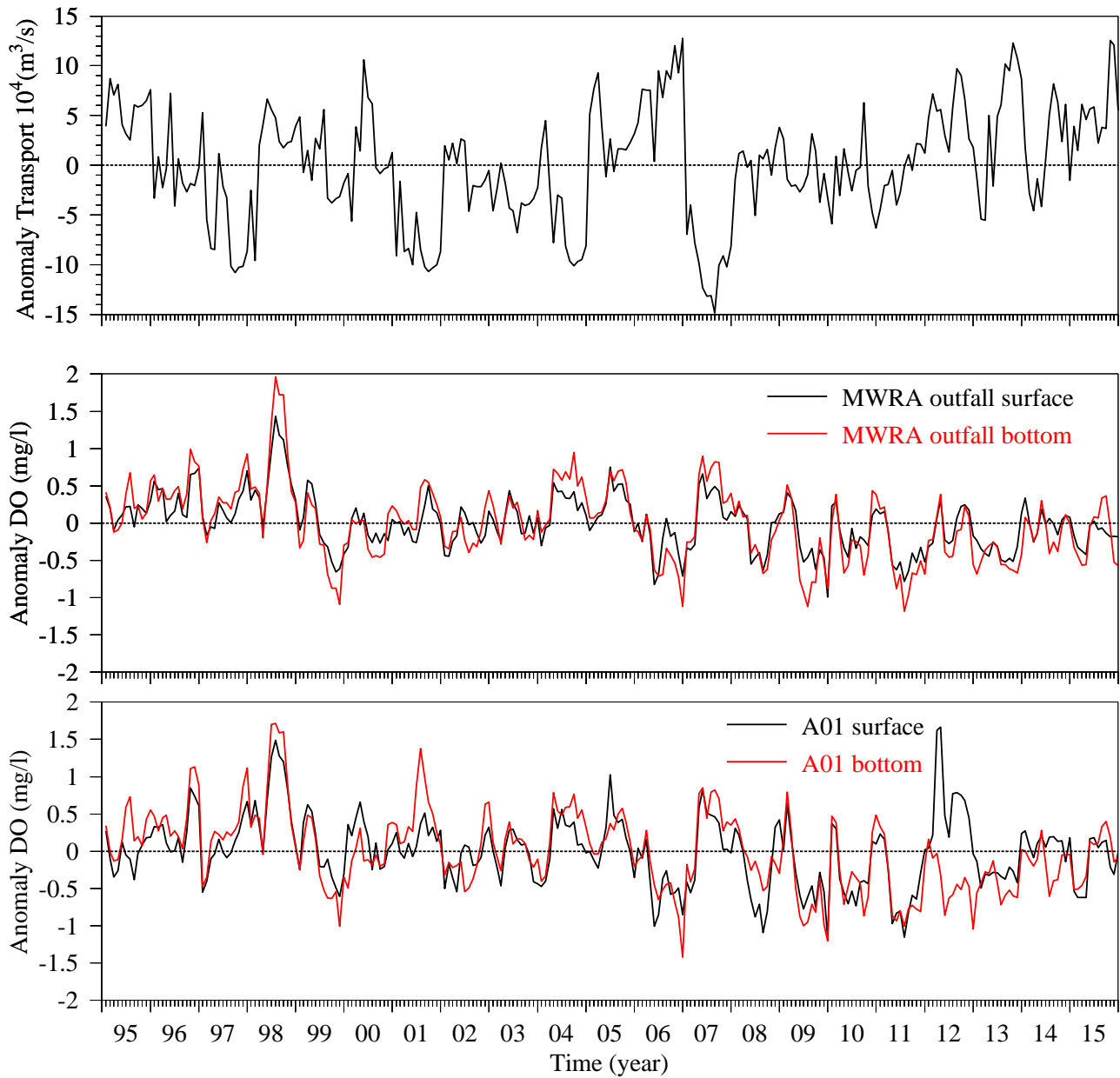


**Figure 6-2.** Transport anomaly and DO concentration anomalies, monthly-means.

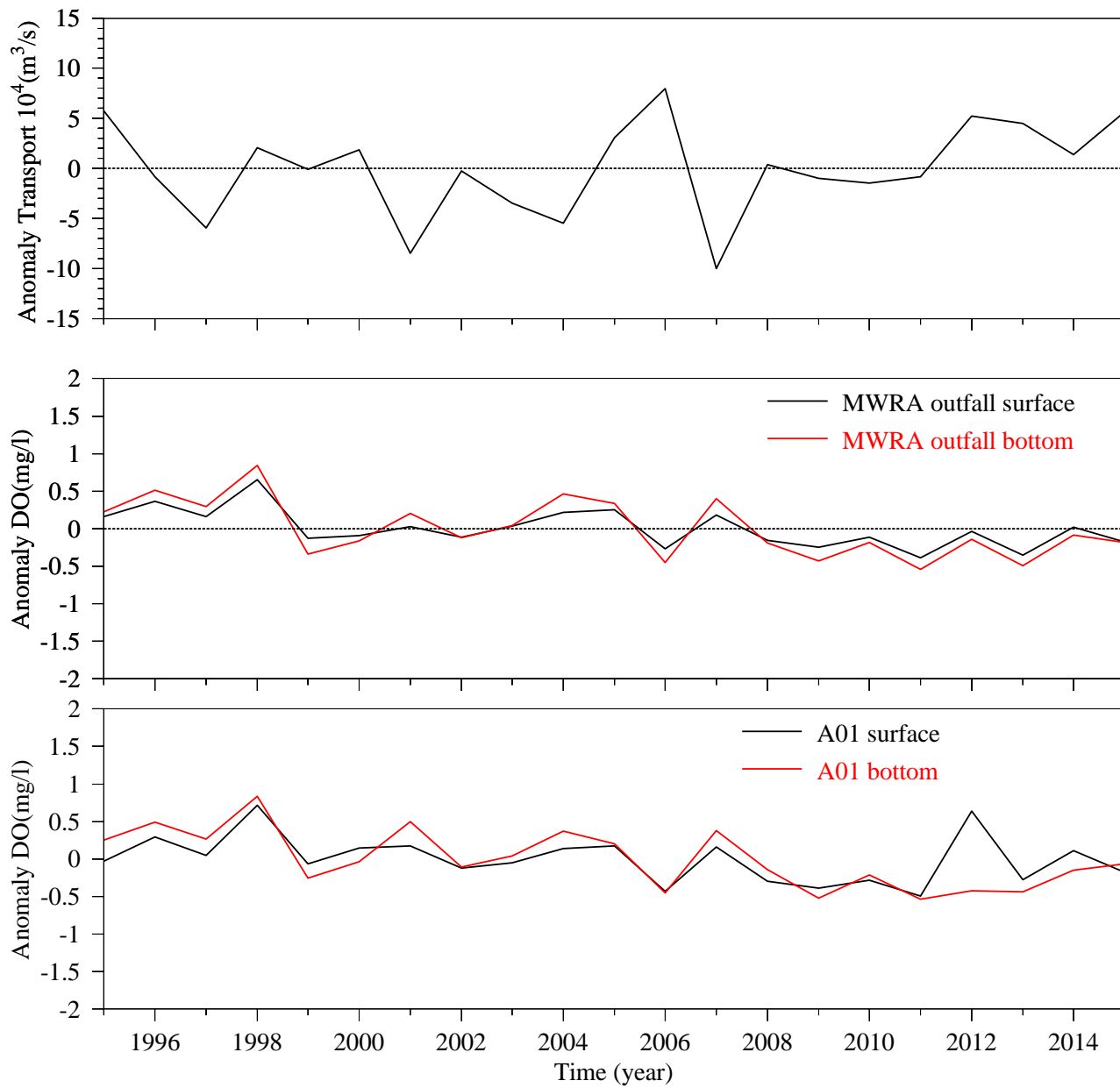


**Figure 6-3.** Transport anomaly and DO concentration anomalies, annual means.

Bay) occurred in winters of 1997, 2001, 2004, and 2007, and positive anomaly peaks were evident in fall-winter of 2000, 2005, 2007, 2012 and 2013.

Variability in model DO at the surface and at the seafloor was investigated at two locations (Figure 1-1): Mooring A01 about 7 km to the south and west of the transport transect, and the MWRA outfall about 24 km farther to the south and west. The near-surface inflow current typically ranges in strength from about 10 to 35 cm s<sup>-1</sup> (Section 4). The advective timescales, or durations it would take for water to travel over those distances at those speeds, range from about 6 hours to about 3.6 days. These are lower bounds because they assume motion in a direct line from point to point, while paths of actual currents are not direct. Near the bottom, currents are weaker, with a representative range roughly between 3 and 10 cm s<sup>-1</sup>, corresponding to a lower-bound advective timescale as long as about 12 days. These timescales are consistent with estimated residence times, for the larger area spanning all of the bay, that range from about 2 weeks to a few months (Geyer et al. 1992).

The 3-day, monthly-mean, and annual-mean surface and bottom anomalies in DO concentration, relative to the long-term (1995-2015) mean, at the outfall and Mooring A01 sites are shown in the middle and bottom frames respectively of Figure 6-1, Figure 6-2, and Figure 6-3. After some of the large negative volume transport anomaly (inflow to the bay) events, the DO anomaly is positive the following year. A prominent example was 1997-1998. Conversely, after some of the large positive anomalies, a negative DO anomaly occurred the following year. Table 6-1 shows results of correlation analysis between transport anomaly and DO concentration anomaly using the 3-day, monthly-mean, and annual-mean data. Correlations are negative, meaning a stronger inflow (negative transport anomaly) is associated with positive DO anomaly (higher DO concentrations). This is consistent with the expectation for higher DO offshore being advected in to the bay. Correlation coefficient magnitudes at the bottom are higher than at the surface, which is consistent with the expectation that advection is a larger contributor to DO variability at depth as opposed to near the surface, where air-sea interactions more strongly influence surface DO. Correlation coefficient magnitudes are highest (up to 0.30-0.42) at the monthly and annual timescales, which is consistent with the conclusions of Xue et al. (2014) that advection is important to seasonal variability and of Geyer et al. (2002) that advection is important to inter-annual variability.

If inward transport off Cape Ann advectively influenced DO at Mooring A01 or at the outfall, DO anomalies in the bay would occur with a time delay relative to transport anomalies off Cape

Table 6-1. Correlation coefficient of transport anomaly and DO concentration anomaly.

| Time    | A01_surf | A01_bot | Outfall_surf | Outfall_bot |
|---------|----------|---------|--------------|-------------|
| 3-day   | -0.07    | -0.21   | -0.09        | -0.18       |
| monthly | -0.12    | -0.35   | -0.18        | -0.30       |
| yearly  | -0.10    | -0.42   | -0.25        | -0.37       |

Ann. Correlations were therefore also computed, using the monthly-mean data, with inclusion of a lag between 0 and 6 months. Lags of up to 6 months were included based on the example of the 1998 positive DO anomaly, which occurred about 6 months later than the peak negative transport anomaly in September 1997. The resulting coefficients (Table 6-2) have lower magnitudes than the original correlations, and they decrease with increasing lag.

Table 6-2. Correlation coefficient of monthly-mean transport anomaly and lagged DO concentration anomaly.

| Time lag (month) | A01_surf | A01_bot | Outfall_surf | Outfall_bot |
|------------------|----------|---------|--------------|-------------|
| 0                | -0.10    | -0.36   | -0.16        | -0.30       |
| 1                | -0.07    | -0.31   | -0.14        | -0.27       |
| 2                | -0.03    | -0.25   | -0.07        | -0.20       |
| 3                | -0.05    | -0.24   | -0.08        | -0.19       |
| 4                | -0.01    | -0.19   | -0.06        | -0.16       |
| 5                | 0.03     | -0.12   | -0.02        | -0.11       |
| 6                | 0.01     | -0.11   | -0.05        | -0.09       |

Anomalies in chlorophyll concentration, computed the same way as the DO anomalies, are shown together with the transport anomalies at 3-day, monthly-mean, and annual-mean timescales in Figure 6-4, Figure 6-5, and Figure 6-6 respectively. Prominent relationships between transport anomaly and chlorophyll anomaly are not apparent on visual inspection. Correlations computed by the same methods as for DO, with and without lags (Table 6-3 and Table 6-4 respectively), give coefficient magnitudes that are mostly much smaller than those for DO. The magnitudes are generally higher at the surface than the bottom, which seems consistent with the known higher concentrations and therefore higher variability of chlorophyll at the surface. However, the signs of

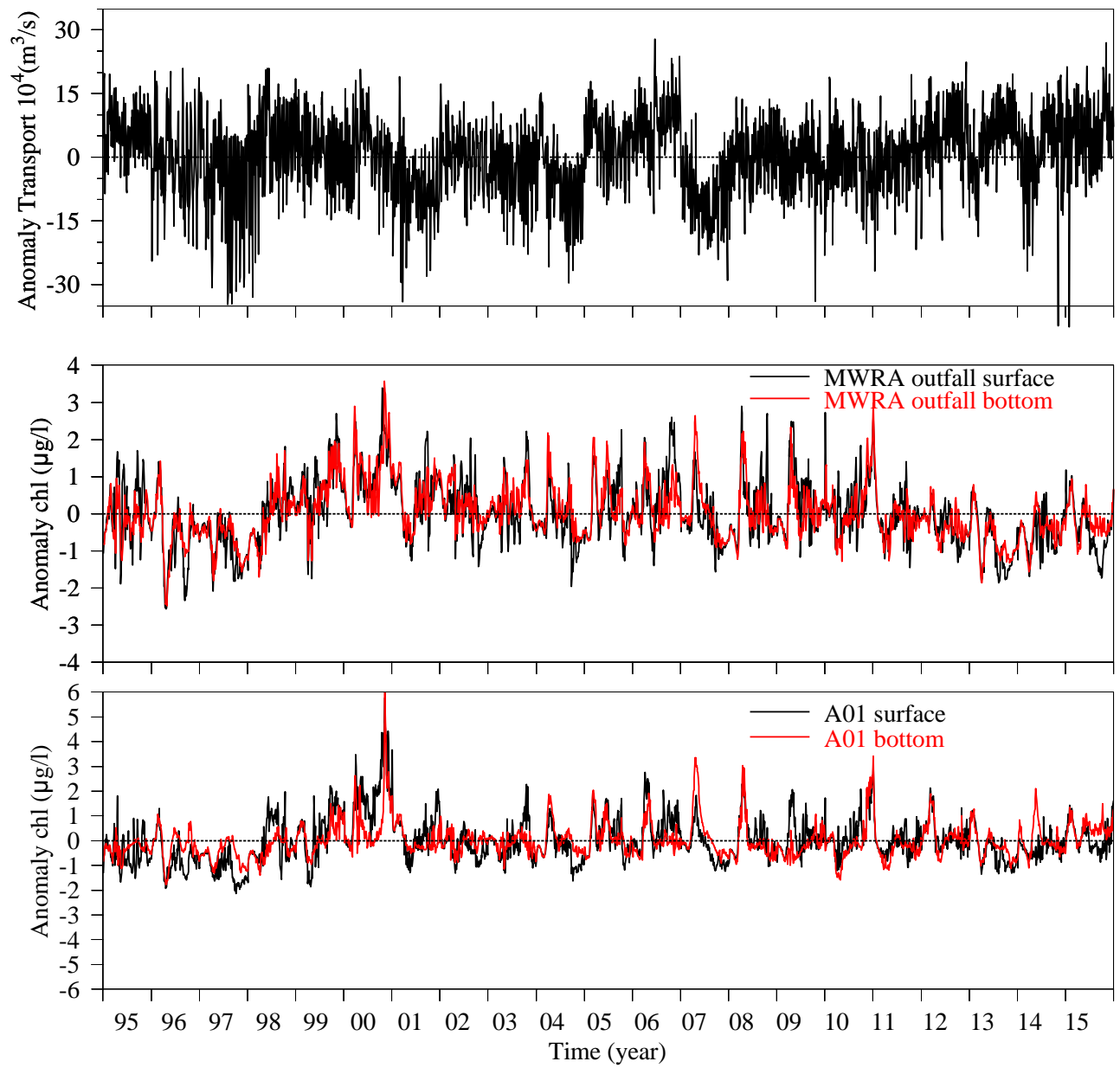


**Figure 6-4.** Transport anomaly and chlorophyll concentration anomalies, 3-day resolution.

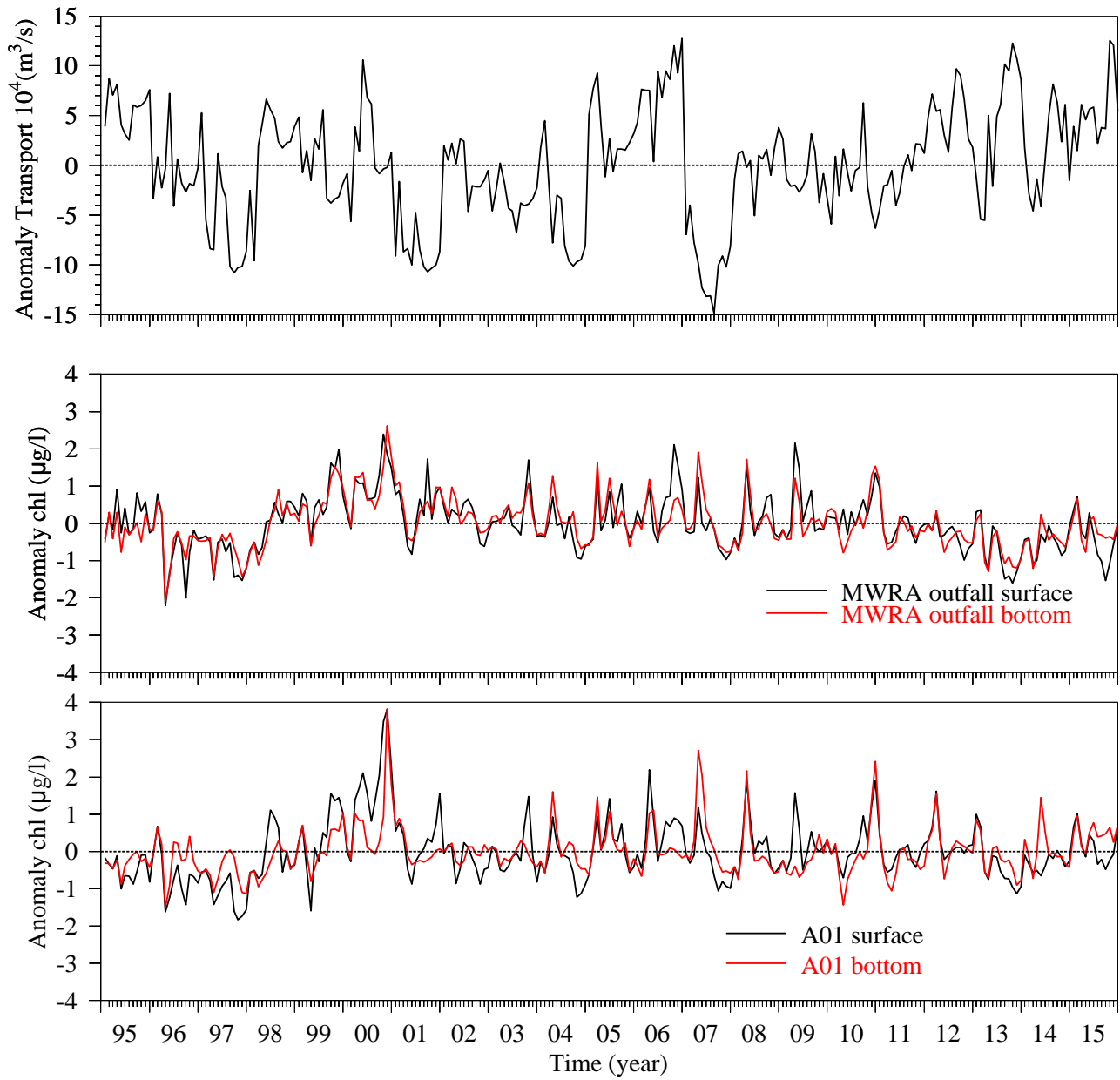


**Figure 6-5.** Transport anomaly and chlorophyll concentration anomalies, monthly means.

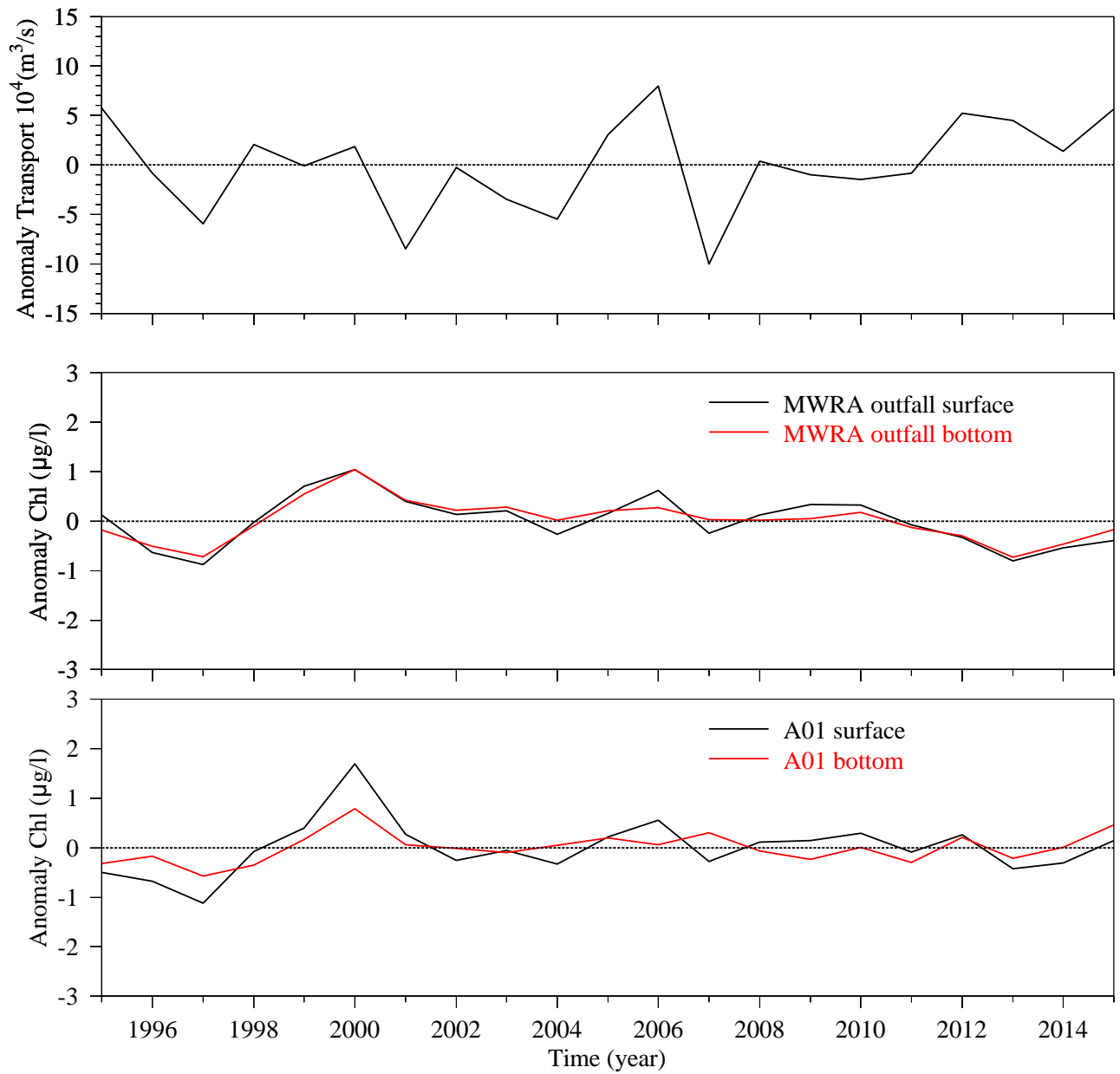


**Figure 6-6.** Transport anomaly and chlorophyll concentration anomalies, annual means.

Table 6-3. Correlation coefficient of transport anomaly and chlorophyll concentration anomaly.

| Time    | A01_surf | A01_bot | Outfall_surf | Outfall_bot |
|---------|----------|---------|--------------|-------------|
| 3-day   | 0.08     | -0.03   | 0.01         | -0.09       |
| monthly | 0.14     | -0.04   | 0.04         | -0.08       |
| yearly  | 0.27     | 0.11    | 0.10         | -0.08       |

Table 6-4. Correlation coefficient of monthly-mean transport anomaly and lagged chlorophyll concentration anomaly.

| Time lag (month) | A01_surf | A01_bot | Outfall_surf | Outfall_bot |
|------------------|----------|---------|--------------|-------------|
| 0                | 0.15     | -0.07   | 0.08         | -0.07       |
| 1                | 0.19     | 0.02    | 0.10         | 0.01        |
| 2                | 0.22     | 0.10    | 0.14         | 0.07        |
| 3                | 0.19     | 0.10    | 0.12         | 0.06        |
| 4                | 0.17     | 0.13    | 0.12         | 0.06        |
| 5                | 0.14     | 0.18    | 0.11         | 0.06        |
| 6                | 0.08     | 0.19    | 0.07         | 0.03        |

the correlation coefficients are mostly positive at the surface and negative at the bottom, for which the responsible process is not obvious. In the lagged correlations, for the surface results at both sites the coefficients at 2 month lag are marginally higher than for other lags. However, the magnitudes of the coefficients are small enough to limit confidence in any conclusions or interpretations that could be made.

In summary, for DO the correlation coefficients with transport have modest magnitudes, signs that are consistent with the expected current advection mechanism, and decreasing values when a lag is included. This suggests the importance of the flow from offshore in influencing seasonal and inter-annual variations of DO in the bay, a result that supports the findings of earlier studies. In contrast, for chlorophyll the correlation coefficients are not as high, and their signs are not easy to interpret in terms of a known process or mechanism. This suggests advection is not a major contributor to chlorophyll variability, based on this preliminary investigation. Differing results for DO and chlorophyll are not unexpected because, while DO and chlorophyll are related to each other, each is influenced by its own set of numerous processes.

In the event that a follow-on investigation was of interest, there are many possible modifications and extensions to the approach taken in this initial analysis. Instead of the volume transport, the

transport of DO or chlorophyll (computed as the product of the velocity and the DO or chlorophyll concentration) through the transect off Cape Ann could be computed and investigated. Additionally, instead of the transport through the transect at all depths, the transport in a near-bottom layer (expected to be more applicable to DO), and the transport in a near-surface layer (expected to be more applicable to chlorophyll), could be computed and investigated independently. Finally, ground-truthing the temporal variations in the model velocities (from which the transports are computed) against observed velocities (available at Mooring A01), and ground-truthing the temporal variations in the model DO and chlorophyll concentrations against observations, would increase confidence that the findings are applicable to Massachusetts Bay.

## 7. Summary

The Marine Ecosystem Dynamics Modeling Laboratory at University of Massachusetts Dartmouth simulated hydrodynamic and water quality parameters for calendar year 2015 in Massachusetts Bay, Cape Cod Bay, and Boston Harbor using the unstructured-grid Bays Eutrophication Model (BEM). BEM consists of a system of nested models including data-assimilative hydrodynamic simulations at global (Global-FVCOM), regional (GOM3-FVCOM), and coastal embayment (MB-FVCOM) scales, together with the UG-RCA water quality model applied within a subset of the latter.

The methods were the same as in the prior year's simulation (described in Zhao et al., 2016) except that the system was upgraded to be based on the regional model of the North East Coastal Ocean Forecast System (NECOFS). One major advantage of the new approach is that NECOFS is an operational product generated for, and being used by, many others meaning it is no longer necessary to independently execute the regional simulations dedicated to this project as has been done in past years.

The main features of observed seasonal cycles in temperature and salinity were captured well by the hydrodynamic model. The seasonal cycle of stratification in the model also agreed well with observations. Comparisons to observed currents were favorable.

Overall patterns in seasonal variations and vertical structure of many water quality parameters in the model were in good agreement with observations. In comparison to field measurements, the model typically showed a smaller range of values, and smaller surface-bottom differences during the stratified season. The well-known observed spring/summer reduction in shallow DIN concentrations due to phytoplankton uptake, and later fall replenishment due to enhanced mixing when stratification breaks down, were apparent in the model and consistent with observations. The model also reproduced the main characteristics of the observed seasonal cycle of DO, with peaks in spring when shallow values increase due to phytoplankton growth, followed by continuous decreases at depth through summer and early fall, with replenishment during the winter mixed period. In addition to these bay-wide patterns, near the seafloor local to the outfall (within 10-20 km) dissolved inorganic nitrogen was elevated, but this was not the case for other water quality parameters including chlorophyll. Agreement of model DON and PON with observations was modest, and model POC showed relatively poor agreement with measurements, particularly with regard to vertical structure. In summary, model-observation agreement was generally strongest for

DIN and DO, modest for DON and PON, and weakest for POC and chlorophyll. Overall, the simulations support the conclusions of the field monitoring program, that the outfall does not have an appreciable influence on bay-wide ecosystem function.

Agreement with observations was generally better for the hydrodynamic model than for the water quality model. This is not unusual, in the context of current research methods for simulations of coastal waterbodies such as Massachusetts Bay and Cape Cod Bay. In part this is a result of the less complete scientific understanding of the complex biological and chemical processes that are represented in water quality models. The model must include such processes but can only use substantially simplified formulations for them, leading to larger differences when compared to observations. In addition, for the biological and chemical parameters of the water quality model, observations available to drive and verify the model are less spatially and temporally extensive compared to parameters important to the hydrodynamic model. An example of the latter is that water temperatures, and the strength and direction of winds, are monitored at least hourly at multiple Gulf of Maine locations. In contrast, the most substantial field sampling effort for water quality parameters has been the MWRA Ambient Monitoring program, which consists of vessel-based surveys 3-4 weeks apart and focuses on measuring and understanding outfall effects, so can only partially characterize the regional nutrient and plankton dynamics.

To help improve understanding of temporal variability of dissolved oxygen and chlorophyll concentrations near the outfall, a preliminary investigation was carried out using a 21-year (1995-2015) hindcast simulation. The focus was the potential importance of variations in physical transport by the inflow to Massachusetts Bay occurring south of Cape Ann, as distinct from the influence of local biological processes which could be impacted by outfall discharge. The volume transport through a transect extending offshore from Cape Ann across the inflow was computed at 3-day temporal resolution, and the transport anomaly was computed relative to the long-term (1995-2015) mean. Near-surface and near-bottom model dissolved oxygen and chlorophyll concentrations from the same years at two locations—the Mooring A01 site between the transect and the outfall, and the outfall site—were used to compute anomalies similarly. Correlations between transport anomaly and dissolved oxygen and chlorophyll anomalies were computed for the 3-day record, monthly means, and annual means; lagged correlations were computed, using the monthly-means, for lags ranging from 0 to 6 months.

Results for dissolved oxygen included modest correlation coefficients, which decreased when lags were included. For the monthly means and annual means the deep anomalies were negatively correlated with the transport. This associates higher inflow (negative transport anomaly) with higher oxygen concentration, which is consistent with the hypothesized mechanism of offshore high-oxygen water moving in to the bay at depth causing an increase in bay concentrations. This is consistent with findings of prior studies, that variations in transport in to the bay are important to variability of DO at seasonal and inter-annual timescales within the bay (Xue et al., 2014 and Geyer et al., 2002, respectively). Results for chlorophyll differed from DO, as may be expected given that although chlorophyll is related to DO it is controlled by a wide range of processes different from those affecting DO. The correlation coefficients between chlorophyll and transport from offshore were low, and their signs were not easily interpretable in terms of the hypothesized mechanism. This preliminary investigation therefore suggests that variations in inflow from offshore do not make a major contribution to chlorophyll variability within the bay. A number of ways to enhance or expand the investigation have been identified and should be useful in the event it is revisited in the future.

## References

- Beardsley RC, EE Adams, D Harleman, A Giblin, JR Kelly, JE O'Reilly, and JF Paul, 1995. Report of the MWRA hydrodynamic and water quality model evaluation group. MWRA Enviro. Quality Dept. Misc. Rpt. No. ms-37. Boston: Massachusetts Water Resource Authority. 58pp. <http://www.mwra.state.ma.us/harbor/enquad/pdf/1995-ms-37.pdf>
- Becker S, 1992. The seasonal distribution of nutrients in Massachusetts and Cape Cod Bays. Masters Thesis, University of New Hampshire, Durham. 127pp.
- Blumberg A, Z Ji, and CK Ziegler, 1996. Modeling outfall plume behavior using a far field model, *J. Hydraulic Engineering*, 112: 610-616.
- Chen C, B Beardsley, GW Cowles, J Qi, Z Lai, G Gao, D Stuebe, Q Xu, P Xue, J Ge, R Hu, R Ji, R Tian, H Huang, H Wu, H Lin, Y Sun, and L Zhao, 2013. An Unstructured grid, Finite-Volume Community Ocean Model-FVCOM User Community-FVCOM user manual, School for Marine Science and Technology, University of Massachusetts Dartmouth, New Bedford, Fourth Edition. SMAST/UMASSD Technical Report-13-0701, 404pp.
- Chen, C, H Haung, RC Beardsley, Q Xu, R Limeburner, GW Gowles, Y Sun, J Qi and H Lin, 2011. Tidal dynamics in the Gulf of Maine and New England Shelf: An application of FVCOM. *J. Geophys. Res.*, 116. C12010, doi: 10.1029/2011JC007054.
- Chen, C, G Gao, Y Zhang, R Beardsley, Z Lai, J Qi, H Lin. 2016. Circulation in the Arctic Ocean: Results from a high-resolution coupled ice-sea nested Global-FVCOM and Arctic-FVCOM system. *Prog. Oceanogr.* 141 (2016), 60-80.
- Chen C, R Tian, RC Beardsley, J Qi, and Q Xu, 2010. Modeling 2008 in Massachusetts Bay using an upgraded unstructured-grid Bays Eutrophication Model. Boston: Massachusetts Water Resources Authority. Report 2010-15. 127pp. <http://www.mwra.state.ma.us/harbor/enquad/pdf/2010-15.pdf>
- Cowles, GW, SJ Lentz, C Chen, Q Xu, and RC Beardsley, 2008, Comparison of observed and model-computed low-frequency circulation and hydrography on the New England Shelf, *J. Geophys. Res.*, 113, C09015, doi:10.1029/2007JC004394.
- Fitzpatrick JJ and RA Isleib, 2003. Post-audit analysis of the impacts of wastewater treatment plant outfall relocation on Boston Harbor, Massachusetts Bay and Cape Cod Bay water quality Proceedings of the Water Environment Federation, WEFTEC 2003, pp. 530-555.
- Geyer, WR, PS Libby, and AE Giblin, 2002. Influence of physical controls on dissolved oxygen variation at the outfall site. Boston: Massachusetts Water Resources Authority. Letter Report, Task Order 35. 20 pp.
- Geyer, WR, G Gardner, W Brown, J Irish, B Butman, T Loder, R Signell, 1992. Physical oceanographic investigation of Massachusetts and Cape Cod Bays. Massachusetts Bays Program. U.S. EPA Region I / Massachusetts Coastal Zone Management Office, Boston, Massachusetts. Technical Report MBP-92-03. 497pp.
- Hunt CD, RK Kropp, JJ Fitzpatrick, P Yodzis, and RE Ulanowicz, 1999. A Review of Issues Related to the Development of a Food Web Model for Important Prey of Endangered Species in

- Massachusetts and Cape Cod Bays. Boston: Massachusetts Water Resources Authority. Report ENQUAD 99-14. 62 pp. <http://www.mwra.state.ma.us/harbor/enquad/pdf/1999-14.pdf>
- HydroQual, 1993. A water quality model for Massachusetts and Cape Cod Bays. Boston: Massachusetts Water Resources Authority. Report 1993-05. 222pp. <http://www.mwra.state.ma.us/harbor/enquad/pdf/1993-05.pdf>
- HydroQual, 1995. A water quality model for Massachusetts and Cape Cod Bays: Calibration of the Bay Eutrophication Model (BEM). Boston: Massachusetts Water Resources Authority. Report 1995-08. 402pp. <http://www.mwra.state.ma.us/harbor/enquad/pdf/1995-08.pdf>
- HydroQual, 2000. Bays Eutrophication Model (BEM): modeling analysis for the period 1992-1994. Boston: Massachusetts Water Resources Authority. Report 2000-02. 158pp. <http://www.mwra.state.ma.us/harbor/enquad/pdf/2000-02.pdf>
- HydroQual, 2001. Analysis of the addition of a third algal group to the Bays Eutrophication Model (BEM) kinetics. Boston: Massachusetts Water Resources Authority. Report ENQUAD 2001-15. 110pp.
- HydroQual, 2002a. Sensitivity of the Bays Eutrophication Model (BEM) to changes in algal model coefficients. Boston: Massachusetts Water Resources Authority Report 2002-16. 236pp. <http://www.mwra.state.ma.us/harbor/enquad/pdf/2002-16.pdf>
- HydroQual, 2002b. Addendum to the 1998-1999 hydrodynamic modeling report. Boston: Massachusetts Water Resources Authority. Report 2002-17. 82pp. <http://www.mwra.state.ma.us/harbor/enquad/pdf/2002-17.pdf>
- HydroQual, 2004. "User's Guide for RCA, Release 3.0", Hydroqual, Inc, New Jersey.
- Jiang M, GT Wallace, M Zhou, PS Libby and CD Hunt, 2007. Summer formation of a high-nutrient low-oxygen pool in Cape Cod Bay, USA, *J. Geophys. Res.*, **112**, C05006, doi:10.1029/2006JC003889.
- Jiang M, and M Zhou, 2004. Calibration of the Massachusetts and Cape Cod Bays hydrodynamic model: 2000-2001. Boston: Massachusetts Water Resources Authority. Report 2004-08. 71pp. <http://www.mwra.state.ma.us/harbor/enquad/pdf/2004-08.pdf>
- Key KE, WS Leo, and PS Libby, 2012. Comparisons of Model-Predicted and Measured Productivity in Massachusetts Bay. Boston: Massachusetts Water Resources Authority. Report 2012-03. 11 p. plus Appendix. <http://www.mwra.state.ma.us/harbor/enquad/pdf/2012-03.pdf>
- Li Y, PS Fratantoni, C Chen, JA Hare, Y Sun, RC Beardsley, R Ji, 2015. Spatio-temporal patterns of stratification on the Northwest Atlantic shelf. *Prog. Oceanog.* 134, p123-137. <http://dx.doi.org/10.1016/j.pocan.2015.01.003>
- Libby PS, DG Borkman, WR Geyer, JT Turner, AS Costa, DI Taylor, and DL Codiga, 2016. 2015 Water column monitoring results. Boston: Massachusetts Water Resources Authority. Report 2016-12. 45 pp. <http://www.mwra.state.ma.us/harbor/enquad/pdf/2016-12.pdf>
- Libby PS, C Gagnon, C Albro, M Mickelson, A Keller, D Borkman, J Turner, and CA Oviatt, 2005. Combined work/quality assurance plan for baseline water quality monitoring: 2004-2005. Boston: Massachusetts Water Resources Authority. Report 2005-09. Version 1. 76 pp., plus appendices. <http://www.mwra.state.ma.us/harbor/enquad/pdf/2005-09.pdf>

- Limeburner, R (Editor), 1985. CODE-2: Moored Array and Large-Scale Data Report. Woods Hole Oceanographic Institution Technical Report 85-35, 234pp.
- Menzie CA, JJ Cura, Jr, JS Freshman, and B Potocki, 1991. Boston Harbor: estimates of loadings. Boston: Massachusetts Water Resources Authority. Report 1991-04. 108pp.  
<http://www.mwra.state.ma.us/harbor/enquad/pdf/1991-04.pdf>
- Menzie-Cura and Associates, 1991. Sources and loadings of pollutants to the Massachusetts Bay. Report to the Massachusetts Bays Program. Report No. MBP-1991-01.
- Montoya JP, KM Rathbun, and CS Mayo, 2003. Information Briefing to Outfall Monitoring Science Advisory Panel. Recent nitrogen isotope data from Massachusetts and Cape Cod Bays. January 6, 2003. 8 pp.
- Sun C, & co-authors, 2010. "The Data Management System for the Global Temperature and Salinity Profile Programme" in Proceedings of OceanObs.09: Sustained Ocean Observations and Information for Society (Vol. 2), Venice, Italy, 21-25 September 2009. Hall, J, DE Harrison, and D Stammer, Eds., ESA Publication WPP-306, doi:10.5270/OceanObs09.cwp.86.
- Sun Y, C Chen, RC Beardsley, D Ullman, B Butman, and H Lin, 2016. Surface circulation in Block Island Sound and adjacent coastal and shelf regions: A FVCOM-CODAR comparison, *Prog. Oceanogr.*, 143, p 26-45, DOI:10.1016/j.pocean.2016.02.005.
- Taylor DI, 2015. Boston Harbor Water Quality 1994-2014. Boston: Massachusetts Water Resources Authority. Report 2015-05. 11 p.  
<http://www.mwra.state.ma.us/harbor/enquad/pdf/2015-05.pdf>
- Tian, RC, C Chen, Q Xu, PF Xue, GW Cowles, RC Beardsley, and B Rothschild, 2009. Massachusetts Bay Eutrophication Model: 2006-2007 Simulation. Boston: Massachusetts Water Resources Authority. Report 2009-11. 147pp.  
<http://www.mwra.state.ma.us/harbor/enquad/pdf/2009-11.pdf>
- Tian, RC, C Chen, LZ Zhao, P Xue, WS Leo, MJ Mickelson, 2010. Modeling 2009 in Massachusetts Bay using the unstructured-grid Bays Eutrophication Model. Boston: Massachusetts Water Resources Authority. Report 2010-22. 100pp.  
<http://www.mwra.state.ma.us/harbor/enquad/pdf/2010-22.pdf>
- Tucker J, and AE Giblin, 2002. Stable isotope analyses of sediment and invertebrate samples from Boston Harbor and Massachusetts Bay. Boston: Massachusetts Water Resources Authority. Report 2002-21. 24 p. <http://www.mwra.state.ma.us/harbor/enquad/pdf/2002-21.pdf>
- Tucker J, AE Giblin, CS Hopkinson, Jr, and D Vasiliou, 2000. Benthic nutrient cycling in Boston Harbor and Massachusetts Bay: 1999 annual report. Boston: Massachusetts Water Resources Authority. Report 2000-11. 63 p. <http://www.mwra.state.ma.us/harbor/enquad/pdf/2000-11.pdf>
- Tucker J, S Kelsey, and AE Giblin, 2010. 2009 benthic nutrient flux annual report. Boston: Massachusetts Water Resources Authority. Report 2010-10. 27 p.  
<http://www.mwra.state.ma.us/harbor/enquad/pdf/2010-10.pdf>
- Werme C, KE Keay, PS Libby, D Wu, DI Taylor, DL Codiga, 2016. 2015 Outfall monitoring overview. Boston: Massachusetts Water Resources Authority. Report 2016-11. 64 p.  
<http://www.mwra.state.ma.us/harbor/enquad/pdf/2016-11.pdf>

- Xue, P, C Chen, J Qi, RC Beardsley, R Tian, L Zhao, and H Lin, 2014. Mechanism studies of seasonal variability of dissolved oxygen in Mass Bay: A multi-scale FVCOM/UG-RCA application. *Journal of Marine Systems*. 131, 102-119.
- Zhao L, C Chen, RC Beardsley, DL Codiga, WS Leo, and MJ Mickelson, 2015a. Modeling 2012 in Massachusetts Bay Using the Unstructured-Grid Bays Eutrophication Model. Boston: Massachusetts Water Resources Authority. Report 2015-02. 102p.  
<http://www.mwra.state.ma.us/harbor/enquad/pdf/2015-02.pdf>
- Zhao L, C Chen, RC Beardsley, DL Codiga, WS Leo, and MJ Mickelson, 2015b. Modeling 2013 in Massachusetts Bay Using the Unstructured-Grid Bays Eutrophication Model. Boston: Massachusetts Water Resources Authority. Report 2015-03. 102p.  
<http://www.mwra.state.ma.us/harbor/enquad/pdf/2015-03.pdf>
- Zhao L, Chen C, Beardsley RC, Codiga DL, Leo W. 2016. Simulations of Hydrodynamics and Water Quality in the Massachusetts Bay System during 2014 using the Bays Eutrophication Model. Boston: Massachusetts Water Resources Authority. Report 2016-03. 105p.
- Zhao, L, C Chen, WS Leo, and MJ Mickelson, 2012. Modeling 2011 in Massachusetts Bay using the unstructured-grid Bays Eutrophication Model. Boston: Massachusetts Water Resources Authority. Report 2011-13. 135pp. <http://www.mwra.state.ma.us/harbor/enquad/pdf/2012-13.pdf>
- Zhao L, R Tian, P Xue, C Chen, WS Leo, and MJ Mickelson, 2011. Modeling 2010 in Massachusetts Bay using the unstructured grid Bay Eutrophication Model. Boston: Massachusetts Water Resources Authority. Report 2011-09. 118 p.  
<http://www.mwra.state.ma.us/harbor/enquad/pdf/2011-09.pdf>



Massachusetts Water Resources Authority  
Charlestown Navy Yard  
100 First Avenue  
Boston, MA 02129  
(617) 242-6000  
[www.mwra.com](http://www.mwra.com)